Homopolymer and Block Copolymer Composites Based on Silica Nanoparticles Coated with Polymeric *Single* or *Double Shells* Synthesized by Atom Transfer Radical Polymerization

Dissertation

zur Erlangung des akademischen Grades
Doktor der Ingenieurwissenschaften
(Dr. -Ing.)
der Technischen Fakultät
der Christian-Albrechts-Universität zu Kiel

Golda Louis Chakkalakal
Kiel
2011

1. Gutachter	Prof. Dr. Volker Abetz
2. Gutachter	Prof. Dr. Rainer Adelung
3. Gutachter	Prof. Dr. Franz Faupel

Datum der mündlichen Prüfung 10.11.2011

Erklärung

Die vorliegende Arbeit wurde von mir selbstständig verfasst und ich habe dabei keine anderen als die angegebenen Hilfsmittel und Quellen benutzt.
Ferner habe ich nicht versucht, anderweitig mit oder ohne Erfolg eine Dissertation einzureichen oder mich der Doktorprüfung zu unterziehen.

Table of Contents

List of Figures

Chapter 3

Chapter 4. Results and Discussions

Chapter 4.3

Chapter 4.4

List of Tables

Page

Chapter 1. Introduction

The application of inorganic nanofillers is increasing exponentially in polymeric systems. Diverse applications of polymer composites are so wide that it can be felt in every walks of our lives. The unique combination of various characteristics of nanomaterials can cause changes in the properties of polymer matrix. The recent trends in the field of nanocomposite research reveal that nanofillers of particular size, shape and dimension when processed properly at small amounts (≤ 5 wt%) can improve the impact strength, tensile properties, resistance to thermal degradation, chemical and flammability resistance, gas impermeability and dimensional stability of polymeric materials.

It is important to recognize that nanocomposite research is extremely broad and encompassing the areas such as communications, data storage, electronics and computing, aerospace materials, defence applications. sporting materials, health medicine, energy, environmental and transportation.[1] Toyota central research laboratories in Japan reported in the early 1990's, that for a very small amount of nanofiller loading can cause pronounced improvement in thermal and mechanical properties of Nylon-6 nanocomposites.[1-2] Thus, polymer nanocomposites have tremendous market potential both as replacements for current composites and in the creation of new markets through their outstanding properties.

Organic/inorganic nanocomposites are generally termed as organic polymer composites with nano-scale building blocks of inorganic materials. They have the combined advantages of organic polymer, such as processability, ductility, flexibility, and dielectric, and that of an inorganic material such as rigidity and thermal stability. The small size of nanofillers leads to a marked enhancement in the interfacial area of polymer nanocomposites when compared to that of conventional composites. Since most of the important physical and chemical interactions in

polymer composites are governed by surface properties, such as, the increased interfacial area creates a significant volume fraction of interfacial polymer with properties different from that of a bulk polymer even at low loadings of filler.

So the nanomaterials can be broadly classified by their geometries: particulate, layered, and fibrous materials. Inorganic nano-scale building blocks includes fibrous materials (e.g., nano-tubes, nano-fibres), layered silicates (e.g., montmorillonite, saponite), and nanoparticles (NP's). Nanoparticles are often defined as particles having diameter less than 100 nm. The NP's can be those derived from non-metal oxides (e.g., SiO_2), metals (e.g., Au, Ag), metal oxides (e.g., TiO_2, Al_2O_3), semiconductors (e.g., PbS, CdS) and others (e.g., SiC).[1] The surface area per unit volume of particles and fibres are inversely proportional to the material's diameter; thus smaller the diameter, greater is the surface area per unit volume.[3]

Among the various polymer nanocomposites, silica-polymer nanocomposites have attracted substantial academic and industrial interest. In fact, among the numerous inorganic/organic nanocomposites, polymer/silica composites are the most commonly reported in the literature. The speciality silica business includes silica gels/aerogels, precipitated silicas and silicates and nanosilicas such as colloidal silicas/silica sols and fumed silica. The estimated global market share of speciality silicas during the period 2009-2010 on the basis of global survey made by Freedonia Group is given by the Figure 1.[4] According to their survey, "the demand for speciality silica will rise 6.3 % per year to 2.7 million metric tons by 2014". The above market values of speciality silicas are based on their applications in the field of plastics and ceramic industry, tire and non-tire rubber products, coatings and inks, electronics and semiconductor devices, speciality papers, cosmetics, food and health care products and in the field of agriculture and animal health care.

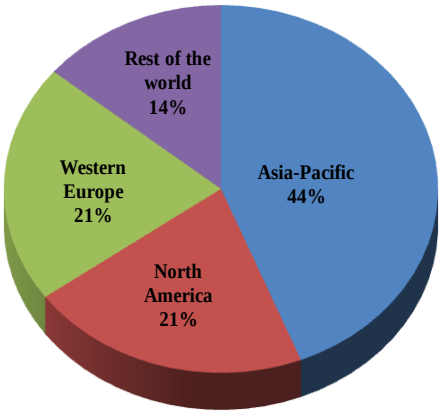

Figure 1.1. Estimated market shares and demand of speciality silicas all over the world on the basis of global survey made by Freedonia Group during the period 2009-2010.[4]

In the past few years, application of colloidal silica suspension prepared by sol-gel process received much attention in the field of nanocomposite research. However, developing the manufacturing process technologies in terms of quantity and value for commercialization poses big challenges. The main challenges are dispersion of NP's and chemical compatibility with matrix materials. The great differences in the properties of polymer (hydrophobic) and silica materials (hydrophilic) can often cause phase separation. So, a direct homogeneous dispersion of NP's in a polymer by physical or simple mechanical mixing is insufficient to overcome the attractive interactions between the nanoparticles (e.g., hydrogen bonding, van der Waals forces) which lead to the agglomeration of particles in the matrix. Therefore, the interfacial interaction between two phases of nanocomposites is the most decisive factor affecting the properties of the resulting materials. A variety of methods have been used to enhance the compatibility between nanosilica and the polymer. The most frequently used method to improve the interfacial interaction and to decrease the phase separation of the polymer/silica nanocomposites is to modify the surface of silica NP's either physically or chemically. Surface modification based on physical interaction is usually implemented by using surfactants or macromolecules adsorbed

onto the surface of silica particles. Chemical methods involve modification either with modifier agents or by grafting polymers. Silane coupling agents are the most commonly used modifier agents.

Surface modification of silica NP's by polymer-grafting is gaining attention. This can be attributed to the fact that polymer-grafting improves the interfacial properties of the resulting organic/inorganic hybrid materials, and at the same time the thermal and mechanical properties of the polymer. In these methodologies, the use of living or controlled polymerization techniques has been critical to incorporate organic (co)polymers of controlled molecular weight, composition and functionality to inorganic substrate. Four major surface-initiated controlled radical polymerizations (SI-CRP)[5] are atom transfer radical polymerization (ATRP), nitroxide-mediated polymerization (NMP), stable free radical polymerization (SFRP) and reversible addition fragmentation transfer (RAFT) polymerization.

Among the above mentioned SI-CRP techniques, ATRP has been most extensively studied and used to graft polymer brushes from the surface of NP's especially from silica. Figure 1.2 displays the recent publication status of various controlled/living radical polymerization techniques.[6] Among the various CRP techniques, studies in the field of ATR polymerization is found to be the most exploiting topic. According to recent review of Mathias Destarac,[7] ATRP has been licensed for the commercial production of speciality polymers by several corporations since 2003. Among them, PPG industries explored it as a suitable method to design functional polymer additives of various controlled architectures like block, gradient, graft, star copolymers with low polydispersity for coating applications. Growing polymer chains from silica particles by ATRP through *"grafting from"*[8] approach has proven to be a versatile approach for incorporating organic (co)polymers. Surface chemistry of core particles plays a vital role on grafting initiator through anchored Silane moiety and finally the kinetics of surface modification by (co)polymer shell. Molecular weight, grafting density, brush thickness, length of the tethered chains and the

size of core silica particles decides the nature of dispersion of silica-(co)polymer hybrid particles and the final property of the composites.

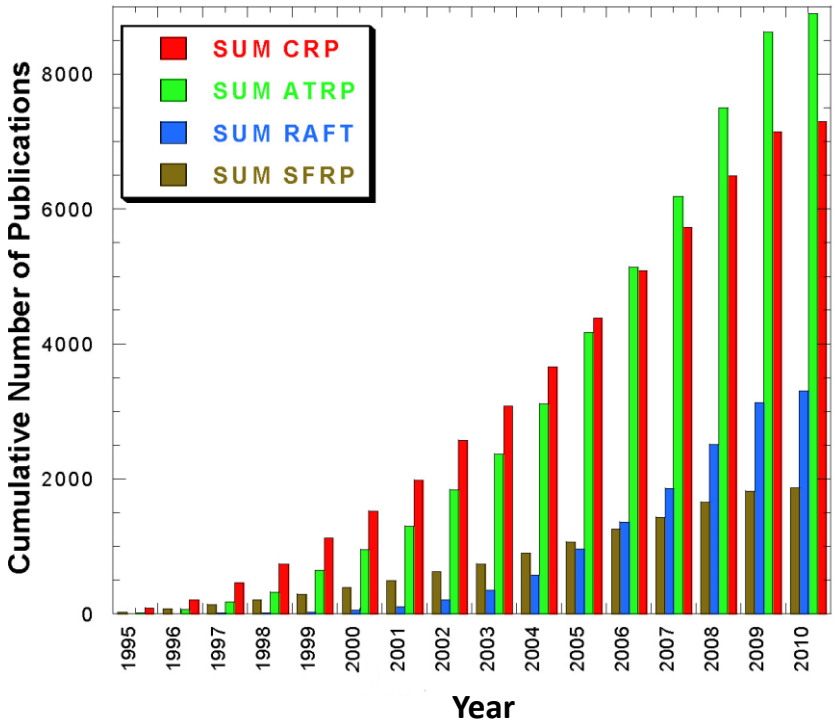

Figure 1.2 A survey of number of publications in the field of (a) all CRP techniques (SUM CRP) (b) ATRP (SUM ATRP) (c) RAFT (SUM RAFT) and NMP or SFRP (SUM SFRP) vs. year of publication (SciFinder Scholar®).[7]

Block copolymer/nano-particle mixture have attracted substantial attention due to the fact that microphase separation of the copolymer can direct the spatial distribution of NP's and thereby tailoring the properties like optical, electrical, mechanical, etc. of the final composites. Bockstaller et al.[9] has validated the size-selective organization of inorganic NP's. The NP's have been found to alter both the orientation[10-11] and the morphology[12-13] of the di-block copolymer microdomains. Most of these studies were focussed on relatively small NP's of either metals or metal oxides relative to the dimensions of block copolymer domains.

Taking into account some of the above mentioned facts, this research work employs colloidal silica suspension for surface functionalization reactions. As a matter of curiosity, silica particles having average core diameters, 12 nm (Si_{12}) and 20 nm (Si_{20}) were chosen for surface modification. Commercially available epoxysilane is chosen as the coupling agent for anchoring the initiator on silica nanoparticles (precursor) for *"grafting from"* ATR polymerization. One of the main challenges, this research work encountered were the reduction of the aggregation of functionalized silica nano-particle precursors. This is achieved to a good extend by keeping the particles in a respective solvent after each step of functionalization (before polymerization) without drying during purification steps.

The second challenge was controlling the concentration of ATRP initiator on silica nanoparticles. This is very important in regulating the efficiency of colloidal silica initiator towards "*grafting from*" polymerization. The coupling efficiency of silane linker is important in the anchoring of ATRP initiator. This is answered by controlling the silane concentration on silica surface under controlled pH conditions. Further, the concentration of anchored initiator on respective silane coupled silica particles was studied under different basic systems and solvents. Obviously one could observe variation in the content of coupled silane and grafting density of initiator under a given reaction condition from both sets of silica particles, arising due to the difference in surface chemistry.

Surface-initiated atom transfer polymerization (SI-ATRP) from silica nanoparticles is not a new topic. Most of the reported works on SI-ATRP were carried out from silica particles having lower bromide concentration. But in the present work, the efficiency of styrene and methyl methacrylate (MMA) grafting polymerization from both Si_{12} and Si_{20} nanoparticles having higher initiator concentration (0.4 mmol/g) are systematically investigated under specific reaction conditions. Also, apart from other reported works, in order to make a comparative analysis, the initiator concentration was kept constant on both types of particles. The

consequences at higher conversions and the effective size distribution of resultant silica grafted polymer brushes were studied.

As known, poly(methyl methacrylate) (PMMA) is one of the most available commodity plastic that has been widely used in industry for many years due to its excellent optical clarity, good weather resistance, high tensile strength and tensile modulus. However, its brittleness manifests itself as a limiting factor for being used in other field of applications. Therefore, a part of the research work is devoted to investigate the impact and tensile properties and dispersion of selective PMMA modified particles in a given PMMA matrix prepared by melt mixing on the basis of some factors such as graft density, varying graft molar mass and silica core size.

The classical way of achieving a significant improvement in toughness of PMMA or other glassy polymers is by adding discrete amount of rubbery like modifier particles with *core-shell* structure. Emulsion polymerization and mechanical blending are the common methods adopted for the preparation of such rubber-toughened PMMA composites.[14-16] The *core-shelled* modifier particles have either a glassy or elastomeric core with an outer shell depending on the nature of the matrix it get dispersed. PMMA composites with silica nanoparticles modified by *double-shell* (block copolymer) with an elastomeric inner shell poly(butyl methacrylate) (PBMA) and PMMA outer shell have not been reported yet. The question is how the silica core and elastomeric inner layer in the double shell particles affect the final impact and tensile properties of composites.

In this research work, we synthesised the *silica core-double shelled* particles with PBMA inner block by ATRP for the first time. The latter part of the work investigates the synergetic effect of silica modified by *double-shelled* block copolymer particles in PMMA composites and then compared with those comprising *single-shelled* particles on the final impact and tensile properties of composites (for low silica content) prepared by melt mixing.

As mentioned above, most of these studies were carried out with very small particles like quantum dots in block copolymer films. Very few works reported with the dispersion

characteristics of silica particles/modified silica particles in block copolymer films. Due to the complex morphological changes occur during melt mixing, almost no works have reported yet with the dispersion characteristics of silica particles in glassy block copolymer matrix. So, in this work, the localization characteristics of PMMA modified silica (*single-shelled*) particles in PS-*b*-PMMA composite prepared by melt mixing for a given morphology and their effect on impact properties is studied.

On the above basis, the present doctoral work is organized as follows: Chapter-2 sketches a theoretical background regarding the synthesis of colloidal silica nanoparticles, importance of surface functionalization by grafting (co)polymers, their mode of dispersion in homopolymer/block copolymer matrices and finally, effect on mechanical properties of resultant composites will be given. Experimental techniques for characterizing surface modified silica nanoparticles and the related silica-(co) polymer nanocomposites are also discussed at the end of same chapter. The experimental procedures employed for the functionalization of silica nanoparticles followed by graft polymerization of (co)polymers, preparation of nanocomposites from (co) polymer and their characterization methods are discussed in Chapter 3.

Chapter 4 deals with results and discussions. It is further divided into five sub chapters. Chapter 4.1 describes the reaction conditions and effect of surface chemistry of Si_{12} and Si_{20} nanoparticles towards epoxy-silanization followed by initiator grafting reactions. Chapter 4.2 comprises an investigation of reaction kinetics of styrene and MMA polymerizations. In the latter part of the same section, the size distribution of polymer grafted silica particles at higher conversions and their selective morphology is discussed. Chapter 4.3 discusses the mechanical properties and selective morphologies of PMMA composites on the basis of factors such as graft density, given matrix and varying graft molar mass and silica core of PMMA modified Si_{12} and Si_{20} particles. Chapter 4.4 describes the dispersion characteristics of PMMA modified silica nanoparticles in PS-*b*-PMMA block copolymer matrix of given morphology. Chapter 4.5 is

devoted to the synthesis and characterization of *silica core-g-(PBMA-b-PMMA)* double shell particles. It further investigates the effect of these particles on improving the mechanical properties of PMMA composites. Finally, Chapter 5 summarizes the conclusions obtained during these investigations.

References

1. F. Hussain, M. Hojjati, M. Okamoto, R. E. Gorga, *J. Comp. Mater*, 2006, 40, 1511-1575.
2. A. Usuki, M. Kawasumi, Y. Kojima, A. Okada, T. Kurauchi, O.J. Kamigaito *Mater. Res*., 1993, 8, 1174.
3. J.J. Luo, I.M. Daniel, *J. Compos. Sci. Technol*., 2006, 63, 1607–1616.
4. *Speciality Silicas*, Global Strategic Analysis, Freedonia Group, 2009-2010.
5. R. Barbey, L. Lavanant, D. Paripovic, N. Schüwer, C. Sugnaux, S. Tugulu, H. A. Klok, *Chem. Rev*., 2009, 109, 5439-5452.
6. Survey of SciFinder Scholar on *"Cumulative publications in the field of CRP techniques"* Up to March 25, 2010.
7. M. Destarac, Macromol. Reac. Eng., 2010, 4, 165-179.
8. O. Pruker, J. Rühe, *Mater. Res. Soc. Symp. Proc.*, 1993, *304*, 1675.
9. M. R. Bockstaller, E. L. Thomas, *Phys. Rev. Lett*., 2004, 93, 166106.
10. J. Y. Lee, Z. Shou, A. C. Balazs, *Phys. Rev. Lett*., 2003, 91,136103.
11. Y. Lin et al., *Nature*, 2005, 434, 55.
12. B. J. Kim, J. J. Chiu, G. R. Yi, D. J. Pine, E. J. Kramer, *Adv. Mat*., 2005, v 17, 2618.
13. Y. S. Sun, U. S. Jeng, K. S. Liang, S. W. Yeh, K. H. Wei, *Polymer*, 2006, 47, 1101.
14. C. B. Bucknal, *Toughened Plastics*, Applied Science Publishers: London, 1977.
15. H. Keskkula, *Rubber-Toughened plastic*, American Chemical Society, New York, 1989, 289.
16. C. Wrottecki, P. Heim, P. Gaillard, *Polym Eng Sci*., 1991, 31, 213.

Chapter 2. Theoretical Background

2.1. Silica nanoparticles

The synthesis of organic-inorganic hybrids, especially silica-polymer hybrid materials, has been extensively investigated in the past few years because of the exceptional opportunities to tailor the properties of these materials. Such kind of particles has real potential as speciality nanofillers, where the organic group can be tailored for compatibility with the matrix. The introductory chapter has already highlighted the growing demand of speciality silicas in the coming years. Applications involving silica nanoparticles (SiNP's) are of interest not only in the academic field, dealing with stability and interactions in dispersion, but also in numerous industrial fields including ceramics, catalysis, chromatography, pigments, pharmaceuticals, automotive, aerospace and electronics.[1-5] Silica nanoparticles is available in the form of dry powder (fumed silica) or colloidal form. Of which, fumed silicas are usually prepared by the pyrolysis of tetraalkoxysilanes. Even though the primary silica particles are nanosized, high surface energy and interparticle hydrogen bonding leads to aggregation or agglomeration of silica while preparing composites with polymer. Even though these particles are widely offered in market, lack of particle stabilization during processing of composites limits its application in polymer technology.[6]

Therefore, colloidal silica, otherwise called as *'white carbon black'* is frequently used as an active nanofiller in many polymeric systems.[6] Colloidal silica is of particular interest in polymer industry for composite preparation due to the ease of synthesis and precise control of the size and distribution of the particles.[5,7] Within the past decades, the sol-gel process has been widely used to create novel organic-inorganic composite (hybrid) materials, which were termed as "ceramers" by Wikes et al. [8] and "ormosils" or "ormocers" by Schmidt et al.[9] The well-

established hydrolytic sol-gel approach by Stöber and co-workers[10] enables the synthesis of unmodified and monodisperse silica. The synthesis involves the hydrolysis and condensation of tetraethyl orthosilicate (TEOS) in a mixture of alcohol, water and ammonia (catalyst). Hydrolysed TEOS monomers generated during the hydrolysis reaction undergo condensation to eventually form silica particles of various size ranges. The resultant silica particles are stabilized by electrostatic repulsion due to the ions in the ammonia solution. The general reaction scheme is shown in following Figure 2.1. The Stöber method was later modified by many research groups and found to be the simplest route to monodisperse silica particles.[11-17]

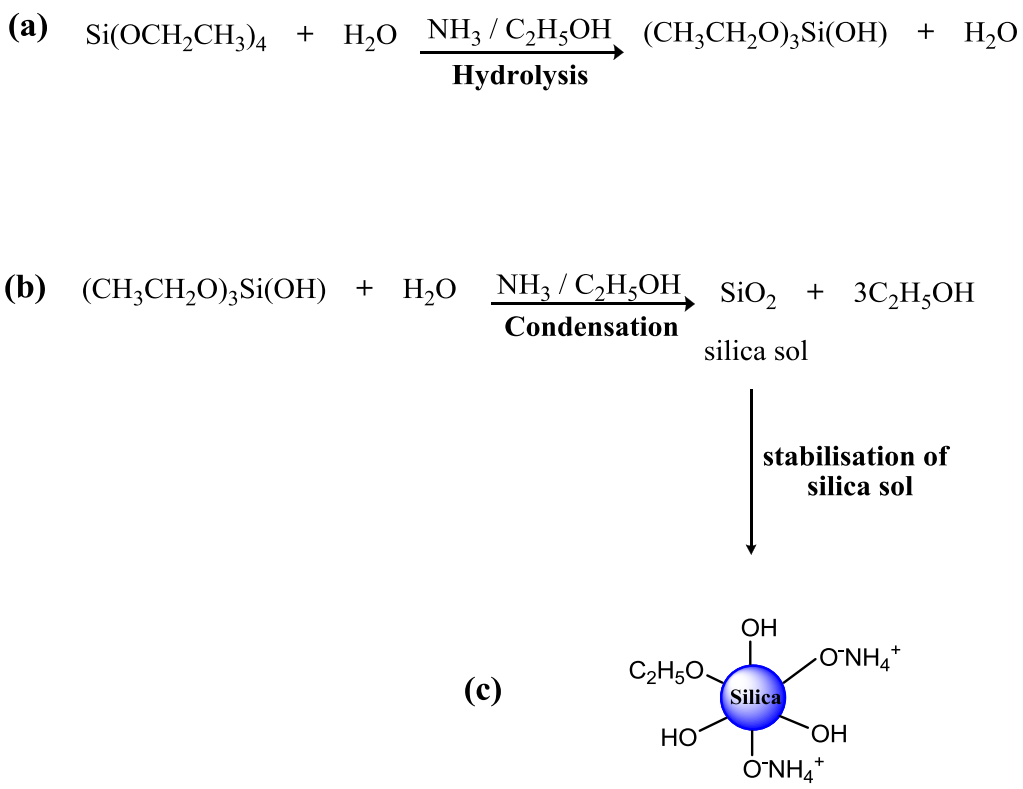

Figure 2.1. General reaction scheme for Stöber process (**a**) hydrolysis (**b**) condensation (**c**) stabilization of silica sol in basic ammonia.[10] Cartoon (c) is taken from reference 5.

Many factors influence the kinetics of hydrolysis and condensation reactions in the sol-gel process, which include the water/silane ratio, catalyst, temperature, nature of solvent and so

forth. Hydrolysis of TEOS can be catalyzed by either acidic or basic medium. Slower hydrolysis and faster polycondensation were observed in the case of base catalysis leading to compact colloidal particles. In contrast, faster rate of TEOS hydrolysis was observed in acidic medium. It has been shown that basic catalysis usually yields hybrid particles with dimensions well above 100 nm and more generally in the micrometer range. Alternatively, if acid catalysis is used, sizes below 100 nm can be obtained. Preparation of unmodified silica nanoparticles via hydrolytic sol-gel approach from tetraalkoxysilane precursors has been extended to the formation of silsesquioxane particles (with empirical formula $[R_2Si_2O_3]_n$) from mixtures of TEOS and organotrialkoxysilane precursors, $RSi(OR')_3$, (with R = methyl, phenyl, octyl, aminopropyl etc., and R' = ethyl or methyl)[13-15] or directly from organically-modified precursors.[18-20]

2.2. Why is surface modification of silica nanoparticle necessary?

The structure of silica nanoparticles has a three dimensional network. The hydrophilic nature of the silica particles is determined by the silanol and siloxane groups that are present on the external as well as the internal structure.[29,17] Polymeric materials generally show improved mechanical and thermal properties after the addition of silica NP's. While, the hydrophilic nature of silica nanoparticles made them to aggregate while preparing composites with hydrophobic polymer matrix. The main challenge is then to control the level of interparticle aggregation. In the present scenario, functionalization of silica particles in colloidal suspension gains attention. Functionalization of silica NP's from colloidal solution makes the particle to be well separated and reduces the chances of aggregation. Silanol groups can be functionalized through different chemical methods. Chemical methods can improve the properties of the silica particles through functionalizing the surface hydroxyl groups by suitable organic modifier agents or by grafting polymers.

Nowadays grafting polymer chains onto inorganic nanomaterials receives much attention. Generally this is achieved chemically through either covalent bonding or by physisorption.[21] Physisorption makes the adsorption reversible, especially during processing and is therefore not a favoured technique. Covalent binding of polymer chains are more preferred in order to maximize a stable interfacial compatibility between the two phases. Covalent attachment on a solid substrate can be accomplished by either "*grafting to*" or "*grafting from*" techniques.[21-22]

The "*grafting to*" technique (see scheme in Figure 2.2) involves the reaction of preformed end-functionalized polymer molecules with chemically activated substrate.[23]

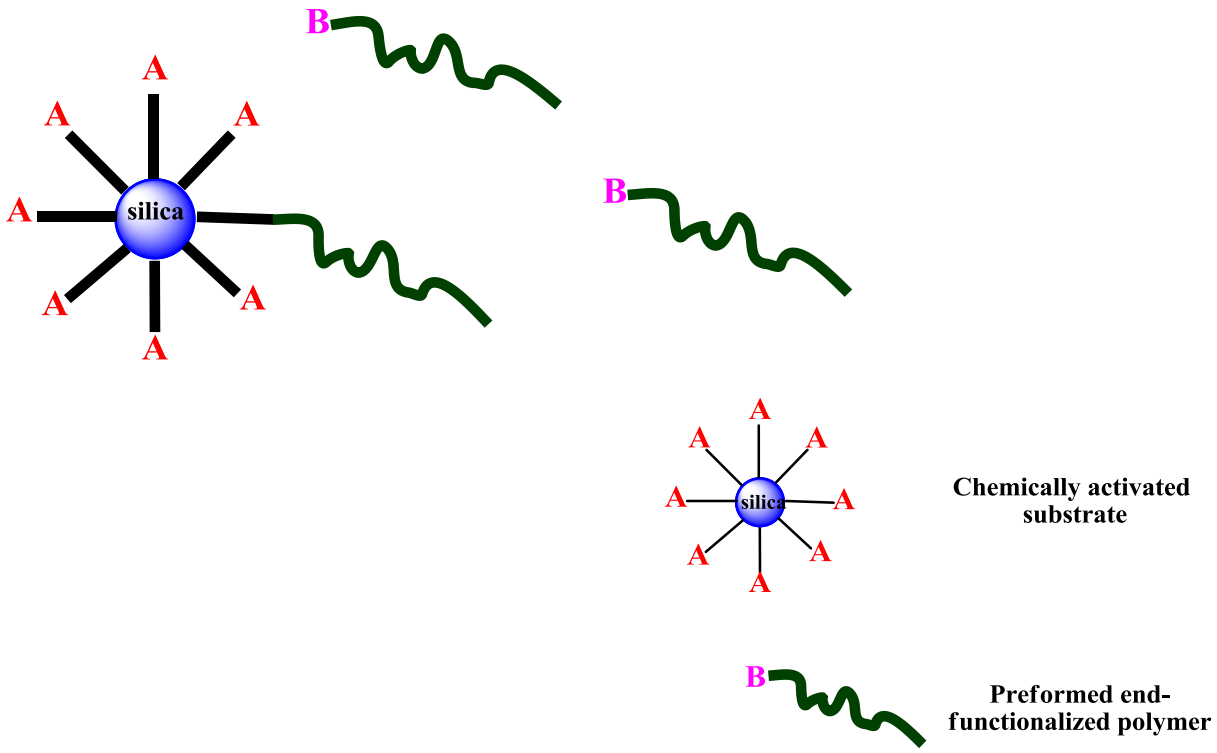

Figure 2.2. General concept of "*grafting to*" approach [5]

Yoshikawa et al.[24] observed that relatively low grafting densities are obtained by this approach. Steric crowding or repulsions of already attached chains on the surface hinder the diffusion of additional chains to the reactive sites, thereby hampering the formation of dense polymer brushes.[25] Furthermore, with increasing polymer molecular weight, the reaction between the polymer end-group and the complementary group on the substrate surface becomes less efficient. One advantage of this method is that polymer chains can be characterized before being attached to the substrate.

2.2.1. Surface modification through "*grafting from*" approach

In the "*grafting from*" approach, initiator molecules are anchored on silane functionalized silica NP's followed by the polymerization reaction with the monomer, which leads to the formation of tethered polymer chains (as schematically shown in Figure 2.3). Polymer brushes of high graft density can be generated, because the small monomer molecules can easily diffuse to reactive sites of the growing polymer chains and thereby circumvent the problem that arised from diffusion barriers as in "*grafting to*" approach.

Conventional free radical polymerization, cationic polymerization, anionic polymerization, ring-opening polymerization, ring-opening metathesis and controlled polymerization reactions can be used for the fabrication of polymer brushes. Free radical processes are more tolerant to functional groups and impurities and are well suited for polar monomers. The *"grafting from"* approach was first reported by Prucker and Rühe.[26-27] The method involves the grafting of azo initiator onto a particle or flat surface followed by polymerization. Polymer brushes of high molecular weight and high graft density were produced. At lower conversion, polymerization kinetics of initiation and propagation step of the growing polymer was similar to that of solution polymerization.

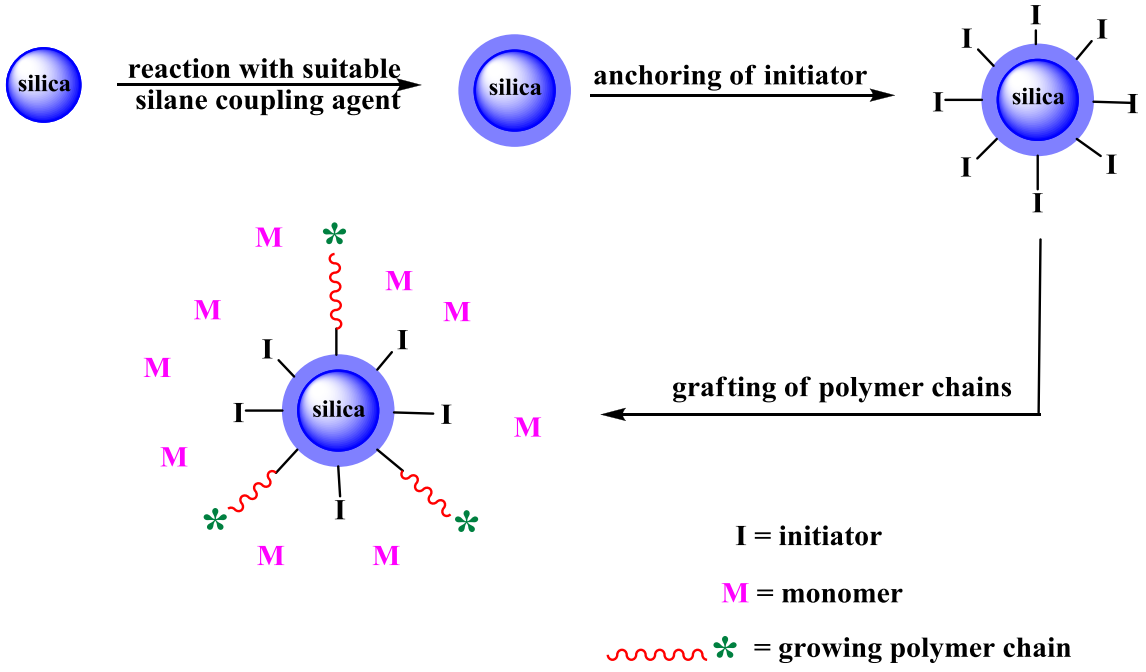

Figure 2.3. General concept of "*grafting from*" approach

However, the kinetics of termination was different. In surface-initiated polymerization, free chains had to diffuse against a concentration gradient into the film thereby reducing the bimolecular termination.[21] In classical free radical polymerization, it is impossible to control the chain transfer and termination. There the rate of propagation is a pseudo first order reaction while termination is of second order. These polymerizations are generally characterized by broad molecular weight distributions, poor control of molecular weight and chain end functionality, and the inability to synthesize well defined block copolymers.[28-29] However, controlled free radical polymerization can overcome most of these drawbacks.

Developments in the field of controlled/living radical polymerization have proven it as a versatile method for growing polymer chains with varied architectures from silica surface.

Through this technique, one can manipulate the structure of the resultant polymer through changes in grafting density, composition and molar mass.[31] Controlled living radical polymerization is a preferential choice for most of the grafting polymerization due to (i) initiating groups attached to the solid surface confer a mobility barrier for termination by coupling and (ii) a limited number of surface initiating groups are needed to promote property changes, thereby reducing the concentration of free radicals in the system. Controlled free radical polymerization maintains a low concentration of radicals at any one time during the course of reaction.[29-31]

Hence, most of the polymer brushes synthesized by *"grafting from"* approach are prepared by surface-initiated (SI) controlled radical polymerization techniques like atom transfer radical polymerization (ATRP), reversible-addition fragmentation chain transfer (RAFT) polymerization, nitroxide-mediated polymerization (NMP) and photoiniferter-mediated polymerization (PIMP). These are commonly referred as *surface-initiated controlled radical polymerization techniques*.[40]

Generally in controlled radical polymerization, polymer chains are formed by the reaction of radicals generated by initiator with monomer molecules. The "capping groups" reversibly deactivates the radicals present on the end of growing polymer chain. The reaction of capping group with a radical polymer chain eliminates the radical, thereby temporarily stopping polymerization. The reaction propagates by the loss of capping group. Hence, polymers can be synthesized with predefined molar mass, low polydispersity, controlled composition and functionality by controlling the life-time of the growing radicals.[5,31] The polydispersity of typical product is ≤ 1.3.

Among the various controlled polymerization techniques, ATRP has been extensively studied and utilised to produce polymer brushes from surfaces. Compared to other controlled radical

polymerization methods, ATRP is chemically versatile and robust and the SI-ATRP is explicitly described in the following chapters.

2.3. Surface-initiated atom transfer radical polymerization (SI-ATRP)

ATRP was simultaneously reported by Matyjaszewski[32] and Sawamoto[33] in the mid of 1990's. The reaction mechanism in ATRP involves a reversible redox activation of a dormant alkyl halide terminated polymer chain end by a halogen transfer to a transition metal complex (Figure 2.4). [34]

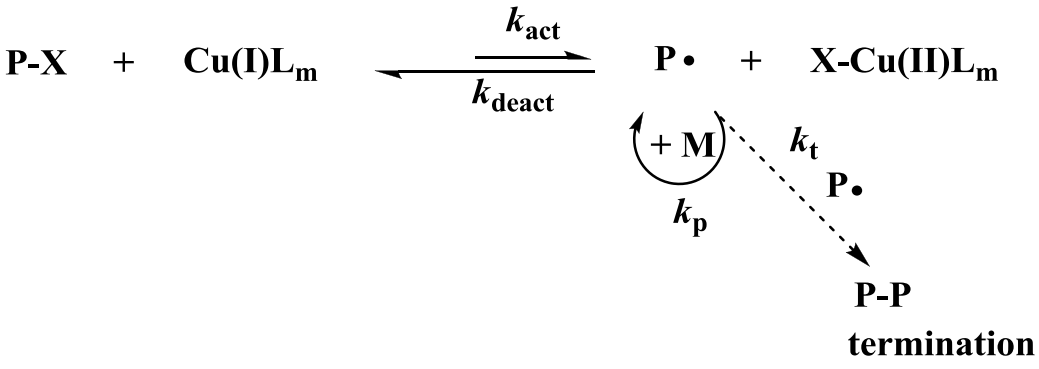

Figure 2.4. General reaction mechanism of copper-catalyzed atom transfer radical polymerization.[34]

Initially, homolytic cleavage of carbon–halogen bond occurs and generates a free and active carbon-centered radical species at the polymer chain end. This activation step is based on the single electron transfer from the transition metal complex to the halogen atom, which leads to the oxidation of the transition metal complex (X-Cu(II)L_m). Then, in a fast reversible reaction, the oxidised form of the catalyst reconverts the propagating radical chain end to the corresponding halogen-capped dormant species. Termination reactions in ATRP occur mainly through radical coupling of two active polymer chains and disproportionation. In a well-

controlled ATRP, no more than a few percent of the polymer chains undergo termination. This termination process generates oxidised metal complexes, (X-Cu(II)), as persistent radicals to reduce the stationary concentration of growing radicals and thereby minimize the contribution of termination.[34]

ATRP is tolerant to impurities and functional groups and hence a wide range of monomers such as styrenes, (meth)acrylates, (meth)acrylamides and acrylonitrile which contain substituents that can stabilize the propogating radicals and can be polymerised in organic as well as aqueous phases. The ATRP initiator (typically, α-halo ester or α-benzyl moiety) is activated in the presence of transition metal salts such as those of copper (Cu), ruthenium (Ru), iron (Fe), cobalt (Co) and others, which can undergo redox reactions with halogens. Copper based catalyst systems are commonly used. The solubility and activity of the transition metal salts are enhanced by ligation with aliphatic or aromatic amines. Many parameters, such as ligand to transition metal ratio, Cu(II) to Cu(I) ratio (in the case of copper catalyst), type of ligand, counter ion, solvent or initiator influence the performance of (SI)-ATRP. This facile polymerization and less stringent experimental conditions promoted the application to polymer brush growth on NP's, especially silica.[34-40] The following paragraphs reviewing important works on SI-ATRP from silica nanoparticles.

SI-ATRP was first reported by Huang and Wirth[41] in 1997 by successfully grafting poly(acrylamide) (PAM) brushes from benzylchloride functionalized silica particles. Later, Ejaz et al.[42] adopted Langmuir-Blodgett technique for the synthesis of poly(methyl methacrylate) (PMMA) brushes from 2-(4-chlorosulfonylphenyl)ethyl silane self-assembled monolayers. They pointed out that addition of free, sacrificial initiator was necessary to achieve a controlled polymerization.

Matyjaszewski et al.[43] successfully demonstrated the addition of small amount of Cu(II) as deactivating species instead of free initiator can control the polymerization of polystyrene (PS)

from bromoisobutyrate-functionalized silicon wafers. Later they made the study with *n*-butyl acrylate and MMA monomers and various core-shell colloids containing tethered AB diblock copolymers were synthesized.[40]

Afterwards, Pattern and von Werne[44] reported the SI-ATRP of PS and PMMA from silica NP's of different sizes (75 nm and 300 nm). Their approach consisted of immobilization of the initiator molecule on the silica particle followed by surface-initiated ATRP (Figure 2.5).

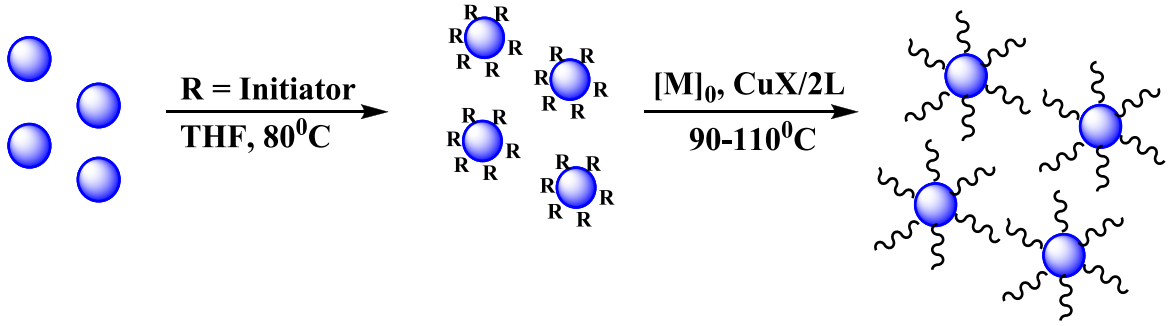

Figure 2.5. Synthesis of surface initiated ATRP from silica particles[44]

The immobilization of initiator on the silica surface was accomplished through the silane coupling agents like [2-(4-chloromethylphenyl)ethyl]dimethylethoxysilane (CPTS), [3-(2-bromo-isobutyryl)propyl]dimethylethoxysilane (BPDS), and [3-(2-bromopropionyl)propyl]dimethylethoxysilane (BIDS). They found that 75 nm sized silica particles exhibited a higher degree of control on molecular weight than larger particles (300 nm). Harrak et al.[45] exploited SI-ATRP to control the interparticle aggregation of NP's for grafting polystyrene chains. This was achieved by maintaining the silica particles in an organic solution throughout the surface modification. Irreversible aggregation was often observed if the particles are redispersed after solvent removal.

Similar to the work done by Patten et al.[44] , Matyjaszewski and his co-workers[46] utilized $CuBr_2$ deactivating species for the synthesis of core-shell colloids containing tethered PS, poly(butyl acrylate), PMMA and AB diblock copolymers.

ATRP of several hydrophilic monomers were successfully carried out in aqueous media by Armes et al.[47-48] Later they extended this process to perform surface modification on silica NP's.[49] Polymers like poly[oligo(ethylene glycol) methacrylate] (POEGMA) and poly[2-(*N*-morpholino)ethyl methacrylate] (PMEMA) were investigated. The colloidal stability of these sterically stabilized particles was studied.

Further, silica particles of average diameter 300 nm were subjected to ATRP of ionic monomers such as sodium-4-vinylbenzote and 2-(diethylamino)-ethyl methacrylate (DEAEMA) in protic solvents. The pH-responsive colloidal stability of these cationic polyelectrolyte-grafted silica particles was investigated. They were colloidally stable at low or neutral pH, but became aggregated at higher pH. However, a reverse effect was found for anionic polyelectrolyte-grafted silica particles.[50]

Vairon et al.[51] observed that films casted from silica hard interior and an elastomeric shell shows enhanced mechanical properties. For their studies, they made use of 12 nm silica particles as the core for the growth of outer elastomeric poly(*n*-butyl acrylate) shell.

Fukuda et al.[52] have successfully grafted high density PMMA brushes onto silica particles using the initiator (2-bromo-2-methyl)propionyloxyhexyltriethoxysilane (reaction procedure is shown in Figure 2.6). These particles were found to have good dispersibility in organic solvents. Transmission electron microscopy (TEM) showed the monolayer formation and an ordered two-dimensional lattice at the air-water interface throughout the monolayer was observed through atomic force microscopy (AFM).

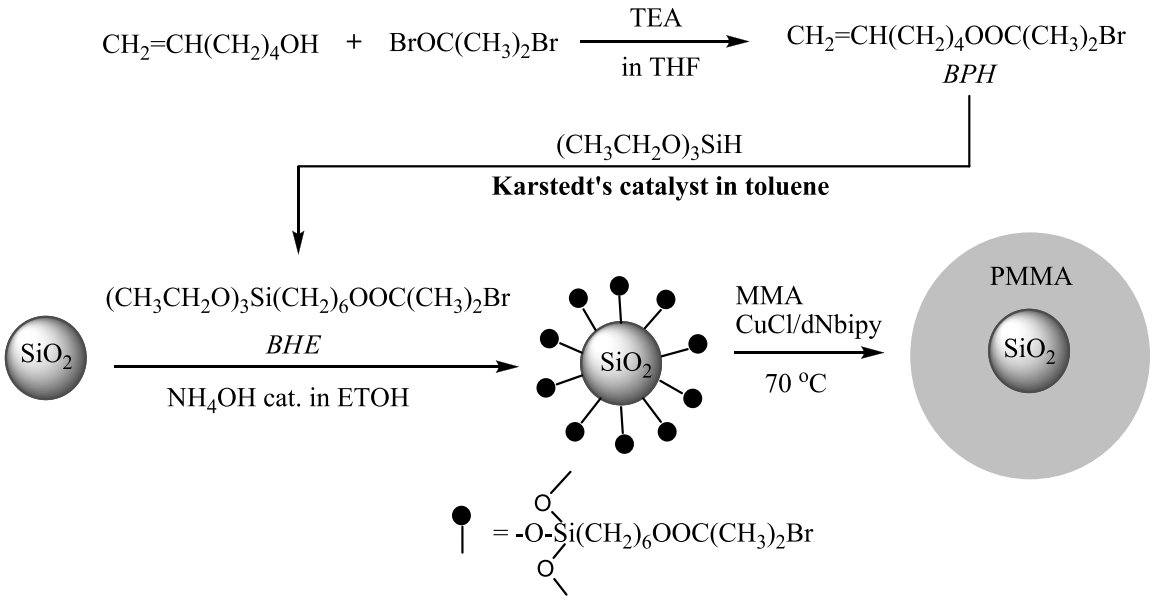

Figure 2.6. Synthesis of high density PMMA-coated silica particle by SI-ATRP[52]

Later, Boettcher et al.[53] focussed on the same ATRP procedure and reported on the graft density of a first and a second generation (block) of polystyrene grafted from silica. They showed that approximately 10-15% of the first generation of the grafts were not active for reinitiation of the second monomer feed.

Müller et al.[54] used an α-bromo type ATRP initiator for grafting hyperbranched polymer on silica particles by self-condensing ATRP. Self-condensing vinyl polymerization (SCVP) was achieved from the above initiator grafted silica particles through an inimer, which had both a polymerisable acrylic group and an initiating group. Relatively high weight fraction and surface coverage of the grafted polymers was observed for SCVP. The above functionalized silica particles could also be subjected to self-condensing vinyl copolymerization (SCVCP), in which one could tune the architecture, chemical and physical properties, and particle morphology by the choice of comonomers and their composition in the feed.

2.4. Kinetics of ATRP from solution and from surface

The general mechanism of copper metal-catalyzed ATRP is shown in Figure 2.4. The rate of polymerization can be expressed as follows:[34]

$$R_p = k_p [M][P^*] = k_p K_{eq} [M][I]_0 \times [Cu^I] / [X - Cu^{II}] \quad \text{(Equation 2.1)}$$

As already mentioned, a reversible redox process catalyzed by a transition metal complex generates the radicals or active species. This complex undergoes a one electron oxidation with concomitant abstraction of a halogen atom, X, from a dormant species, P-X. This process occurs with a rate constant of activation, k_{act}, and deactivation k_{deact}. Similar to a conventional radical polymerization, polymer chains grow by the addition of the intermediate radicals to monomers with a rate of propagation, k_p. In the absence of any side reactions other than radical termination by coupling or disproportionation, the magnitude of the equilibrium constant ($K_{eq}=k_{act}/k_{deact}$) determines the polymerization rate.[34]

The dependence of conversion of polymerization as a function of time and semilogarithmic coordinates is shown by Figure 2.7. If there is a constant concentration of propagating species in the polymerization and first-order kinetics with respect to monomer, hence a semilogarithmic plot of monomer conversion vs. time should be linear. “Nevertheless, a linear semilogarithmic plot is often observed”.[34] The reason may be due to the initial presence of excess Cu(II) species limited the solubility of the copper complexes.[34,55]. Kinetically, the optimum ratio of ligand to copper can vary with regard to changes in the monomer, counter ion, ligand, temperature and other factors.

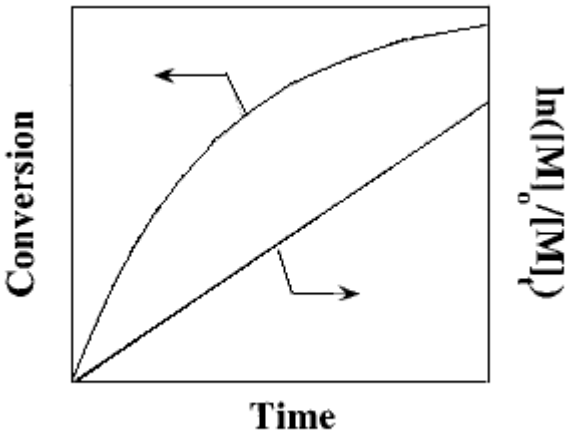

Figure 2.7. Schematic representation of the dependence of the conversion on time in linear and semilogarithmic coordinates.[34]

A reactive organic radical is generated along with a stable Cu(II) species in the atom transfer step can be regarded as a *persistent metalloradical*.[56-58] The coupling of organic radicals will occur if the initial concentration of deactivator Cu(II) in the polymerization is not sufficiently large thereby increasing the Cu(II) concentration in the reaction system. If there is sufficient amount of deactivating Cu(II) species and the radical concentration is low enough, radical termination will occur. Under these conditions, the rate of combination of radicals ($k_t[R^1]^2$) will become much slower than the rate of reaction of radicals with the Cu(II) complex ($k_{deact}[R^1][Cu(II)]$) in a deactivation process, as a result a controlled ″living″ polymerization will proceed.[34]

So far, the kinetics of ATRP from solution is discussed. A key difference in SI-ATRP from untethered solution ATRP is the presence of initiating groups at high local concentrations due to immobilization on surfaces. This is in direct contrast to small molecule initiators that are homogeneously distributed throughout the reaction media, along with the monomer and catalyst. So, control over polymerization does not necessarily result from the application of conditions

suitable for solution polymerization. Termination reactions are sometimes enhanced by the proximity of radicals tethered to a surface. Prucker and Rühe[27] investigated the kinetics and mechanism of free-radical polymerization initiated from immobilized azo initiators and concluded that the main differences between surface and solution occur due to changes in termination reactions. Several studies of SI-ATRP have shown that the growth in film thickness decreases with time, suggesting termination.

Matyjaszewski et al.[59] made simulation studies for the growth of polymer chains by SI-polymerization considering "the transfer of the monomer to the growing surface and changes in polydispersity index (M_w/M_n) with time and concluded that the initiator coverage is a major factor in defining whether the growth in layer thickness depends linearly on the reaction time". Also they found that "the lack of molecular weight control was manifested as a reason for the abrupt increase in film thickness at short polymerization times and was a consequence of the low initiator concentration in the system".

On the basis of reported studies,[44,46] the addition of ″deactivator″ or ″sacrificial″ free initiator to the polymerization system were two methods for inducing molecular weight control. The addition of free initiator served to decrease the initial monomer-to-initiator ratio and to increase the overall initiator concentration, thereby allowing some radical coupling in solution to build up the concentration of deactivator. The addition of the Cu(II) as deactivator in Cu(I) catalyzed ATRP system mitigated the insufficient formation of deactivator from the small initial concentrations of initiator and Cu(I) catalyst.

2.5. Dispersion characteristics of modified silica nanoparticles in homopolymer and block copolymer matrices

One important factor taken into care of while preparing composites is the rational control of filler clustering or aggregation, which often adversely affects material properties

(thermal, mechanical, optical, electrical properties, etc.). In the past few years, several research groups have modified the surface of nanoparticle fillers in an effort to improve their dispersion in (co)polymer matrix. For example, if nanoparticles are grafted with chains compatible with the matrix polymer, filler dispersion is favored.[60-65] The nature of dispersion of grafted nanoparticles in a homopolymer matrix is determined by several controllable parameters including the (a) graft density, (b) the molecular weight, degree of polymerization and chemical composition of the graft and matrix polymers, (c) graft chain length and (d) the size or the surface chemistry of the nanoparticles.

The grafted polymer chains form a brush on the curved particle surfaces; this topic has been investigated extensively in the context of colloidal stabilization.[66-68] Bates et al.[62] investigated the dispersion of polystyrene (PS) grafted silica particles in PS films and found that, when the molecular weight of matrix polymer is lower (higher) than that of grafted polymer, the nanoparticles disperse (aggregate). This behaviour is shown by the Figure 2.8.

Recently, Kumar and his co-workers[69] showed that spherical silica nanoparticles grafted with polystyrene chains can self-assemble into a range of superstructures when they are dispersed into the corresponding homopolymer films. The particular structures formed are sensitively determined by their grafting density and the ratio of the brush to matrix molecular weights. Theory and simulation showed that this assembly is driven by "the microphase separation arising from the immiscibility between the inorganic particle core and the polymeric grafted chains; a process analogous to the self-assembly of block copolymer or other amphiphiles".

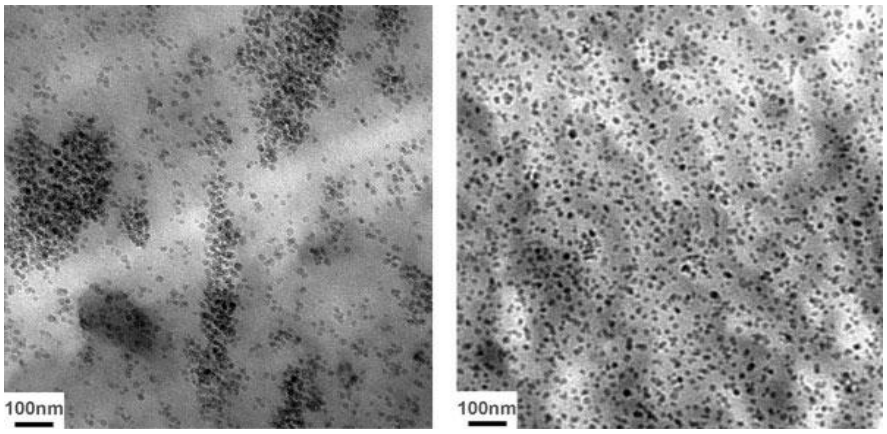

Figure 2.8. These TEM images reveal how the matrix molecular weight controls the degree of dispersion of Si-32 (3 vol % silica core and 32 is the molecular weight of graft polystyrene in kg/mol) particles. Left and right panels correspond to PS-120 and PS-18, respectively (120 and 18 for matrix molecular weights of polystyrene matrices in kg/mol).[62]

The effect of chain "confinement" on local dynamics has been observed at the interfaces of thin films[70-71] and in bound polymer layers around nanoparticles arises due to the attraction between the polymer and the nanoparticles.[72-75] Additionally, Kumar et al.[76] extended their studies towards the "*wetting*" and "*dewetting*" behaviour of 15 wt% of PMMA grafted silica particles in PMMA matrix films by varying the graft and matrix molecular weights for a given graft density. Rheological experiments showed that the composites display solid-like behaviour only when the particles are aggregated. Whereas a different behaviour was shown in their previous studies,[69] this difference is attributed to the presence of percolating particle clusters in the agglomerated samples which allows for stress propagation through the system.

As it is known, block copolymers are naturally nanostructured owing to the covalent bonds that hold chemically different blocks within a molecular dimension. Block segregation, resulting from thermodynamic block incompatibility, leads to ordered structures and domain morphologies,[77] with dimensions ranging from roughly 5–100 nm. Experimental studies

revealed that nanoparticles can be selectively placed within films of specific block copolymer microdomains, as predicted theoretically.[78-82] This phenomenon can be well exemplified by the segregation of PS grafted gold particles to the center of PS domain in poly(styrene-*block*-vinyl pyridine) (PS-*b*-PVP) diblock copolymer.[80, 82-83] The associated microdomain swelling can induce morphological transitions, for example from lamellae to cylinders[71-72] in accordance with theoretical calculations.[83-84] Most of the above reported studies were focussed on relatively small nanoparticles (especially metallic nanoparticles) when compared to the block copolymer dimensions.

Very few studies report the mixing behaviour of grafted silica particles (having larger core diameters compared to previous studies) in block copolymer films. Bates et al.[62] reported the nature of dispersion of PS chains of varying molecular weights grafted on silica nanoparticles having a core diameter of 14 nm (on the basis of dynamic light scattering measurements) in poly(styrene-*block*-butadiene) (PS-*b*-PB) block copolymer as a function of overall molecular weight. They stated that the grafted nanoparticles with PS-*b*-PB diblock copolymers appear to be governed by two factors, the overall block copolymer molecular weight and the ratio of particle diameter to microdomain dimension. Increasing the overall block copolymer molecular weight, and reducing the particle graft molecular weight at constant particle size, the degree of dispersion was enhanced. Also, the grafted particles tend to occupy either domain of the block copolymer (shown in Figure 2.9).

Since most of these works were done in films, a part of the present work is dedicated to study the localisation behaviour of PMMA grafted silica particles in PS-*b*-PMMA block copolymer composites prepared by melt-mixing (discussed in Chapter 4.4).

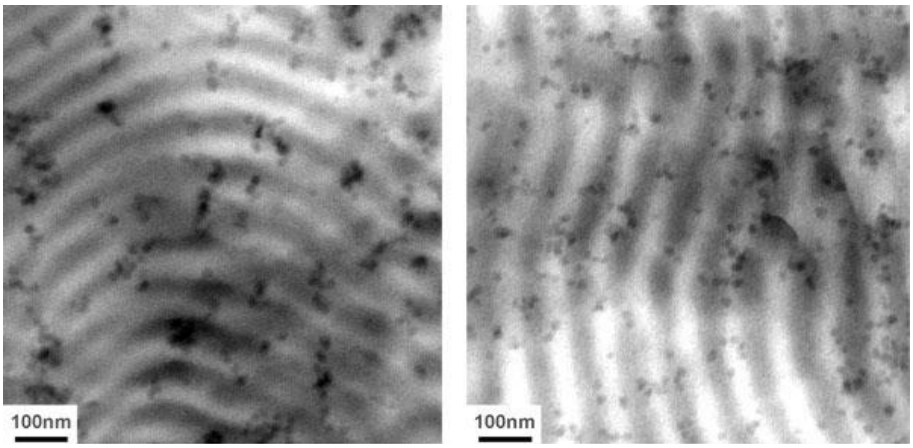

Figure 2.9. TEM images obtained from mixtures of Si-8 (left panel) and Si-16 (right panel) nanoparticles (1 vol % silica core; 8 and 16 correspond to graft molecular weights of polystyrene in kg/mol) blended with PS-PB-465 (465 stands for the molecular weight of matrix block copolymer in kg/mol). The specimens have been lightly stained with OsO_4 to reveal the underlying lamellar morphology without obscuring the particles. These images show that the particles are distributed in both the PS and PB domains.[62]

2.6. Mechanical properties of polymer composites with modified silica nanoparticles

A primary reason for adding inorganic nanofillers to (co)polymers is to improve their mechanical performance already at small loadings. One of the major requirements of polymer nanocomposites is to optimise the balance between the strength/stiffness and the toughness by keeping its inherent properties as much as possible.[85] Nanocomposites are usually evaluated by measuring several properties including tensile strength, impact strength, flexural strength, hardness, fracture toughness and so forth. Among these, Young's modulus, tensile strength, elongation at break and impact strength are the four main parameters that can vary with silica content. Surface modified silica NP's by suitable techniques mentioned above can improve their dispersion in (co) polymer matrices and thereby improving the compatibility inorder to achieve desired properties. These properties can vary with (co)polymers and silica

content. Even though there are numerous studies that have been carried out in polymer/silica composites, only some of the selective studies based on polymer-modified silica composites are described in the following paragraphs.

Zhang et al.[86] reported an improvement in mechanical properties and dispersion characteristics of polypropylene matrix by the addition of various polymer modified silica particles for a net silica content of 3.31 vol%. Shang and his co-workers[87] illustrated the influence of silica content on the mechanical properties of polyisoprene-silica hybrids prepared by sol-gel process. In that case, the hybrid films show a linear increase in Young's moduli (E) with silica content. Whereas, the tensile strength (σ_b) and elongation at break (ε_b) was increased up to 10 wt% loadings of unmodified silica and up to 20 wt% for those modified by suitable coupling agent.

Yang et al.[88] also reported that the mechanical properties such as impact strength, tensile strength, and elongation at break of polyamide 6-modified silica nanocomposites prepared by in situ polymerization also show a tendency to increase and then decrease with increasing silica content and have maximum values at 5 wt% silica content. Modified silica containing composites showed good dispersion and interfacial adhesion with the polymer matrix. Hong et al.[89] noticed an improvement in tensile, impact and impact properties of PMMA slices doped with modified silica particles. The properties of the PMMA composites were improved in the order of pristine < silane modified < PMMA modified silica particles. In general, some of the reported studies in silica filled epoxy composites show a dramatic improvement in tensile, impact and flexurial properties.[90-91]

Among the various commodity plastics, PMMA is one of the widely used thermoplastics and moreover the latter part of the research work is concentrated on how to improve the mechanical properties of PMMA composites. This is because of its excellent optical clarity, good weathering resistance, high tensile strength and tensile modulus. However, PMMA is brittle and notch

sensitive, which limits its applications. Therefore, by increasing its toughness while maintaining its inherent (good) properties like transparancy, the application field of PMMA can be widened.

The incorporation of rubber particles into the bulk of thermoplastic brittle polymers is a well known technique to improve the toughness of plastics,[92-95] for what high impact polystyrene (HIPS) is the most known example. Its application has been extended to PMMA matrix as well. The two general methods adopted for preparing rubber-toughened polymers are (a) interpenetrating polymer networks and (b) preformed spherical particles.

Usually, preformed mono-disperse modifier particles are prepared by emulsion polymerization. These spherical particles are added either directly to the acrylic monomer before polymerization or to molten low molecular weight PMMA using a screw extruder. The nature of particle dispersion in the matrix depends on the mixing conditions and on the chemical nature of the particle surface. An efficient toughening occurs through a sufficient stress transfer between the matrix and modifier phases. This can be achieved by a *core shell particle structure* (Figure 2.10).[95-96] Such a core-shell particle structure not only enables good adhesion to the matrix but also reduces particle agglomeration.

The *core-shell* particle structure can have both (a) an elastomeric shell between inner glassy core and an external shell or (b) an elastomeric core covered with an external shell. The external shell is made from macromolecules that are thermodynamically compatible with the matrix in the melt, grafted on to the rubbery domains of the particles. Usually, the glassy core is made up of glassy polymers. The strong polymer-polymer interaction resulting from the interpenetration and entanglement of the external shell with matrix ensures adequate adhesion. In order to regain the inherent optical clarity of PMMA matrix, the composition of core shell modifiers is usually chosen in such a way that they are having similar refractive index with that of PMMA. The rubber content, overall size of the core-shell modifier and the molecular weight of the outer shell also plays important role in dispersing particles. A significant improvement in tensile and impact

properties and fracture toughness was observed for PMMA matrices containing *core-shell* modifier particles.[95-97] Contrary to the composition of the above mentioned three layered *core-shell* structure, glassy polymeric core is substituted by silica nanoparticle in the present research work. More general, silica nanoparticles were coated with a diblock copolymer *double shell* having an elastomeric inner block. These particles were synthesized through well known ATRP. Chapter 4.5 of results and discussions is devoted to the study of the mechanical properties of PMMA matrix with these particles. More details will be discussed in this chapter.

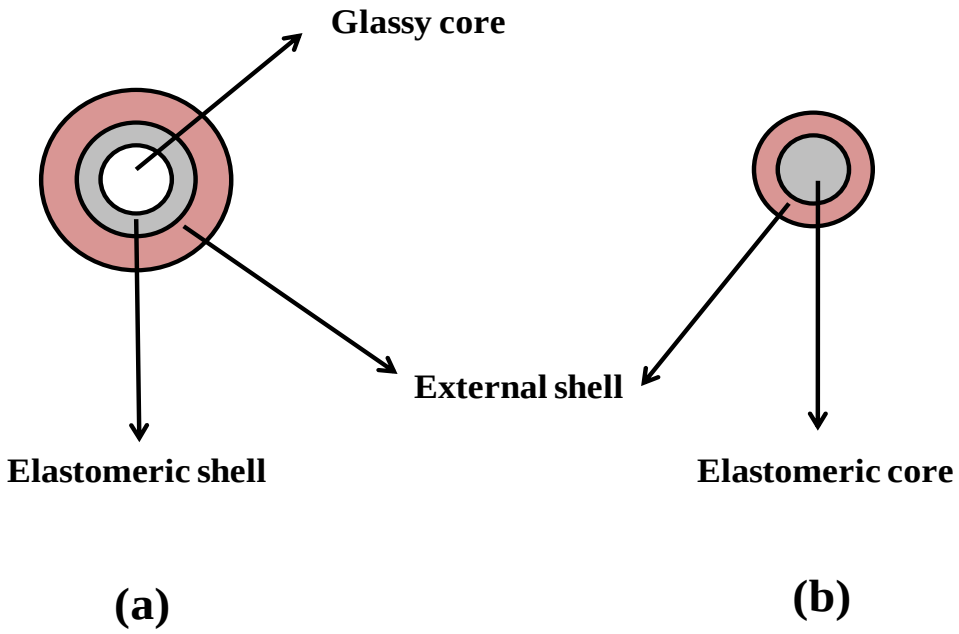

Figure 2.10. Core shell modifiers (a) three layered core-shell particle and (b) two layered core-shell particle[96]

2.7. Characterization of modified silica nanoparticles and their composites

Various spectroscopic techniques such as nuclear magnetic resonance (NMR), infrared (IR) and X-ray photoelectron (XPS) spectroscopy are widely used to characterise modified silica particles. High resolution solid-state NMR spectra can provide more information than that is

available from corresponding solution NMR spectra. For this, special techniques such as magic-angle spinning (MAS), cross polarization (CP) etc are required. Hence, solid state ^{29}Si and ^{13}C CP-MAS NMR spectroscopy are widely used to determine the nature of silica surface after silanization followed by immobilization of initiator layers, respectively.[98] The characteristic peaks for the initiator and polymer bound to the silica surface can be analyzed through diffuse reflectance infrared fourier transform (DRIFT) spectroscopy. This technique is sensitive and appropriate to determine the relatively low coverage of immobilized groups on the silica surface. The carbonyl absorption is particularly useful in the characterization of bonded phase.

Armes et al.[49] successfully analyzed the relative abundance of atomic species, including the presence of different oxidized states of atoms, presence of the grafted polymer layer and silica core by means of XPS.

Gravimetric techniques like thermogravimetric analysis (TGA) and differential scanning calorimetry (DSC) provide a bulk compositional property of the hybrid material. Matyjaszewski and his co-workers[99] used DSC to study the effect of tethering and chain mobilisation on the glass transition temperature of the polymer shell-polystyrene.

Dynamic light scattering (DLS) is also extensively used to study the stability of dispersion and size distribution of modified silica particles. Electrophoretic studies were also used as a tool to study the effect of grafted polyelectrolyte chains on the colloidal stability of silica particles. Armes et al.[49] combined DLS and aqueous electrophoresis to show the colloidal stability of polyelectrolyte-grafted silica particles. Harrak et al.[45] utilised small angle neutron scattering (SANS) to determine size and state of dispersion of modified and unmodified silica particles. Recently, Chevigny et al.[100] precisely characterized polystyrene grafted silica nanoparticles using SANS coupled with a neutron contrast variation method.The light scattering techniques helped to study the role of polymer brush in preventing aggregation of silica particles.

In the field of polymer nanocomposites, several studies reported that fourier transform infrared spectroscopy (FTIR) can also supply evidence of the existence of hydrogen bonding or covalent bonding between organic and inorganic phases in polymer/silica nanocomposites.[101-104]

Microscopic studies have been used to determine the size and nature of silica particles before and after each stage of modification. Techniques such as transmission electron microscopy (TEM), scanning electron microscopy (SEM), atomic force microscopy (AFM) and brewster angle microscopy (BAM) have proven to be useful. Analysis of high density PMMA brushes on silica particles using TEM and AFM techniques was successfully carried out by Fukuda et al.[52] The bright field TEM images of film of PMMA-silica core by dropping a suspension in toluene onto water surface showed the silica core as uniformly dispersed dark circles, while the PMMA chains formed fringes around the core. Sometimes the organic components of the sample would be decomposed by the electron beam; this can be avoided by using cryogenic microscopy (cryo-TEM), where the specimen is measured at liquid nitrogen or liquid helium temperatures in a frozen state. High resolution TEM (HRTEM) can afford a much closer look at the samples.[98]

The AFM images of the above mentioned films showed protrusions composed of a silica core and the polymer layer at uniform spacing on the substrate. The *in situ* information about the long-range structure of a silica particulate layer is given by BAM analysis. The above microscopic techniques are powerful tools to observe the morphology of homopolymer/block copolymer silica nanocomposites. The recent application of electron energy loss spectroscopy imaging techniques to TEM (ESI-TEM) can provide information on the composition of polymer surfaces. The internal nanomorphologies of thermoplastics such as vinyl polymer/silica nanocomposites were assessed using ESI.[105] In order to get a better picture of the nature of dispersion of graft particles in the corresponding matrix, quasi-elastic neutron scattering (QENS)

technique is adopted. Since QENS is primarily sensitive to the dynamics of the protons, the segmental dynamics of the graft and the matrix segments can be probed through the use of selective labelling.[76]

Small angle X-ray scattering (SAXS) in combination with TEM is a useful method to characterise the morphology of hybrid organic-inorganic materials. A combined investigation of both methods on thermoplastic nanocomposites such as copolymer of poly(methyl methacrylate) (PMMA) and 2-hydroxyethylmethacrylate (HEMA), poly(MMA-*co*-HEMA) filled with 10 nm silica particles with different surface coatings provided complete information about the complete morphology of the materials.[106] TEM analysis gave visible information on the extent of particle separation on the surface modification over a broad scale range including especially large sized aggregates. Macromolecular scale structure has been widely studied by SAXS in which the source for the scattering of X-rays is the heterogeneities in the sample.[98] SAXS analysis enabled acquisition of more detailed information about size distributions of primary particles and mean size aggregates in the real nanosize range below 20 nm. Wide angle X-ray diffraction (WAXD) was performed in order to analyse the degree of crystallinity in polypropylene-silica and polyurethane-silica nanocomposites.[107-108] The WAXD patterns showed that increasing silica content (5 wt%) induces the formation of crystals with the β-modification in polypropylene. Similarly, wide angle X-ray scattering (WAXS) is also used to investigate the changes in crystalline structure polyamide66-silica nanocomposites.[109-110]

2.8. References

1. Y. Wei. L. M. Fan, L. R. Chen, *Chromatoraphia*, 1997, 46, 637.
2. J. P. Mathew, M. Srinivasan, *Polym. Int*., 1992, 29, 179.
3. Y. Mizutani, S. Nago, *J. Appl. Polym. Sci*., 1999, 72, 1489.
4. K. L. Mittal, Ed. *Adhesion Aspects of Polymeric Coatings*, Plenum: New York, 1983.
5. R. Ranjan, "*Surface modification of silica nanoparticles*", Doctoral Thesis, 2008.

6. J. Chruściel, L. Ślusarski, *Mater. Sci*., 2003, 21, 461-469.
7. Y. Yu, W. Chen, *Mat. Chem. Phys*., 2003, 82, 388.
8. H. H. Huang, B. Orler, G. L. Wilkes, *Polym. Bull*., 1985, 14, 557.
9. H. Schmidt, *J. Non-Cryst. Solids*, 1985, 73, 681.
10. W. Stöber, A. Fink, E. Bohn, *J. Colloid Interface Sci*., 1968, 26, 62.
11. R. K. Iler, *The Chemistry of Silica*, Wiley, New York, 1979.
12. A. K. van Helden, J. W. Jansen, A. Vrij, *J. Colloid Interface Sci*., 1981, 81, 354.
13. F. Hatakeyyama, S. Kanzaki, *J. Am. Ceram. Soc*., 1990, 73, 2107.
14. A. van Blaaderen, A. Vrij, *J. Colloid Interface Sci*., 1993, 156, 1.
15. C. R. Silva, C. Airoldi, *J. Colloid Interface Sci*., 1997, 195, 381.
16. H. C. Kim, G. Dubois, *Dekker Encyclopedia of Nanoscience and Nanotechnology*; Taylor & Francis: New York, 2005, 1-10.
17. H. Zou, S. Wu, J. Shen, *Chem. Rev*., 2008, 108, 3893-3957.
18. R. Yin, R. M. Ottenbrite, *Polym. Prepr*., 1996, 36, 265.
19. K. Katagiri, K. Hasegawa, A. Matsuda, M. Tatsumisago, T. Minami, *J. Am. Ceram. Soc*., 1998, 81, 2501.
20. A. Matsuda, T. Sasaki, T. Tanaka, M. Tatsumisago, T. Minami, *J. Sol-Gel Sci. Tech*., 2002, 23, 247.
21. B. Zhao, W. Brittain, *J. Prog. Polym. Sci*., 2000, 25, 677.
22. G. F. Belder, G. ten Brinke, G. Hadziioannou, *Langmuir* 1997, 13, 4102.
23. P. Mansky, Y. Liu, E. Huang, T. P. Russell, C. Hawker, *Science* 1997, 275, 1458.
24. S. Yoshikawa, N. Tsubokawa, *Polym. J*. 1996, 28, 317.
25. Y. Lyatskaya, A. C. Balazs, *Macromolecules*, 1998, 31, 6676.
26. O. Pruker, J. Rühe, *Macromolecules*, 1998, 31, 592.
27. O. Pruker, J. Rühe, *Macromolecules*, 1998, 31, 602.
28. K. Matyjaszewski, T. P. Davis, Eds. *Handbook of Radical Polymerization*, Wiley: Hoboken, NJ, 2002.
29. B. Radhakrishnan, R. Ranjan, W.J. Brittain, *Soft Matter*, 2006, 2, 386-396.
30. C. J. Hawker, *J. Am. Chem. Soc*., 1994, 116, 1185.
31. K. Matyjaszewski ed., *Controlled Radical Polymerization*, American Chemical Society, Washington DC, 1997, 685.
32. J. S. Wang, K. Matyjaszewski, *J. Am .Chem. Soc*., 1995, 117, 5614.
33. M. Kato, M. Kamigaito, M. Sawamoto, T. Higashimura, *Macromolecules*, 1995, 28, 1721.
34. K. Matyjaszewski, J. Xia, *Chem. Rev*., 2001, 101, 2921-2990.
35. K. Matyjaszewski, B. Göbelt, H. J. Paik, C. P. Horwitz, *Macromolecules*, 2001, 34, 430.
36. A. K. Nanda, K. Matyjaszewski, *Macromolecules*, 2003, 36, 1487.

37. W. Tang, N. V. Tsarevsky, K. Matyjaszewski, *J. Am. Chem. Soc*., 2006, 128, 1598.
38. W. Tang, K. Matyjaszewski, *Macromolecules*, 2006, 39, 4953.
39. N. Cheng, O. Azzaroni, S. Moya, W. T. S. Huck, *Macromol. Rapid Commun*., 2006, 27, 1632.
40. R. Barbey, L. Lavanant, D. Paripovic, N. Schüwer, C. Sugnaux, S. Tugulu, H. A. Klok, *Chem. Rev*., 2009, 109, 5439-5452.
41. X. Y. Huang, M. Wirth, *J. Anal. Chem*., 1997, 69, 4577.
42. M. Ejaz, S. Yamamoto, K. Ohno, Y. Tsujii, T. Fukuda, *Macromolecules*, 1998, 31, 5934.
43. K. Matyjaszewski, P. J. Miller, N. Shukla, B. Immaraporn, A. Gelman, B. B. Luokala, T. M. Siclovan, G. Kickelbick, T. Vallant, H. Hoffmann, T. Pakula, *Macromolecules*, 1999, 32, 8716.
44. T. von Werne, T. E. Patten, *J. Am. Chem. Soc*., 1999, 121, 7409.
45. A. E. Harrak, G. Carrot, J. Oberdisse, C. Eychenne-Baron, F. Boué, *Macromolecules*, 2004, 37, 6376.
46. J. Pyun, S. Jia, T. Kowalewski, G. D. Patterson, K. Matyjaszewski, *Macromolecules*, 2003, 36, 5094.
47. X. S. Wang, S. F. Lascelles, R. A. Jackson, S. P. Armes, *Chem. Commun*.,1999, 18, 1817.
48. X. S. Wang, S. P. Armes, *Macromolecules* 2000, 33, 6640.
49. C. Perruchot, M. A. Khan, A. Kamitsi, S. P. Armes, T. von Werne, T.E. Patten, *Langmuir* 2001, 17, 4479.
50. X. Chen, D. P. Randall, C. Perruchot, J. F. Watts, T. E. Patten, T. von Werne, S. P. Armes, *J. Colloid Interface Sci.* 2003, 257, 56.
51. G. Carrot, S. Diamanti, M. Manuszak, B. Charleux, J. P. Vairon, *J. Polym. Sci., Part A: Polym. Chem*., 2001, 39, 4294.
52. K. Ohno, T. Morinaga, K. Koh, Y. Tsujii, T. Fukuda, *Macromolecules*, 2005, 38, 2137.
53. H. Boettcher, M. L. Hallensleben, S. Nub, H. Wurm, *Polym. Bull., (Berlin)* 2000, 44, 223.
54. H. Mori, D. C. Seng, M. Zhang, A. H. E. Müller, *Langmuir* 2002, *18*, 3682.
55. K. Matyjaszewski, *ACS Symp. Ser.* 1998, 685, 2.
56. J. L. Wang, T. Grimaud, K. Matyjaszewski, *Macromolecules*, 1997, 30, 6507.
57. V. Percec, B. Barboiu, A. Neumann, Ronda, *Macromolecules*, 1996, 29, 3665.
58. A. T. Levy, M. M. Olmstead, T. E. Patten, *Inorg. Chem*., 2000, 39, 1628.
59. W. Tang, A. K. Nanda, K. Matyjaszewski, *Macromol. Chem. Phys*., 2005, 206.
60. S. E. Harton, S. K. Kumar, *J. Polym. Sci., Part B: Polym. Phys.*, 2008, 46, 351–358.
61. M. K. Corbierre, N. S. Cameron, M. Sutton, K. Laaziri, R. B. Lennox, *Langmuir*, 2005, 21, 6063–6072.
62. Q. Lan, L. F. Francis, F. S. Bates, *J. Polym. Sci., Part B: Polym. Phys*., 2007, 45, 2284–2299.
63. E. Glogowski, R. Tangirala, T. P. Russell, T. Emrick, *J. Polym. Sci., Part A: Polym. Chem*., 2006, 44, 5076–5086.

64. R. Krishnamoorti, *MRS Bull*., 2007, 32, 341–347.
65. V. Causin, B. X. Yang, C. Marega, S. H. Goh, A. Marigo, *J. Nanosci. Nanotechnol*., 2008, 8, 1790–1796.
66. I. Borukhov, L. Leibler, *Macromolecules*, 2002, 35, 5171.
67. C. M. Wijmans, E. B. Zhulina, G. J. Fleer, *Macromolecules*, 1994, 27, 3238.
68. A. P. Gast, L. Leibler, *J. Phys. Chem*., 1985, 89, 3947.
69. P. Akcora, H. Liu, S. K. Kumar, J. Moll, Y. Li, B. C. Benicewicz, L. S. Schadler, D. Acehan, A. Z. Panagiotopoulos, V. Pryamitsyn, V. Ganesan, J. Ilavsky, P. Thiyagarajan, R. H. Colby, J. F. Douglas, *Nat. Mater*., 2009, 8, 354–359.
70. R. L. Jones, S. K. Kumar, D. L. Ho, R. M. Briber, T. P. Russell, *Nature*, 1999, 400, 146–149.
71. K. Shin, S. Obukhov, J. T. Chen, J. Huh, Y. Hwang, S. Mok, P. Dobriyal, P. Thiyagarajan, T. P. Russell, *Nat. Mater*., 2007, 6, 961–965.
72. A. Bansal, H. Yang, C. Li, K. Cho, B. C. Benicewicz, S. K. Kumar, L. S. Schadler, *Nat. Mater*., 2005, 4, 693–698.
73. K. Chrissopoulou, S. H. Anastasiadis, E. P. Giannelis, B.J. Frick, *Chem. Phys*., 2007, 127, 144910.
74. P. Rittigstein, R. D. Priestley, L. J. Broadbelt, J. M. Torkelson, *Nat. Mater*., 2007, 6, 278–282.
75. S. E. Harton, S. K. Kumar, H. Yang, T. Koga, K. Hicks, H. Lee, Y. Mijovic, M. Liu, R. S. Vallery, D. W. Gidley, *Macromolecules*, 2010, 43, 3415–3421.
76. P. Akcora, S. K. Kumar, V. G. Sakai, Y. Li, B. C. Benicewicz, L.S. Schadler, *Macromolecules*, 2010, 43, 8275-8281.
77. F. S. Bates, G. H. Fredrickson, *Ann. Rev. Phys. Chem*., 1990, 41, 525.
78. M. R. Bockstaller, E. L. Thomas, *Phys. Rev. Lett*., 2004, 93, 166106.
79. M. R. Bockstaller, Y. Lapetnikov, S. Margel, E. L. Thomas, *J. Am. Chem. Soc*., 2003, 125, 5276.
80. J. J. Chiu, B. J. Kim, E. J. Kramer, D. J. Pine, *J. Am. Chem. Soc*., 2005, 127, 5036.
81. S. Yeh, K. Wei, *Macromolecules*, 2003, 36, 7903.
82. B. J. Kim, J. Bang, C. J. Haeker, E. J. Kramer, *Macromolecules*, 2006, 39, 4108.
83. B. J. Kim, J. J. Chiu, G. Yi, D. J. Pine, E. J. Kramer, *Adv. Mater*., 2005, 17, 2618.
84. M. R. Bockstaller, R. A. Mickiewicz, E. L. Thomas, *Adv. Mater*., 2005, 17, 1331.
85. R. Lach, G. M. Kim, G. H. Michler, W. Grellmann, K. Albrecht, *Macromol. Mater. Eng.* 2006, 291, 263.
86. M. Z. Rong, M. Q. Zhang, Y. X. Zheng, H. M. Zeng, R. Walter, K. Friedrich, *Polymer*, 2001, 42, 167.
87. X. Y. Shang, Z. K. Zhu, J. Yin, X. D. Ma, *Chem. Mater*., 2002, 14, 71.
88. F. Yang, Y. C. Ou, Z. Z. Yu, *J. Appl. Polym. Sci*., 1998, 69, 355.
89. R. Y. Hong, H.P. Fu, Y. J. Zhang, L. Liu, J. Wang, H. Z. Li, Y. Zheng, *J. Appl. Polym. Sci*., 2007, 105, 2176-2184.

90. P. Rosso, L. Ye, K. Friedrich, S. Sprenger, *J. Appl. Polym. Sci*., 2006, 100, 1849.
91. G. Ragosta, M. Abbate, P. Musto, G. Scarinzi, L. Mascia, *Polymer*, 2005, 46, 10506.
92. C. B. Bucknall, *Toughened Plastics*, Appl. Sci. Pub., London, 1977.
93. C. K. Riew, ed., *Rubber-Toughened Plastics*, Advances in Chemistry Series 222, ACS, Washington, D.C.
94. C. J. Hooley, D. R. Moore, M. Whale, *Plastics Rubb. Proc. Appl*., 1981, 1, 381.
95. C. Wrottecki, P. Heim, P. Gaillard, *Polym. Eng. Sci*., 1991, 31, 213-217.
96. Y. G. Suu, "*Studies on Mechanical Properties of Poly(methyl methacrylate) and Poly(methyl methacrylate)-Modified Natural Rubber Blend*", Master Thesis, 2008.
97. C. Wrottecki, P. Heim, P. Gaillard, *Polym. Eng. Sci*., 1991, 31, 218-222.
98. G. Kickelbick, In *Hybrid Materials. Synthesis, Characterization, and Applications*; Ed. Wiley-VCH: Weinheim, Germany, 2007.
99. D. A. Savin, J. Pyun, G. D. Patterson, T. Kowalewski, K. Matyjaszewski, *J. Polym. Sci. Part B: Polym. Phys*., 2002, 40, 2667.
100. C. Chevigny, D. Gigmes, D. Bertin, J. Jestin, F. Boúe, *Soft Matter*, 2009, 5, 3741-3753.
101. W. Zhou, J. H. Dong, K. Y. Qiu, Y. Wei, *J. Polym. Sci., Part A: Polym. Chem*., 1998, 36, 1607.
102. S. L. Huang, W. K. Chin, W. P. Yang, *Polymer*, 2005, 46, 1865.
103. J. Jang, H. Park, *J. Appl. Polym. Sci*., 2002, 83, 1817.
104. S. M. Lai, C. K. Wang, H. F. Shen, *J. Appl. Polym. Sci*., 2005, 97, 1316.
105. J. I. Amalvy, M. J. Percy, S. P. Armes, C. A. P. Leite, F. Galembeck, *Langmuir*, 2005, 21, 1175.
106. C. Becker, B. Kutsch, H. Krug, H. Kaddami, *J. Sol-Gel. Sci. Technol*., 1998, 13, 499.
107. S. Jain, H. Goossens, M. van Duin, P. Lemstra, *Polymer* 2005, 46, 8805.
108. Z. S. Petrovic´, I. Javni, A. Waddon, G. Ba´nhegyi, *J. Appl. Polym. Sci.* 2000, 76, 133.
109. R. Sengupta, A. Bandyopadhyay, S. Sabharwal, T. K. Chaki, A. K. Bhowmick, *Polymer* 2005, 46, 3343.
110. R. Sengupta, S. Sabharwal, A. Bhowmick, A. K. Bhowmick, *Polym. Degrad. Stab*. 2006, 91, 1311.

Chapter 3. Experimental

3.1. Materials

Silica suspensions (Ludox-HS and Ludox-TM) were provided by Sigma-Aldrich Chemicals and used as received. Both of these suspensions consisted of 40 wt % of colloidal silica nanoparticles in water. According to the distributor, Ludox-HS dispersion of silica nanoparticles shows an average diameter of 12 nm (specific area = 220 ± 30 m^2/g, denoted by Si_{12}) and 20 nm in the case of Ludox-TM (surface area = 140 ± 30 m^2/g, denoted by Si_{20}) dispersion. Surface silanol group densities present on Si_{12} and Si_{20} nanoparticles are 4.7 OH groups/nm^2 and 4.5 groups/nm^2, respectively, as determined by thermogravimetric analysis (TGA). Dynamic light scattering measurements (DLS) show that Si_{12} and Si_{20} particles exhibit a size distribution of 14 ± 3 nm and 22 ± 4 nm respectively.

Homopolymer, poly(methyl methacrylate) (Plexiglas 6N glassklar provided by Evonik industries) having a number average molecular weight (M_n) of 49 kg/mol and a polydispersity of 1.8 was used for composite preparation.

The block copolymer poly(styrene-*block*-methyl methacrylate) (PS-*b*-PMMA) having lamellar (denoted as SM_L) and cylindrical (denoted as SM_C) morphologies used for composite preparation were synthesized by sequential anionic polymerization and provided by the Polymer Synthesis Department, HZG, Geesthacht. Size exclusion chromatography showed a number average molar mass of 148 kg/mol with a total PS molar fraction of 0.51 and polydispersity (M_w/M_n) of 1.07 for SM_L. Whereas SM_C showed a molar mass of 158 kg/mol and polydispersity (M_w/M_n) 1.08 with a total PS molar fraction of 0.69.

(3-glycidoxylpropyl)trimethoxysilane(GPS, >98%), triethylamine(Et_3N, >99%), *N*-methylmorpholine (>99.5%), dimethylaminopyridine (DMAP,≥99%), 2-bromoisobutyrylbromide (2-BriB), 98%), ethyl-2-bromoisobutyrate (2-EBriB, 98%), *N*,*N*,*N'*,*N'*,*N''*-pentamethyldiethylenetriamine (PMDETA, 97%), tetrahydrofuran (THF), toluene, acetone (≥ 99.5%), methanol, chloroform ($CHCl_3$, ≥ 99%), copper(I) bromide (CuBr, 99.99%, stored under vacuum), copper(II) bromide ($CuBr_2$, 99.8%, stored under vacuum), hydrofluoric acid (HF, 48 wt %) and aliquot-336 (*N*-methyl-*N*,*N*-dioctyloctan-1-ammonium chloride, 98%) were all used as received.

Monomers used for polymerization were styrene (St, ≥ 99.8%), *n*-butyl methacrylate (*n*-BMA, ≥ 99.5%) and methyl methacrylate (MMA, ≥ 99.9%). They were purified by first passing through an alumina column followed by drying over calcium hydride (CaH_2) and further distillation. All the chemicals were purchased from Sigma-Aldrich.

3.2. Surface functionalization of silica nanoparticles

3.2.1. Anchoring of epoxysilane coupling agent on silica and concurrent ring-opening of the epoxy groups.

The silica suspension (12 g of the 40 wt % SiO_2 suspension in water) was added to a round bottom flask with a magnetic stir bar fitted with a reflux condenser. (3-glycidoxypropyl)trimethoxysilane (GPS) (20 ml, 0.09 mol) was added. The system was diluted with deionised water in order to reach a concentration of silica in the whole reaction media not greater than 0.2 g/mL while maintaining the total pH at 11 by the addition of NaOH solution, and it was then sonicated (bath sonicator, Elma S3OH, Elmasonic, *f*=25 kHz) for 5 min. The reaction mixture was then refluxed for concurrent silanol condensation and epoxy hydrolysis leading to

diol functionalized nanoparticles (reaction scheme is shown in Figure 3.1). The reaction period was varied from 8 h to 36 h. The reaction mixture was then cooled down to room temperature. The clear dispersion was then added to methanol in order to precipitate colloids. The excess of GPS present in the solution was removed by centrifuging (Sigma Laborzentrifugen 3K15) four to five times for a period of 15 min at 11,000 rpm. The silica particles were redispersed in methanol after each washing step and sonicated for 5-7 min. Further details of characterization are detailed in Chapter 4.1 of Results and Discussions. The GPS grafted silica particles are denoted as Si_xG^y, where subscript *x* stands for average particle diameter in nm and superscript *y* for weight fraction (%) of coupled silane measured from thermogravimetric analysis (TGA).

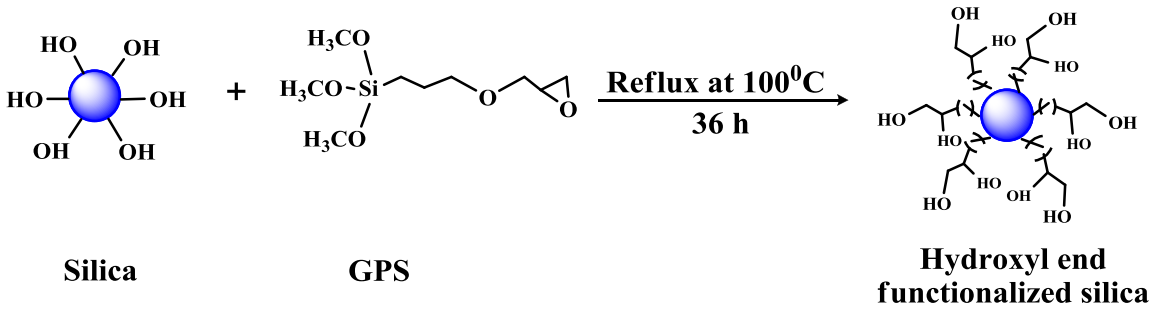

Figure 3.1. Reaction scheme for the silanization of silica nanoparticles

3.2.2. Grafting of ATRP initiator onto the diol functionalized nanoparticles

The solvent of the methanol dispersion of silane modified silica was exchanged with THF without passing through the dry state. The remaining methanol was removed by centrifuging the dispersion in THF at least four to five times. The dispersion was then charged into a bi-necked round bottom flask with a magnetic stir bar. The amount of THF in the final solution was

adjusted to have a concentration of silanized silica not greater than 0.065 g/ml and it was sonicated for 5 min. Then, the flask was purged with nitrogen followed by the addition of triethylamine (0.047 mol, 6.5 mL) and kept stirring for 30 min. As an alternative to triethylamine, the reaction was also carried out with the weak base *N*-methylmorpholine (0.058 mol, 6.4 mL) for both systems in the presence of a catalytic amount of DMAP (0.004 mol, 0.443g). 2-Bromoisobutyryl bromide (0.028 mol, 3.5 mL) was then added drop wise at 0°C (water/ice bath). The bromination reaction was also carried out in solvent toluene under the same conditions described above but in the absence of DMAP (reaction scheme is shown in Figure 3.2). The details are shown in Table 4.1.2 of Chapter 4.1 in results and discussions. When the addition of the initiator was completed, the reaction system was slowly heated up to room temperature and kept stirring for 48 h.

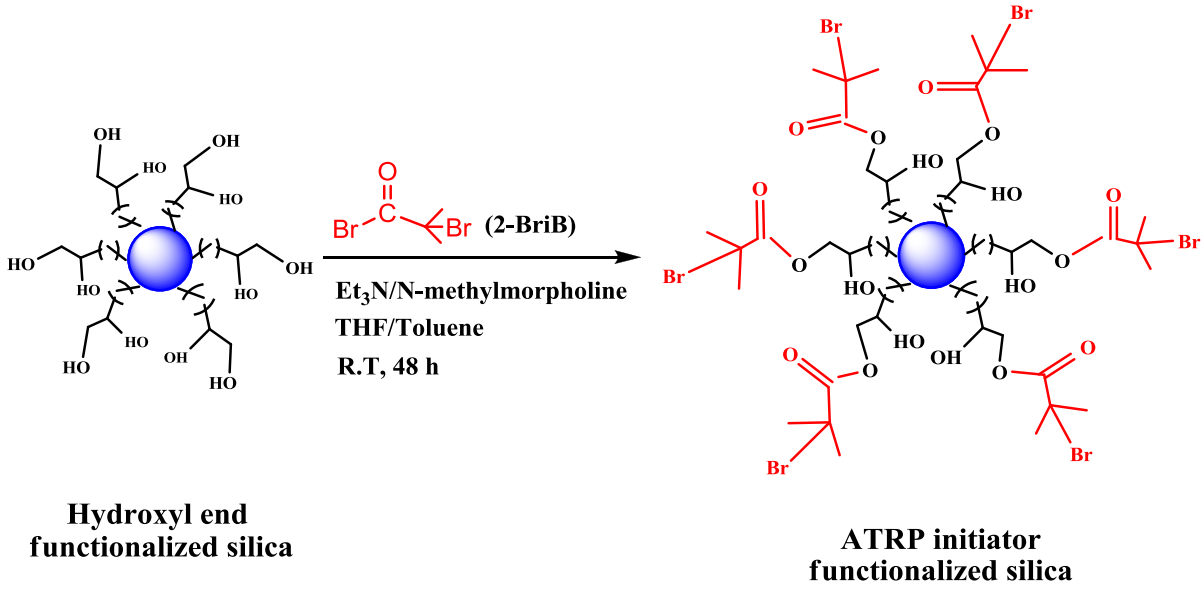

Figure 3.2. Reaction scheme for grafting ATRP initiator onto silanized silica nanoparticles

After reaction, the colloids were precipitated by adding drop wise to a methanol/H_2O mixture (3:1 vol). The initiator-grafted silica particles were recovered by washing and centrifugation (six

to seven times) with methanol. The recovered particles were dried under vacuum at 60 °C for 48 h. The brominated particles are denoted as Si_xBr^y. The subscript *x* stands for average particle diameter in nm and superscript *y* for bromide concentration of grafted ATRP inititator in mmol/g measured from TGA.

3.3. "*Grafting from*" atom transfer radical polymerization (ATRP) from functionalized silica particles

3.3.1. Synthesis of polystyrene grafted silica (Si_x-*g*-PS, *single core-shell*) particles

Silica colloidal initiators (500.0 mg, 0.2 mmol of ATRP initiator), Cu(I)Br (0.028 g, 0.2 mmol) and Cu(II)Br_2 (0.003 g; 0.013 mmol) were added to the reaction flask. Styrene (11.5 mL, 0.1 mol) (bubbled with nitrogen before use) was added to the flask. The system was purged with nitrogen and finally PMDETA (42 µL, 0.2 mmol) was added. The reaction flask was then placed in an oil bath at 90 °C. Samples were taken periodically for kinetic analysis of the polymerization. After reaction, samples were diluted with tetrahydrofuran and centrifuged two to three times to remove free polymer and precipitated into 500 mL of 3:1 ratio of methanol and water. After filtration, the precipitated polymer was dried in a vacuum oven at 40 °C for 48 h. The polymer for GPC analysis was degrafted from silica using hydrofluoric acid and aliquot 336 (phase transfer catalyst) and then precipitated into methanol (reaction scheme is shown in Figure 3.3). The grafted particles are denoted by $Si_xPS_y^a$, where the subscripts *x* and *y* for average particle diameter in nm and weight fraction of grafted polystyrene (PS) in % measured from TGA and superscript *a* represents the graft molecular weight of PS in kg/mol.

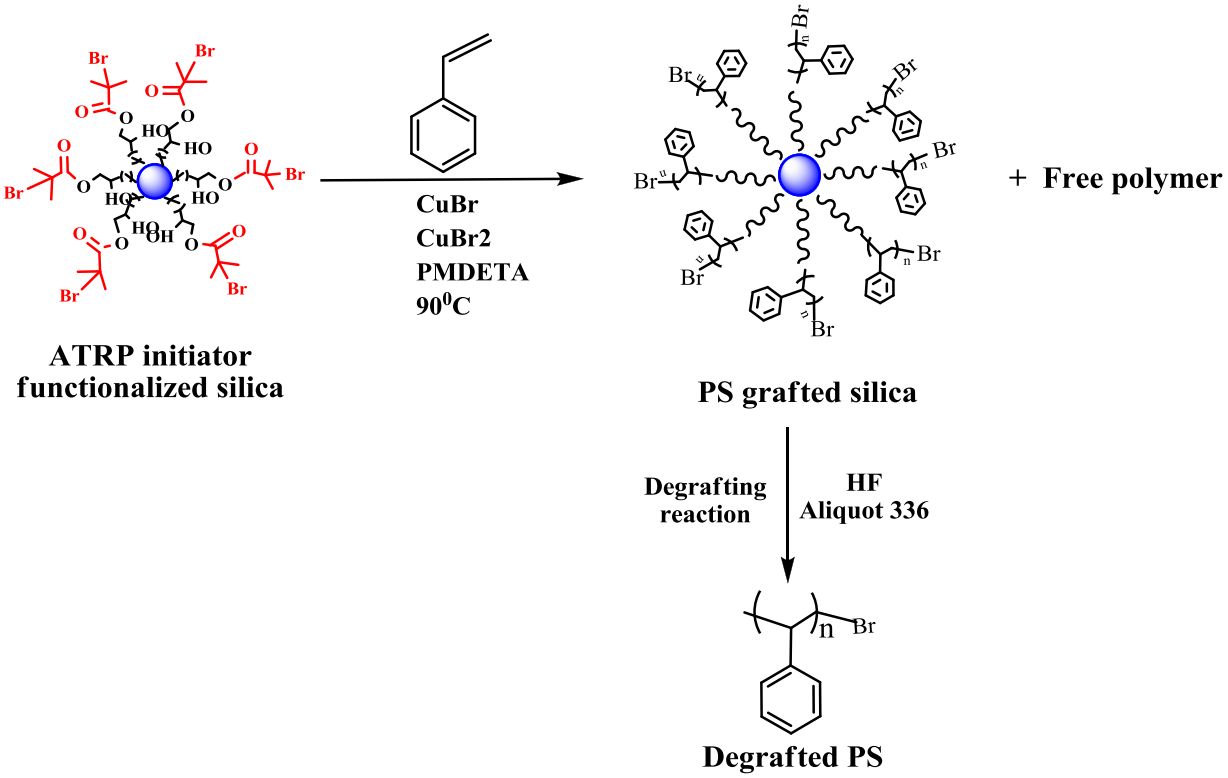

Figure 3.3. Reaction scheme for grafting polystyrene from initiator functionalized silica nanoparticles

3.3.2. Synthesis of PMMA grafted silica (Si_x-*g*-PMMA, *single core-shell*) particles

Silica colloidal initiators (500.0 mg, 0.2 mmol) and Cu(I)Br (0.023g, 0.16 mmol) were added to the reaction flask. Methyl methacrylate (10.7 mL, 0.1 mol) (bubbled with nitrogen before use) was then added via syringe. After this, the system was purged with nitrogen. Ethyl-2-bromoisobutyrate (1.8 µL, 0.012 mmol) and finally PMDETA (33 µL, 0.16 mmol) were added to the flask. The reaction flask was then placed in a previously heated oil bath at 70 °C. Samples were taken periodically for kinetic analysis of the polymerization.

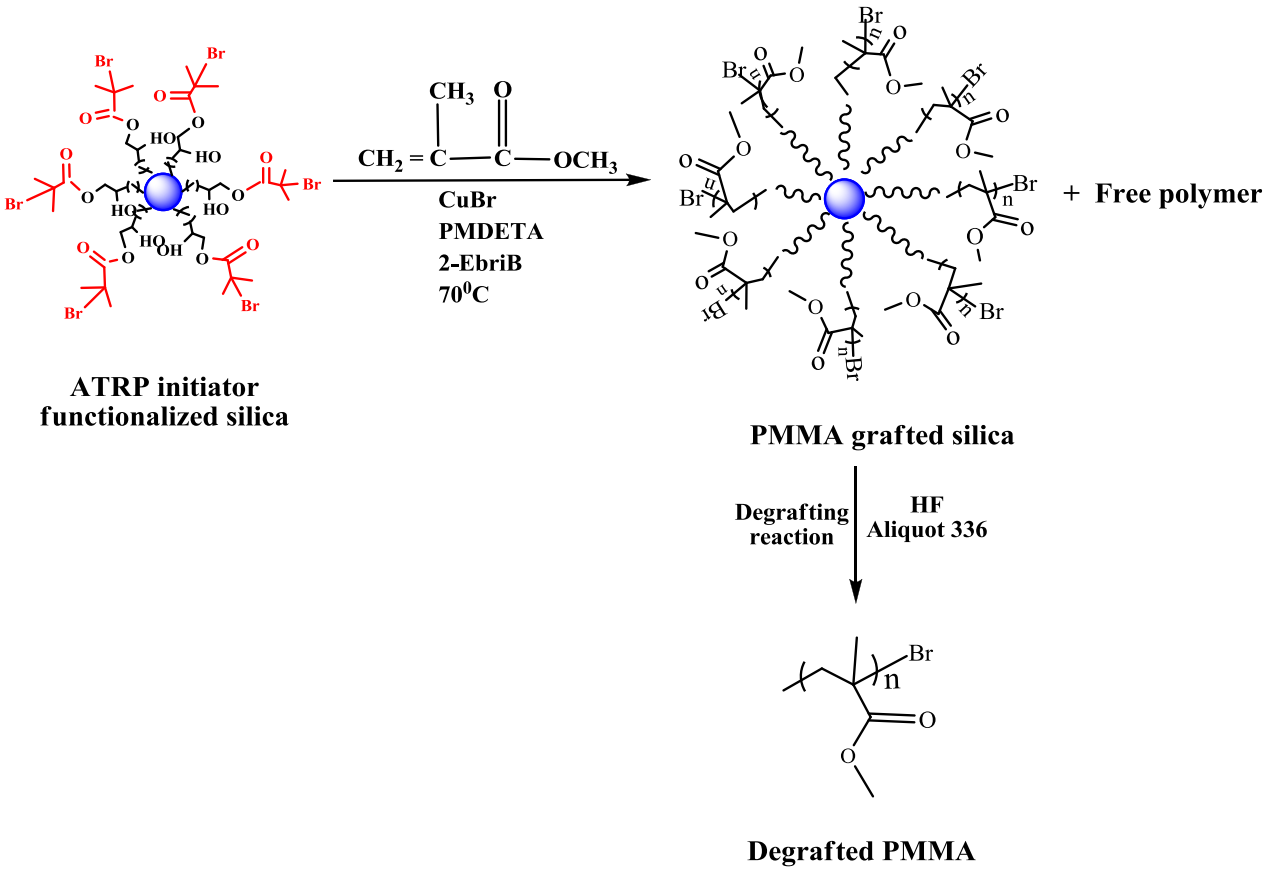

Figure 3.4. Reaction scheme for grafting PMMA from initiator functionalized silica nanoparticles.

After reaction, samples were diluted with tetrahydrofuran and centrifuged two to three times to remove free polymer and precipitated into 500 mL of 3:1 ratio of methanol and water. After filtration, the precipitated polymer was dried in a vacuum oven at 40 °C for 48 h. The polymer sample for GPC analysis was degrafted using the same procedure as mentioned for styrene polymerization (reaction scheme is shown in Figure 3.4). The grafted particles are denoted by $Si_xM_y^b$, where the subscripts *x* and *y* stands for average particle diameter in nm and weight percentage of grafted poly(methyl methacrylate) (M)and superscript *b* for the graft molecular weight in kg/mol.

3.3.3. Synthesis of PBMA grafted silica (Si_x-*g*-(PBMA)-Br, *macroinitiator*) particles

Silica colloidal initiators (500.0 mg, 0.16 mmol of ATRP initiator), Cu(I)Br (0.022 g, 0.16 mmol) were added to a round bottom flask and degassed and back-filled with nitrogen. Deoxygenated acetone (6 mL) was added to the flask followed by *n*-BMA (5.6 mL, 0.04 mol) under nitrogen atmosphere. The solution was magnetically stirred in order to disperse the colloidal initiator. Finally the ligand, PMDETA (33 µL, 0.16 mmol) was added. The reaction mixture was placed in a previously heated oil bath at 50 °C (reaction scheme is shown in Figure 3.5).

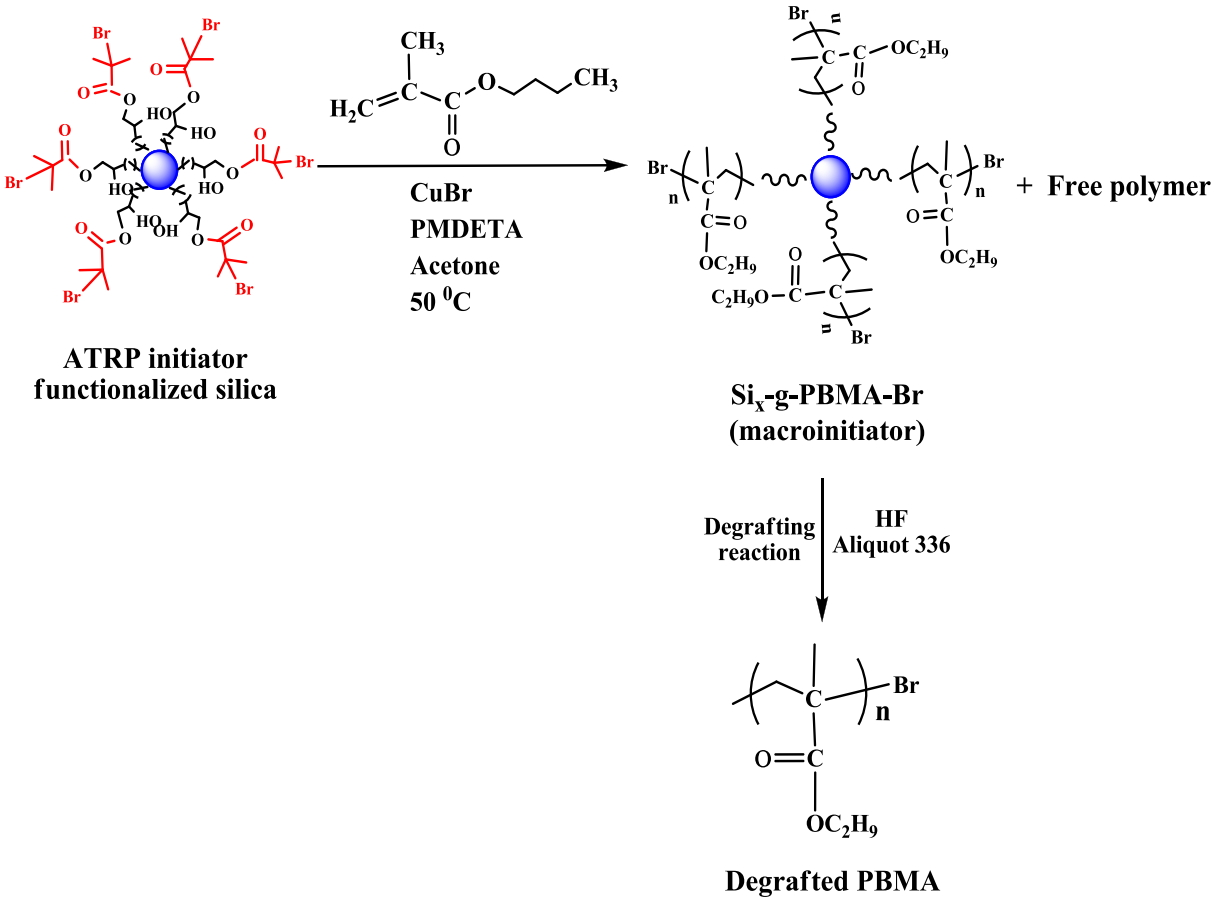

Figure 3.5. Reaction scheme for grafting PBMA macroinitiator from functionalized silica nanoparticles

After reaction, the reaction mixture was dissolved in THF and centrifuged to remove free polymer and precipitated in 6:1 ratio of methanol and water, filtered and dried at 40 ^{o}C for 48 h. The resultant grafted polymer was cleaved from silica after treatment with HF and aliquot 336 for GPC analysis. The grafted particles are denoted by $Si_xPBMA_y^c$, where subscripts *x* and *y* for average particle diameter in nm and weight fraction of grafted PBMA in % and superscript *c* presents the graft molecular weight in kg/mol.

3.3.4. Synthesis of (PBMA-*b*-PMMA) grafted silica (Si_x-*g*-(PBMA-*b*-PMMA), *silica core-double shell*) particles

Si_{12}-*g*-(PBMA)Br hybrid nanoparticles (500 mg, 0.05 mmol), Cu((I)Br (0.0072 g, 0.05 mmol) were added to a round bottom flask. It was degassed and backfilled with nitrogen. MMA (6 mL, 0.056 mol) was added to the flask under nitrogen atmosphere with stirring. PMDETA (10.4 μL, 0.05 mmol) was added to the reaction flask and then transferred to a previously heated (85 °C) oil bath (reaction scheme is shown in Figure 3.6). After reaction, the reaction mixture was precipitated in 4:1 ratio of methanol and water, filtered and dried. The resultant grafted block copolymer was cleaved from silica after treatment with HF for GPC analysis. The grafted particles are denoted by Si_x(PBMA-*b*-PMMA)$_y^d$, where subscripts *x* and *y* stands for average particle diameter in nm and weight fraction of grafted block copolymer (PBMA-*b*-PMMA) in % measured from TGA and superscript *d* presents the grafted molecular weight in kg/mol.

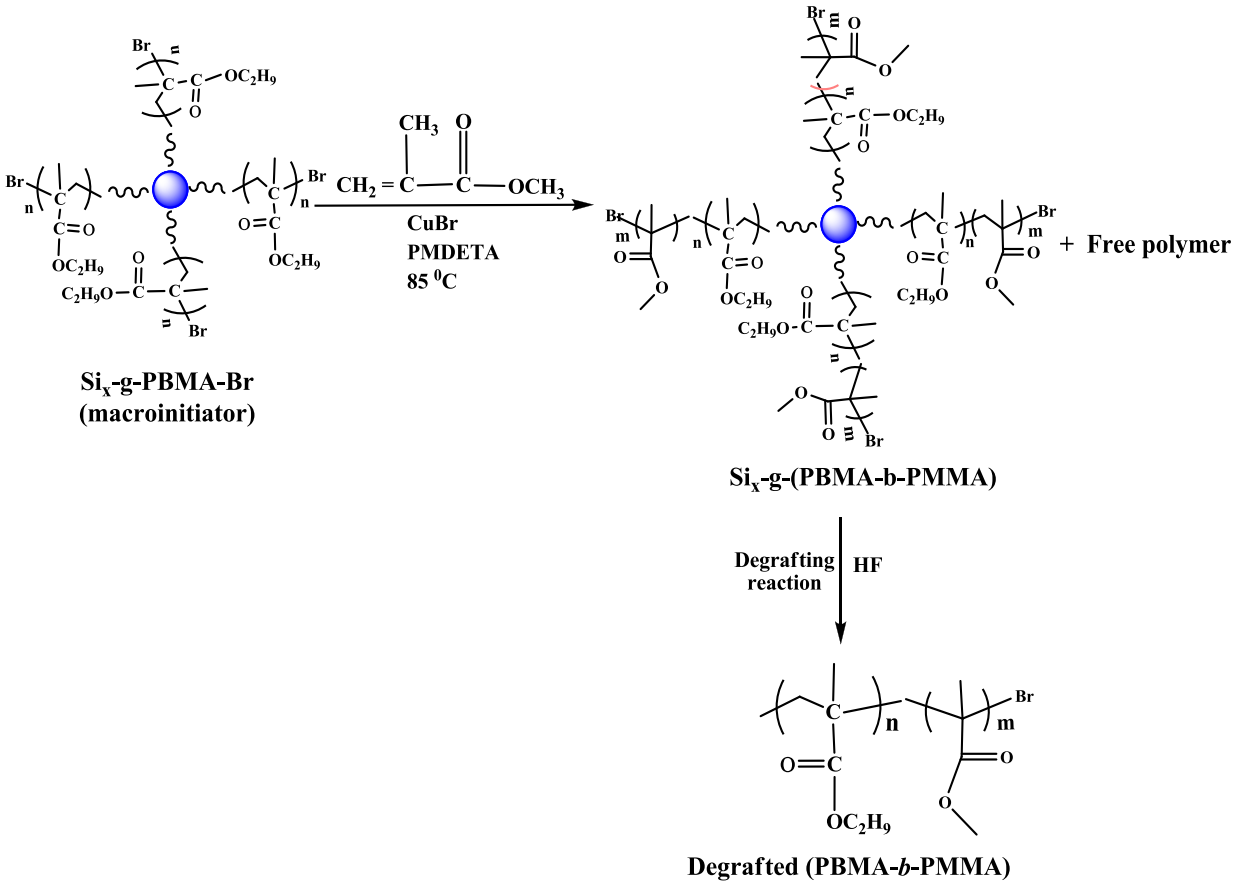

Figure 3.6. Reaction scheme for grafting Si$_x$-*g*-(PBMA-*b*-PMMA) from functionalized silica nanoparticles

3.4. Preparation of homopolymer/block copolymer-modified silica nanocomposites

The general strategy of nanocomposite preparation involves the quantitative addition of modified/unmodified silica nanoparticles in a homopolymer/block copolymer matrix film (prepared by solvent casting) followed by the melt-mixing of composite films and injection moulded into respective specimens for mechanical analysis. General procedure for preparing the composites is shown in Figure 3.7.

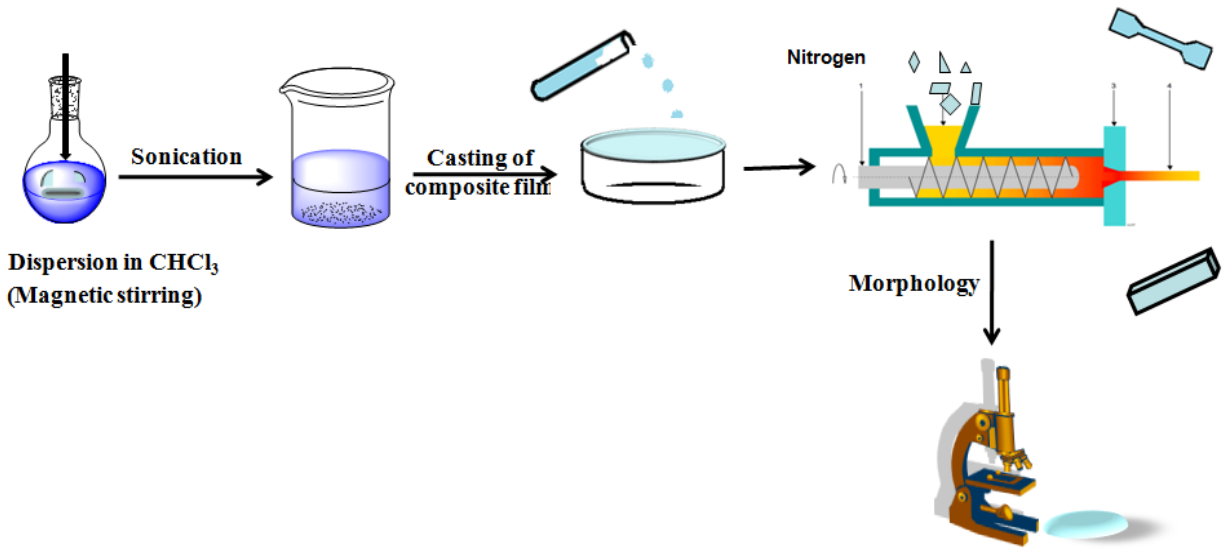

Figure 3.7. General procedure for preparing homopolymer or block copolymer composites for mechanical and morphological characterization

Homopolymer/block copolymer was dissolved in solvent chloroform, to which desired amount of *single shell* or *double shell* grafted silica particles were added and magnetically stirred for 48 h and then sonicated (ELMA S3OH, Elmasonic , f = 25 kHz) for 15 min. The dispersion was then cast on Teflon® supports and kept drying for few days at ambient temperature. The resultant film was dried in an oven under vacuum at room temperature for 24 h followed by heating under vacuum for not less than one and a half week. The small stripes of the above composite films were compounded in a miniextruder (Micro 15cc Twin Screw Compounder, DSM Xplore Netherlands) at 210 °C under nitrogen atmosphere for a period of 20 min and extruded into respective specimens for mechanical characterization.

3.5. Characterization Techniques

3.5.1. Size Exclusion Chromatography (SEC)

SEC measurements were performed using a Waters instrument. The instrument is equipped with four PSS columns with a porosity range from 102 to 105 Å coupled with a differential refractometer (Waters TM 2410 RI) and a UV detector (Waters TM 486, at 254 nm). The samples were dissolved in THF (2 % wt/v) and measured at 28 °C with a flow rate of 1 ml/min using toluene as internal standard. The results were calibrated against polystyrene standards (for degrafted PS samples) and PMMA standards (for degrafted PMMA, PBMA and PBMA-*b*-PMMA samples).

3.5.2. Elemental Analysis

The content of bromine atoms was determined after anchoring of the initiator groups on the surface of the Si_{12} and Si_{20} particles (Chapter 4.1). Percentage content of carbon and hydrogen atoms was also determined. For this, the modified silica nanoparticles were combusted and the oxidized gases produced were reduced and analysed by gas chromatography. The bromine content was determined by potentiometric titration.

3.5.3. Attenuated total reflection-fourier transform infrared spectroscopy (ATR-FTIR)

The samples were powdered well and ATR-FTIR characterization was carried out on Bruker Equinox 55 with 32 scans at a spectral resolution of 1 cm^{-1} under nitrogen atmosphere using a ZnSe ATR crystal set at 45°. The resulting single-beam spectra ranged from 400 - 4000 cm^{-1}.

3.5.4. Nuclear Magnetic Resonance Spectroscopy (NMR)

^{1}H nuclear magnetic resonance spectroscopy (^{1}H-NMR) of polymer grafted samples was measured using the solvent peak as a reference. The modified particles were dispersed in $CDCl_3$ and sonicated (ELMA S3OH, Elmasonic, *f*=25 kHz) before measurements. The ^{1}H-NMR, solid state cross polarised/magic angle spinning (CP/MAS) ^{13}C, and ^{29}Si NMR spectra were carried out on a Bruker AV-300 FT-NMR spectrometer at 300 MHz.

3.5.5. Thermogavimetric analysis (TGA)

Thermal gravimetric analysis (TGA) measurements were carried out on a Netzsch TG209 F1 Iris. The experiments were conducted under a constant Nitrogen flow (20ml/min), from 25 °C to 900 °C, at a constant rate of 20 °C/min.

3.5.6. Differential Scanning Calorimetry (DSC)

Differential scanning calorimetry (DSC) experiments were performed using a Netzsch DSC Phoenix. The equipment was calibrated using indium and cyclohexane. Standard aluminum pans of 50 µl were used to encapsulate the samples of 10 mg ± 1 mg. Dynamic heating and cooling scans were performed. The samples were first heated to180 °C, held for 3 min, cooled down to 25 °C, held for another 3 min, and finally heated to 180 °C. All the measurements were done under N_2 atmosphere at a constant rate of 10 °C/min.

3.5.7. Transmission Electron Microscopy (TEM)

The TEM experiments were done using a FEI Tecnai G2 F20 operated at 200 kV. The modified silica nanoparticles were dispersed in $CHCl_3$ (15 mg in 4 mL) for 24 hours at ambient temperature. After 24 hours, the dispersion were homogenised by sonication (ELMA S3OH, Elmasonic, *f* = 25 kHz) for 1 min and one drop (~5 µl) was placed on a carbon coated copper

grid. The resultant thin film was analysed to see the mode of dispersion of modified particles. The morphology of homopolymer/block copolymer silica nanocomposites were obtained by analysing ultra thin sections of these samples made using a Reichert-Jung Ultracut E microtome equipped with a diamond knife. Contrast between the microphases of the block copolymer was achieved by exposing the nanocomposites to RuO_4 vapour for approximately 1 min. The TEM analyses have the limitation that only specific areas of the sample can be observed. For this reason, several images of the nanocomposites were taken in order to verify the description given in the discussion, and selected representative images were chosen.

3.5.8. Dynamic Light Scattering (DLS)

The particle sizes in solution were determined by dynamic light scattering (DLS). An ALV CGS-3 goniometer (ALV-Laser Vertriebsgesellschaft GmbH, Langen, Germany) equipped with a 22 mW He-Ne Laser (λ_0 = 632.8 nm, vertically polarized; Model 1145 P, JDS Uniphase Corporation Santa Rosa, CA, USA) was employed. A cylindrical sample cell was used (detection volume at a scattering angle of 90° of 0.3 mm^2) which was immersed in a refractive-index-matching vat of toluene. During the measurements the toluene temperature was monitored using a Pt-100 temperature probe and used to correct the solvent viscosity. Dynamic light scattering measurements were conducted at angles θ ranging from 40° to 140° (20° steps). The intensity of the scattered light was recorded with a solid-state avalanche photo diode. Apparent hydrodynamic radii, $R_h^{app}(q)$, were calculated from the correlation functions employing either a second order cumulant fit or the so-called ALV-Regularized Fit of $g^2(t)$-type (based on the CONTIN algorithm) covering a time interval ranging typically from 375 ns to 1ms.[1-2]

3.5.9. Small angle X-ray scattering (SAXS) experiments

SAXS experiments were performed at the A2 beamline of DORIS III, HASYLAB at DESY in Hamburg, Germany. The sample to detector distance used was set to 2.85 m and the wavelength of the beam was 1.5 Å.

3.5.10. Stress-strain experiments

The strain-stress experiments were carried out on Zwick model Z020, with a load cell of 20 kN. The measurements were done with a crosshead speed of 1.5 mm/min at ambient temperature, according to the standard ASTM D882. The samples were prepared according to ISO 527-2B standard.

3.5.11. Impact measurements

The impact measurements were carried using the Charpy impact tester from Zwick model Hit 25 P. Specimens were prepared according to ISO 179 standards. Unnotched specimens with rectangular dimensions of 80 x 10 x 4 mm were fractured at 4 J with an impact speed of 2.9 m/s at ambient temperature. The distance between the support span was kept constant to 62 mm.

3.6. References

1. W. Schärtl, *Light Scattering from Polymer Solutions and Nanoparticle Dispersions*, Springer-Verlag, Berlin, Heidelberg, 2007.
2. S. W Provencher, *Computer Physics Communications* 1982, 27, 213.

Chapter 4. Results and Discussions

4.1. Functionalization of Colloidal Silica Nanoparticles: Efficiency of Epoxy Silane as a Suitable Coupling Agent for Anchoring ATRP Initiator-a Precursor for "*grafting from*" Polymerization

4.1.1. Introduction

Among the various types of fillers, silica nanoparticles have been used in various field of applications for many years (reviewed in Chapter 2). Unmodified silica NP's themselves have the tendency to aggregate in (co) polymer matrices. One of the biggest challenges is to reduce the extent of aggregation in order to achieve the desired properties of composite materials. Recently, surface functionalization of silica nanoparticles (SiNP's) with polymer brushes received much attention as the polymer coating alters the interfacial properties.[1-4] Polymer hybrid SiNP's serve as an interesting example of spherical brushes, which enable better dispersion in a polymer matrix. There the chains are stretched away from the colloidal silica core in order to minimise steric crowding. Physical properties of organically modified nanoparticles are governed by both the size and shape of the silica core and the surrounding organic layer.

Colloidal silica NP's are of particular interest due to their precise size control and distribution of the particles.[5] As already discussed, the "*grafting from*"[6] technique is widely used for tethering polymer chains especially through controlled polymerization reactions like ATRP, because of its ability to achieve high grafting density and controlled molecular weight distribution. Generally, the ATRP initiator is anchored on silica NP's through a coupled silane. Various reported methods regarding surface initiated (SI)-ATRP[1-4, 7] from SiNP's were discussed in detail in Chapter 2. In the past few years, organosilane coupling agents especially epoxy silanes are finding increased use

in ceramic particle-based coatings.[8-10] They have a general formula R´-Si-$(OR)_3$, where R´ is a short hydrocarbon chain (usually 3-6 backbone carbons) with an organic functional group such as amino or epoxy group, and R is an alkyl group.[11] Different types of silanes used for various applications are shown in Table 4.1.1.[12] Usually, hydrolysis of the alkoxide groups produces silanols (Si-OH) and through condensation, hydrolyzed molecules form siloxane bonds. The hydrolysis and condensation reactions are pH dependent.[13]

In the present scenario, hydrolyzed molecules are bonded to silica NP's through condensation to form siloxane bonds with the surface hydroxyls. Here we adopted (3-glycidoxypropyl)trimethoxysilane (GPS, highlighted by bold letters in Table 4.1.1) as the coupling agent for anchoring ATRP initiator, 2-bromoisobutyrylbromide (2-BriB) on colloidal silica particles, based on the studies by Etienne and co-workers.[14] Patten et al.[15] reported the grafting efficiency and molecular weight distribution from silica particles having average diameters, 75 nm and 500 nm respectively. Since the aim of the current research work is more towards further investigation of properties of modified NP's in composites, silica particles having smaller size distribution (12 nm, Si_{12} and 20 nm Si_{20}) are chosen for these studies. Grafting of ATRP initiator on suitable silane coupled silica is not a new procedure. In the present research, we investigated systematically (a) the coupling efficiency of epoxy silane both on Si_{12} and Si_{20} particles under specific pH of the reaction medium, (b) grafting efficiency of ATRP initiator from above modified particles under different basic conditions and in the presence of catalyst, and (c) we checked the grafting efficiency of polystyrene and poly(methyl methacrylate) from initiator modified Si_{12} and Si_{20} particles.

As already mentioned, controlling the extent of aggregation is the biggest challenge in the surface functionalization reactions. For this, we tried to keep the particles in solution until the initiator grafting step.

Table 4.1.1. Typical silane coupling agents used for surface modification of silica NP's[12]

Abbreviation for silanes	Name	Chemical structure
APMDES	aminopropyl methyldiethoxysilane	$H_2N(CH_2)_3(CH_3)Si(OC_2H_5)_2$
APMDMOS	(3-acryloxypropyl)methyldimethoxysilane	$CH_2=CHCOO(CH_2)_3(CH_3)Si(OCH_3)_2$
APTES(APTS,APTEOS, APrTEOS	(3-aminopropyl)triethoxysilane	$H_2N(CH_2)_3Si(OC_2H_5)_3$
APTMS (APTMOS, APrTMOS)	(3-aminopropyl)trimethoxysilane	$H_2N(CH_2)_3Si(OCH_3)_3$
APTMS (APTMOS)	(3-acrloxypropyl)trimethoxysilane	$CH_2=CHCOO(CH_2)_3Si(OCH_3)_3$
APTMS (APTMOS)	aminophenyltrimethoxysilane	$H_2NPhSi(OCH_3)_3$
TESPT	bis(triethoxysilylpropyl)tetrasulfane	$(C_2H_5O)_3Si(CH_2)_3S_4(CH_2)_3Si(OC_2H_5)_3$
DDS	dimethyldichlorosilane	$(CH_3)_2SiCl_2$
GPS(GPTS, GOTMS, GPTMOS, KH560)	**(3-glycidoxpropyl)trimethoxysilane (3-glycidyloxypropyl)trimethoxysilane**	**$CH_2(O)CHCH_2O(CH_2)_3Si(OCH_3)_3$**
ICPTES	(3-isocyanatopropyl)triethoxysilane	$OCN(CH_2)_3Si(OC_2H_5)_3$
MMS	methacryloxymethyltriethoxysilane	$CH_2=C(CH_3)COOCH_2Si(OC_2H_5)_3$
PS(MPTMS, MPTS, MAMSE, MAT MSMA, TPM, MEMO, KH570)	nethacylic acid 3-(trimethoxysilyl)propyl est 3-(trimethoxysilyl)propyl methacrylate, 3-methacryloxpropyltrimethoxysilane	$CH_2=C(CH_3)COO(CH_2)_3Si(OCH_3)_3$
MPTES	methacryloxypropyltriethoxysilane	$CH_2=C(CH_3)COO(CH_2)_3Si(OC_2H_5)_3$
MPTS	mercaptopropyltriethoxysilane	$SH(CH_2)_3Si(OC_2H_5)_3$
MTES	methyltriethoxysilane	$CH_3Si(OC_2H_5)_3$
PTMS	phenyltrimethoxysilane	$PhSi(OCH_3)_3$
VTES	vinyltriethoxysilane	$CH_2=CHSi(OC_2H_5)_3$
VTS	vinyltrimethoxysilane	$CH_2=CHSi(OCH_3)_3$

4.1.2. Discussion of Results

4.1.2.1. Coupling reaction of epoxysilane with silica NP's in aqueous suspension and concurrent ring-opening of epoxy groups.

As shown in Figure 3.1 (Chapter 3), the reaction was performed in two steps. The silica particles used were initially dispersed in a basic aqueous suspension stabilised by Na^+ ions. The purpose of the two-step reaction is to control initiator immobilization and prepare a well-dispersed particle system.

The first step involved the silanization of the particles with an epoxy end group containing silane and, concurrently, the formation of vicinal diols by the addition of OH^- on the epoxy group. As mentioned before, sol-gel methods are composed of three reactions: hydrolysis, adsorption and condensation. The coupling mechanism depends on a link between the organo functional groups

and the hydrolysable groups. In water, alkoxy groups of the organic binder are hydrolysed to build the silanol groups. It is known that acid or base can catalyse the hydrolysis reaction. Pohl and Osterholtz[13] showed that the rate of hydrolysis is fast at low pH and slow at pH 7. Plueddemann[11] followed by Kim et al.[17] studied in detail the pH and viscosity changes with the hydrolysis and condensation reactions of epoxy silanes. The first reaction step was easy and straight forward. A trimethoxysilane-based coupling agent was chosen rather than a monoalkoxysilane due to its higher efficiency for grafting onto a silica surface.

One drawback may arise due to the possibility to generate a polycondensed silane network. Since the aqueous silica suspension is basic, methoxysilyl group hydrolysis into silanols followed by their condensation with the silane functions present at the silica NP's surface takes place. Moreover, the simultaneous epoxy ring opening reaction occurs. In the present case, silanization reaction from Si_{12} particles was found to be effective at a pH between 11 and 11.7 whereas a pH between 10 and 10.7 was good for Si_{20} particles. The amount of coupled silane will be different for Si_{12} and Si_{20} nm silica particles, due to the difference in the surface area of both particles. Among the silica NP's, Si_{12} has a surface area of 220±30 m^2/g (based on the data provided by suppliers) with 4.7 OH groups/nm^2 (calculated from TGA) and for Si_{20} particles, 140±30 m^2/g with 4.5 OH groups/nm^2.

However, the Dynamic light scattering (DLS) measurements carried out in the laboratory showed an average size distribution of 14±4 nm for Si_{12} and 22±4 nm for Si_{20} particles respectively. If the system is concentrated, i.e., the ratio of silane to silica dispersion exceeds beyond a limit, the self condensation among epoxy silane molecules takes place predominantly rather than between silica Si-OH groups and leads to a gel formation.

Table 4.1.2. Anchoring of epoxy silane followed by grafting of (2-bromoisobutyryl) bromide: details of each step of surface modification from Si_{12} and Si_{20} particles and the effect of basic systems during the esterifications step.

Sample code[a]	coupled GPS (wt%)$_{TGA}$	GPS gps/nm^2 (calc)[b]	base reactant (no. of equiv.)	[Br]/nm^2 (calc)[C]	[Br]$_{mmol/g}$ (elemental analysis)[d]	[Br]$_{mmol\ /\ g}$ (TGA)[e]
20A	14.2	4.6	*N*-Morpholine,6	4.3	1	1.2
20B	8.7	3	*N*-Morpholine,6	2	0.42	0.51
20A	12.4	4	Et_3N,3.5	3.4	0.78	0.82
20B	6.8	2.2	Et_3N,3.5	1.6	0.37	0.4
12A	21.2	4.4	*N*-Morpholine,6	3	1.1	1.1
12B	12.2	2.5	*N*-Morpholine,6	1.2	0.41	0.5
12A	23.2	4.7	Et_3N,3.5	3.7	1.28	1.32
12B	14.3	3	Et_3N,3.5	2.3	0.8	0.85

a = 12 and 20 denotes average particle diameters of silica core in nanometres. **A** and **B** stands for 11 and 5 equiv. of GPS for Si_{12} and 14 and 5 equiv. for Si_{20} particles used for coupling reaction (molar equiv are calculated on the basis of available OH/nm^2 on the silica particles). [15,18] **b =** no: of GPS groups/nm^2
$\boldsymbol{M}_{GPS}$ = molar mass of GPS undergoes decomposition in g/mol; $\boldsymbol{S}_{sp}$= specific surface area of silica core in nm^2/g
c = calculated from elemental analysis results and specific surface
d= reaction carried out in the presence of solvent THF in the presence of catalytic amount of DMAP and bromide concentration calculated from elemental analysis
e= reaction carried out in the presence of solvent toluene without DMAP
Note: 20 A and 20 B were carried out at pH 10.7 and 10 respectively, whereas, 12A and 12B were carried out at pH 11.7 and 11 respectively.

Therefore the system is diluted with deionised water while maintaining the pH at the optimal value in such a way that silica concentration in the net reaction medium should not exceed 0.2 g/ml. If the pH is low, then the required pH is achieved by the addition of NaOH solution prepared from deionised water. The quantity of coupled silane was determined by TGA for the samples dried at a temperature of 100 °C for 48 h. Table 4.1.2. shows the influence of coupling efficiency of GPS from Si_{12} and Si_{20} particles having different surface areas. For Si_{12} particles, maximum amount of coupled silane was 23.2 wt% for 11 mol equivalents of GPS for a reaction duration of 36 h. whereas for Si_{20} particles, it was 14.2 wt % for 14 mol equivalents GPS for a reaction duration of 48 h. These quantities indicate a nearly complete conversion of silanol functions on the surface of silica.

ATR-FTIR spectroscopy was carried out to account for the success of the grafting reactions (see Figure 4.1.1). The signal in the range of 1120 cm^{-1} (see Figure 4.1.1, curve a) comes from the typical Si-O-Si stretching vibration from silica particles.

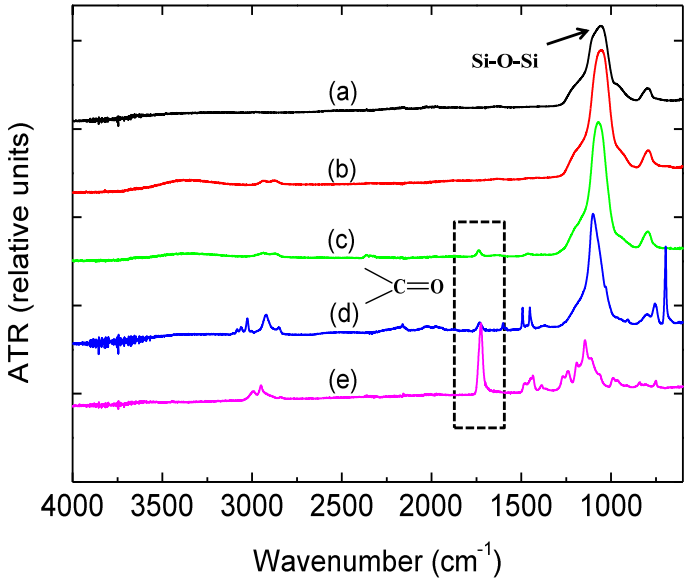

Figure 4.1.1. Selective ATR-FTIR spectra of silica particles after each step of surface modification (a) pristine silica particles, Si_{20} (b) silica particles after coupling with epoxy silane, $Si_{20}G^{14}$ (superscript 14 stands for weight fraction of GPS from TGA in %) (c) initiator grafted silica, $Si_{20}Br^{0.4}$(superscript 0.42 denotes [Br] in mmol/g (d) PS modified silica particles, $Si_{20}PS^{34}$ (PS stands for polystyrene and superscript 34 denotes molar mass of grafted PS on silica in kg/mol (e) PMMA modified silica particles, $Si_{20}M^{31}$(M for PMMA and superscript 31 stands for grafted PMMA in kg/mol).

The broad stretching band near 3400-3450 cm^{-1} corresponds either to the –OH groups from the silica or from the hydrolysed epoxy groups obtained after silanization (see Figure 4.1.1, curve b). The analysis of ^{13}C CP/MAS NMR spectra of $Si_{20}G^{14}$ (see Figure 4.1.2) in solid phase was carried out in order to confirm that epoxy silane immobilized on silica undergoes ring opening reactions. The peak located at 63 ppm is characteristic of primary alcohol and the one at 70 ppm corresponds to the secondary alcohol (together with -CH_2's in α of the ether group). Moreover, no significant peak typical of the methylene of the epoxy group (at 40 ppm) indicates a rather complete hydrolysis of the epoxy ring. From the overall initiator immobilization reactions, one can see a

good control of grafting density through controlled coupling reactions with the epoxy silane from the two different types of silica particles.

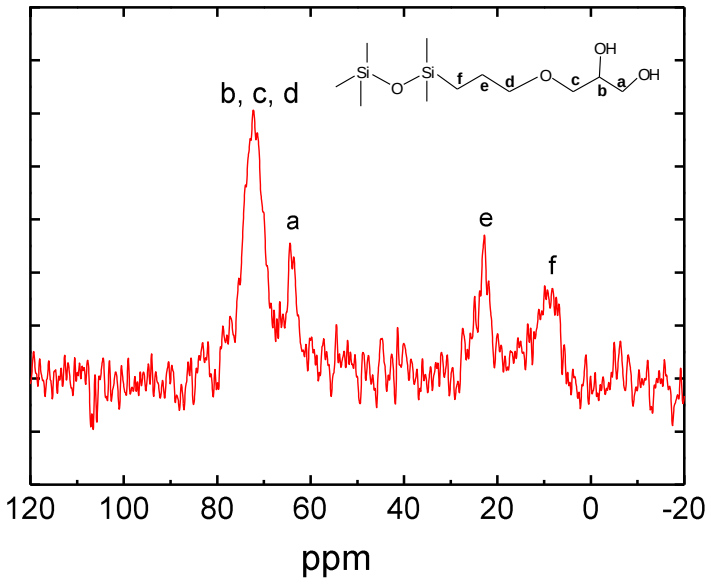

Figure 4.1.2. Solid state ^{13}C CP/MAS NMR spectrum of $Si_{20}G^{14}$ silica particles coupled with hydrolyzed epoxy silane. G^{14}, the superscript 14 corresponds to the % of weight loss of GPS from TGA.

Further, from ^{29}Si CP/MAS NMR spectra it is possible to differentiate the different types of silicon atoms present in the silica particles before after silane modification: Q^4, Q^3 and Q^2, that is, in the bulk, on the surface bonded to one OH and to two OH group, respectively. The patterns T^1, T^2 and T^3 correspond to the silicon atoms contained in the silane molecule which have formed one (or two, or three, respectively) Si-O-Si bond with the silica particle, or one Si-O-Si binding between two silanes. Possible types of signals from silica core and those obtained after silane modification of silica surface is shown by Figure 4.1.3 (a and b).

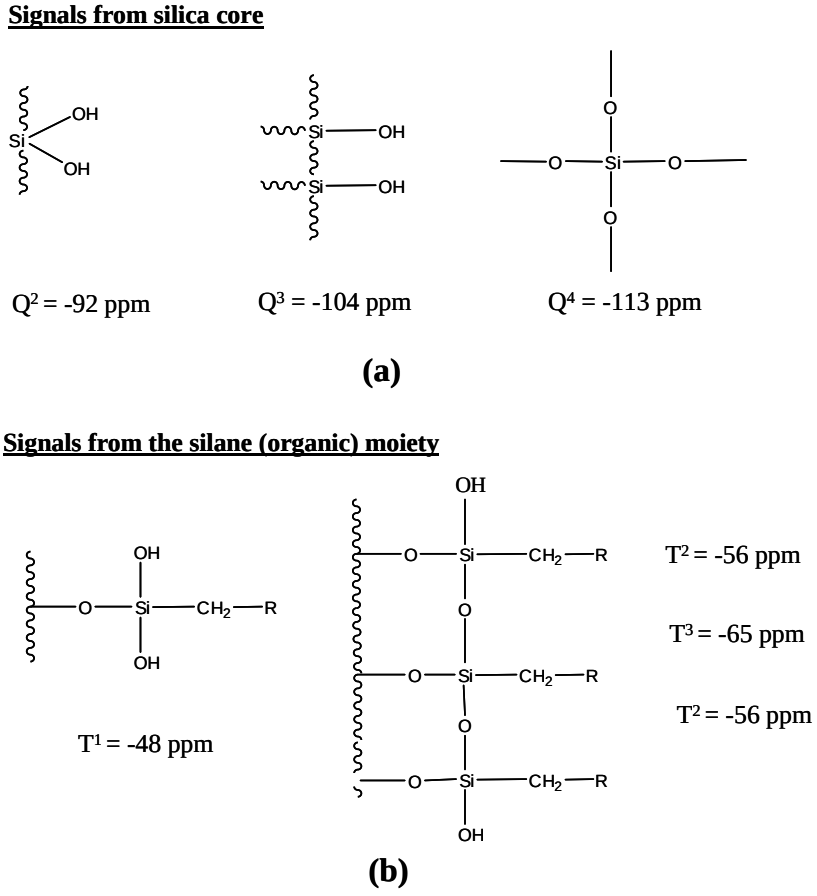

Figure 4.1.3. Possible signals that can be obtained from ^{29}Si spectra of (a) pristine silica particles and (b) after silane modification of silica surface.[20]

Figure 4.1.4 represents the ^{29}Si CP/MAS NMR spectra of unmodified Si_{12} and Si_{20} particles and those contained 23 wt% ($Si_{12}G^{23}$) and 14 wt% ($Si_{20}G^{14}$) of hydrolyzed silane respectively. In the Figure 4.1.4 (curve a and b), the chemical shifts of the Q^4 and Q^3 silicon nuclei were observed as a bimodal signal at -114 ppm (main peak, correspond to bulk silica) and -104 ppm (shoulder peak, silica surface bonded to one OH group), respectively. The Q^2 peak is not visible in the spectra. After the silanization reaction, signals due to T^2 and T^3 patterns (Figure 4.1.4, curve c and d) appear at -58 and -70 ppm, respectively correspond to the silicon atoms contained in the epoxy silane molecule which have formed Si-O-Si bond with the silica particles. After silanization, the shoulder peak in the range -104 ppm diminishes. The number of hydrolysed silane molecules

calculated through TGA analysis from both Si_{12} and Si_{20} particles indicate 100 % silanization reaction from surface OH groups rather than polycondensation reaction between silane molecules. The disappearance of shoulder peak at -104 ppm supports this interpretation.

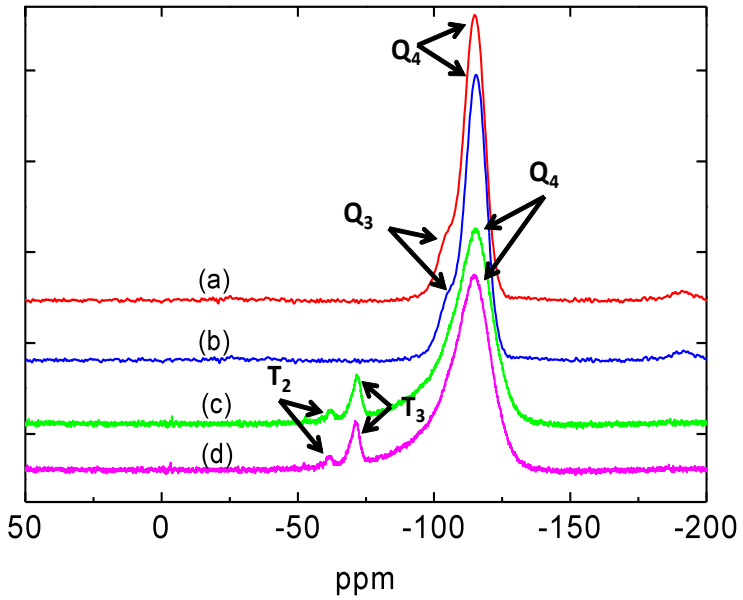

Figure 4.1.4. Solid-state ^{29}Si CP/MAS NMR spectra of the pristine and hydrolysed epoxy silane modified silica particles. (a) Si_{12} (b) Si_{20} (c) $Si_{12}GPS$[23] (d) $Si_{20}G$[14]

Selected TEM images of Si_{12} and Si_{20} after GPS grafting reaction is shown in Figure 4.1.5 (a and b). From the TEM images, one could observe the discrete distribution of particles. The curves c and d of Figure 4.1.4, correspond to the epoxy silanization reaction of Si_{12} particles with 11 mol equiv. and Si_{20} particles with 14 mol equiv. of GPS, respectively. Further, the TEM image of dried silane modified silica films shows a well dispersed system. The narrow particle size distribution (measured from TEM) indicates that the silane layer thickness (1 ± 2 nm) on silica particles is more or less the same.

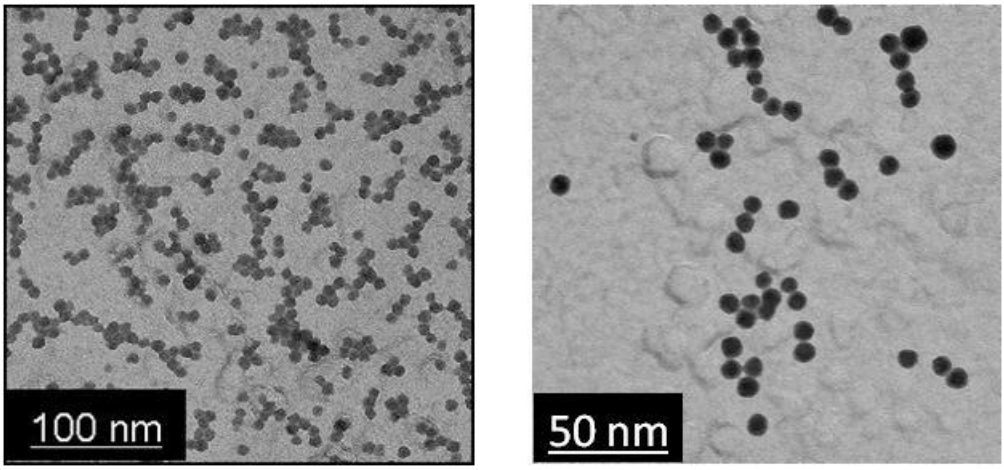

(a) (b)

Figure 4.1.5. TEM images of GPS functionalized (a) $Si_{12}G^{23}$ and (b) $Si_{20}G^{14}$ colloids obtained by casting the dispersion onto carbon-coated copper grid.

4.1.2.2. Grafting of 2-bromoisobutyryl bromide initiator onto diol functionalized silica NP's as a precursor for Styrene and MMA polymerization.

The second step was a grafting reaction which consisted in an esterification of the terminal hydroxyl group of vicinal diol with the 2-bromoisobutyryl bromide. Through this procedure, one can adjust the degree of initiator immobilization up to a certain level of accuracy. The procedure for anchoring ATRP initiator was described in experimental part (Chapter 3).

The amount of epoxy silane condensed on the silica is responsible for the concentration of bromo initiator to be grafted in the second stage of surface modification. The grafting efficiency of the bromo initiator was conducted with different basic systems like *N*-methymorpholine (pK_a = 8.3) and the commonly used triethylamine (pK_a=10.8). Also, the effect of a catalytic amount of 4-(dimethylamino)pyridine (DMAP) (pK_a = 9.7) along with the above basic systems was evaluated.

Reactions in the presence of DMAP were carried out in tetrahydrofuran. Those without DMAP were carried out in toluene. The different percentages of initiator grafted onto silica particles (bromide concentration obtained from elemental analysis) are also given in Table 4.1.2. It is reported in the literature that the best catalytic effect can be expected from bases with higher pK_a, not only due to the higher pK_a value but also from the stability of the formed salts.[17]

Already some of the studies reported the grafting efficiency of ATRP initiator using different bases.[19] In this study we expected a better grafting efficiency in the presence of a strong base like triethylamine rather than *N*-methylmorpholine. For Si_{12} particles, the initiator grafting efficiency was found to be better when using triethylamine. However, the reaction was found to be going well when using the less basic *N*-methylmorpholine for both particle systems. Reaction in the presence of a catalytic amount of DMAP does not show any significant improvement in grafting efficiency when compared to other sets of reactions carried out in toluene. This indicates that the solvents used in the present study do not play an important role in the initiator anchoring reactions. For the above reaction conditions, the reactivity of terminal hydroxyl group of diol functionalized silica particles towards ATRP initiator grafting reaction was confirmed by the elemental analysis of bromide content. Finally, on the basis of above results described in Table 4.1.2, one could conclude that it is possible to control the initiator concentration on silica particles from lower to higher values from controlled epoxysilane functionalized silica particles. ATR-FTIR spectra shows an absorption band near 1740 cm^{-1} (Figure 4.1.1, curve c) that comes from the C=O stretching vibration after the esterification by the ATRP initiator.

Further, the efficiency of the above initiator immobilized silica particles was verified by grafting polymerization reactions with MMA and styrene. The ^{1}H-NMR spectra of grafted polystyrene (shown in Figure 4.1.6, curve A) and PMMA (shown in Figure 4.1.6, curve B) chains proves the efficiency of grafting reactions.

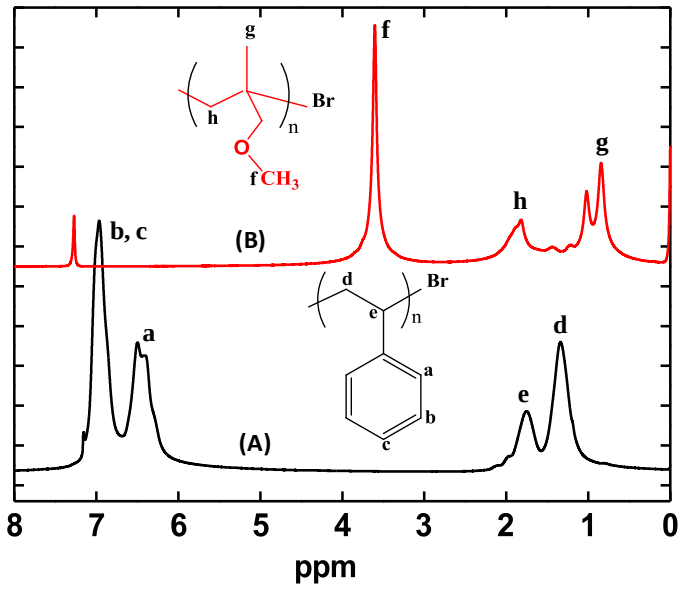

Figure 4.1.6. Selective ^{1}H-NMR spectra of grafted (A) polystyrene, $Si_{12}PS_{62}^{34}$ (B) poly(methyl methacrylate), $Si_{12}M_{58}^{31}$ chains from Si_{12} nanoparticles.

Further, the ATR-FTIR spectra, curves d and e in Figure 4.1, gives a valid interpretation to the grafting efficiency of styrene and MMA polymerization respectively. The SI-ATRP kinetics and further details of grafting polymerization of MMA and styrene will be discussed in the forthcoming Chapter 4.2. After MMA polymerization, the C=O stretching band was found to be stronger near 1750 cm^{-1}, as observed by curve e in Figure 4.1.1. Moreover, the antisymmetric C-O-C stretching mode in esters gives rise to a very strong and quite broad band near 1200 cm^{-1}. The grafting of polystyrene from the particles was confirmed by the appearance of the C=C stretching of the phenyl rings at 1491 and 1451 cm^{-1} in the respective spectra (see Figure 4.1.1, curve d). Further, Selective TEM images of initiator grafted Si_{12} and Si_{20} particles are shown by Figure 4.1.7 (a and b). Both set of the initiator grafted particles show the same nature of distribution.

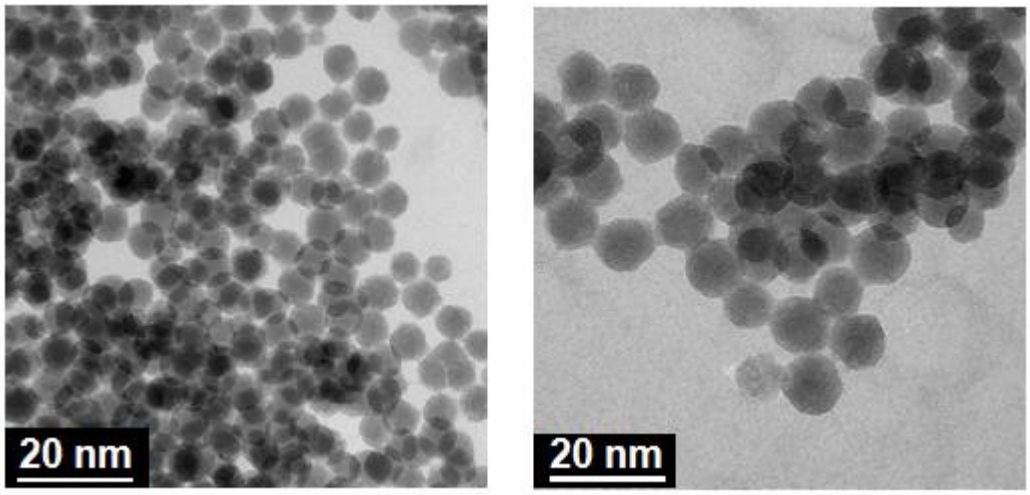

(a) **(b)**

Figure 4.1.7 TEM images of initiator (2-BriB) grafted (a) $Si_{12}Br^{0.4}$ and (b) $Si_{20}Br^{0.41}$ colloids obtained by casting the dispersion onto carbon-coated copper grid.

4.1.3. Conclusions

The efficiency of (3-glycidoxypropyl)trimethoxy silane as a coupling agent for anchoring ATRP initiator was studied in this section. The amount of coupled silane can be varied under controlled reaction conditions. The ^{13}C spectrum of silane modified particles confirms the ring opening reaction of epoxy moiety coupled on silica particles. Further, ^{29}Si spectral analysis of silane modified silica particles discards the possibility of polycondensation of silane molecules under present reaction conditions. Esterificaton reaction was controllable in order to maintain the bromide concentration of ATRP initiator. The bromination reaction of the terminal OH group of vicinal diol of silane modified silica is controllable. The initiator grafting reactions and the distribution of particles were further confirmed by ATR-FTIR analysis.

4.1.4. References

1. B. Radhakrishnan, R. Ranjan, W. J. Brittain, *Soft Matter*, 2006, 2, 386.
2. T. Werne, T. E. Patten, *J. Am. Chem. Soc*., 2001, 123, 7497-7505.
3. J. Pyun, S. Jia, T. Kowalewski, G. D. Patterson, K. Matyjaszewski, *Macromolecules* 2003, 36, 5094-5104.
4. R. Barbey, L. Lavanant, D. Paripovic, N. Schüwer, C. Sugnaux, S. Tugulu, H. A. Klok, *Chem. Rev*., 2009, 109, 5439-5452.
5. M. García, W. E. Van Zyl, M. G. J. Ten Cate, J. W. Stouwdam, H. Verweij, M. S. Pimplapure, G. Weickert, *Ind. Eng. Chem. Res*., 2003, 42, 3750.
6. O. Pruker, J. Rühe, *Mater. Res. Soc. Symp. Proc.*, 1993, *304*, 1675.
7. M. Alexandre and P. Dubois in *"Macromolecular Engineering: Precise Synthesis,Materials Properties, Applications"*, Vol.4, Chapter 2, K. Matyjaszewski, Y. Gnanou and L. Leibler. Wiley-VCH; Weinheim, 2007, 2033-2070.
8. J. D. Blizzard, L. J. Cottington, U.S. Patent, 1995, 5, 403, 535.
9. M. W. Daniels, L. Chu, L. F. Francis, in "*Better Ceramic Through Chemistry* VII: Organic/Inorganic Hybrid Materials" (B. K. Coltrain, C. Sanchez, D. W. Schaefer, G. L. Wilkes, Eds.), Materials Research Society, Pittsburg, PA, 1996, 215.
10. L. Chu, M. W. Daniels, L. F. Francis, *Chem. Mater.*, 1997, 9, 2577.
11. E. P. Plueddemann, "*Silane Coupling Agents*" Plenum, New York, 1982.
12. H. Zou, S. Wu, J. Shen, *Chem. Rev*., 2008, 208, 3896.
13. E. R. Pohl, F. D. Osterholtz, in "*Molecular Characterization of Composite Interfaces*" (H. Ishida and G. Kumar, Eds.) Plenum, New York, 1985, 157.
14. S. Etienne, C. Becker, D. Ruch, B. Grignard, G. Cartigny, C. Detrembleur, C. Calberg and R Jerome, *J. Therm. Ana. and Calori*., 2007, 87, 101-104.
15. V. Werne,T.; T. E. Patten. *J. Am. Chem. Soc*., 2001, 123, 7497-7505.
16. E. R. Pohl, F. D. Osterholtz, *Molecular Characterisation of Composite Interfaces*, Plenum Press, New York, 1985.
17. H. U. Kang, J. K. Park, S. H. Kim, *Korea-Australia Rheology Journal*, 2004, 16, 175-182.
18. M. Save, G. Granvorka, J. Bernard, B. Charleux, C. Boissière, D. Grosso, C. Sanchez, *Macromol. Rapid Commun*., 2006, 27, 393-398.
19. A. E. Harrak ; G. Carrot ; J. Oberdisse ; C. E. Baron ; F. Boue, *Macromolecules*, 2004, 37, 6376-638.
20. M. W. Daniels, L. F. Francis, *J. Colloid and Interface Sci*., 1998, 205, 191-200.

4.2. Surface-Initiated ATRP (SI-ATRP) Kinetics of Styrene and MMA Polymerization from Functionalized Si_{12} and Si_{20} Nanoparticles: Morphological Characterization and Size Distribution of Polymer Grafted Particles at Higher Conversions

4.2.1. Introduction

Among the different controlled radical polymerization techniques, the chemical versatility and robust behaviour make atom transfer radical polymerization (ATRP)[1-6] to be intensively explored in the field of surface initiated (SI) reactions (reviewed in Chapter 2). One fact is that, for ATRP reactions, catalyst systems, as well as surface immobilisable initiators are commercially available or can be synthesized relatively easy from an experimental point of view. Hybrid nanoparticles prepared by SI-ATRP[7-10], in which polymer chains stretch away from the colloidal silica core help to minimise the steric crowding and enable good dispersion in the polymer matrix[11] (depending on the molar mass of matrix and grafted polymer). Nanoparticle physical properties are governed by both the size and shape of the silica core and the surrounding organic layer. Most of the studies were carried out with styrenic and acrylate types of monomers. The normal kinetics of copper catalysed ATRP[12-17] is influenced by many parameters, such as ligand to transition metal ratio, Cu(II) to Cu(I) ratio, type of ligand, counterion, solvent, temperature, type of initiator. Moreover, surface chemistry of the nanoparticles plays an important role in the grafting reactions. By varying the above parameters, one can fine tune the SI-ATRP reactions. Ejaz et al.[8] found that addition of sacrificial initiator was necessary to achieve a controlled polymerization. In the absence of sacrificial initiator, the initiator concentration and, related to this, the concentration of the deactivating Cu(II) species was too low to allow a controlled polymerization. Instead of adding a sacrificial initiator, another strategy to overcome the

insufficient deactivator concentration that results from surface confined ATRP is to add the deactivating Cu(II) species directly to the polymerization solution. This was successfully demonstrated by Matyjaszewski et al.[9,18] for the synthesis of polystyrene (PS) brushes from bromoisobutyrate-functionalized wafers. Patten et al.[19] made similar studies and differentiated the behaviour of polymer chain growth from silica particles (70 nm and 300 nm) having different surface chemistry.

Kinetic studies of SI-ATRP from silica nanoparticles are well known. But in most of the reported studies, comparatively lower initiator concentrations on particle surface were adopted. So in the present work, we tried to investigate the behaviour of styrene and MMA polymerization simultaneously from both smaller silica particles (12 and 20 nm) having higher bromide concentration than in the reported studies. On the basis of reviewed literatures and best of our knowledge, the bromide concentration of ATRP initiator on both Si_{12} and Si_{20} particles were kept constant for comparative kinetic studies of styrene and MMA polymerizations under suitable reaction conditions. Table 4.2.1 gives an exemplary summary about the details of some relevant works dealing with SI-ATRP kinetics of styrenic and acrylic types of monomers from silica particles with various core diameters. Apart from those studies on silica particles with bigger core diameters (Table 4.2.1), Carrot et al.[20] was the first who reported the SI-ATRP of *n*-butyl acrylate (*n*-BA) from smaller silica particles (Si_{12}). In contrast to other works found in the literature, the bromide concentration of ATRP initiator on both Si_{12} and Si_{20} particles was kept constant for comparative kinetic studies of styrene and MMA polymerizations.

Table 4.2.1. Comparative analysis of present work with the relevant works dealing with SI-ATRP kinetics of styrenic and acrylic types of monomers from various types of silica nanoparticles.

Litr. Code	Works on SI-ATRP from silica NP's (year of Pub.)	Monomer subjected to SI-ATRP	SiNP's Si_x(nm)	Initiator concentration (mmol/g)
1	Patten et al.[21](1999)	Styrene	Si_{70}	0.14
2	Patten et al. [19](2001)	Styrene, MMA	Si_{75} and Si_{300}	0.25 (BPDS on Si_{75}) 0.073 (BPDS on Si_{300}) 0.17 (BIDS on Si_{75}) 0.086 (BIDS on Si_{300})
3	Carrot et. al.[20] (2001)	n-butyl acrylate	Si_{12}	shown as 1.4 initiators/nm^2
4	Patterson et al.[11](2002)	styrene	Si_{20}	0.31
5	Matyjaszewski et al.[22] (2003)	Styrene, MMA, n-butyl acrylate	Si_{20}	0.26
6	Carrot et al.[23] (2004)	Styrene	Si_{14}	concentration varied from 0.035-0.119
7	Fukuda et al.[24](2005)	MMA	Si_{130}, Si_{290}, Si_{740} and Si_{1550}	0.08 on Si_{130}

Moreover, the bromide concentration on a given amount of silica particles utilized for the present studies (0.4 mmol/g) is significantly higher than those adopted in reported studies. This concentration is found to be higher than those reported by Patterson et al.[11] (0.31 mmol/g) and Matyjaszewski and his co workers[22] (0.26 mmol/g) for the polymerization of styrene/MMA from functionalized 20 nm sized silica particles. Later, Carrot et al.[23] also carried out the kinetic studies of styrene polymerization from silica nanoparticles of average core diameter 14 nm (Si_{14}) with low initiator concentration. The control on polymerization beyond 20 % conversion was checked by DSC characterization of either polymer modified silica nanoparticles. Also, the consequences of molar mass distributions at different stages of conversion (especially at higher conversions) and respective size distributions of resultant spherical polymer brushes from these particles were investigated. Styrene and MMA polymerizations were carried out in the presence of deactivator ($CuBr_2$) and sacrificial initiator, respectively.

4.2.2. Discussion of Results

4.2.2.1. SI-ATRP kinetics of styrene from initiator functionalized Si_{12} and Si_{20} particles

Grafting polymerization of styrene was carried out from initiator modified silica particles, Si_{12} and Si_{20}, by the general procedure described in Chapter 3. Table 4.2.2 summarises the combined results of styrene and MMA polymerization reactions conducted from the two types of nanoparticles up to 20% conversions under respective conditions. In order to increase the control over the polymerization processes, the ATRP reaction of styrene was conducted in the presence of deactivator $CuBr_2$.[11,25-26] The temperature of all styrene polymerization reactions were kept at 90 °C. A comparative kinetic study was carried out with modified silica particles ($Si_{12}Br$ and $Si_{20}Br$) by maintaining similar molar concentration (0.4 mmol/g) of bromide initiator on silica surface. The [Br] concentration adopted for the present study is slightly higher than the ones in the reported studies of Matyjaszewski and his coworkers.[26] Let us go through the overall effect of the two different modified particle systems towards the styrene polymerization. Polymerization reactions up to a monomer conversion of 20 % are shown in Table 4.2.2, and the consequences at higher conversions will be discussed in the following paragraphs. This low degree of conversion was chosen to avoid gelation arising from interparticle radical coupling reactions.[26] The efficiency of silica colloidal initiators was already verified by the polymerization of either styrene or MMA monomers and they were characterized through ATR-FTIR spectroscopy (Chapter 4.1) The grafting of polystyrene from the particles was confirmed by the apparition of the C=C stretching of the phenyl rings at 1491 and 1451 cm^{-1} in the ATR-FTIR spectrum (Chapter 4.1, Figure 4.1.1. curve d) and from the ^{1}H-NMR spectrum (Chapter 4.1, Figure 4.1.1. curve A).

Table 4.2.2. Conditions for the ATRP of styrene (Sty) and methyl methacrylate (MMA) from 2-bromoisobutyrate functionalized colloidal silica particles.

No: code	**Silica initiator**	**Monomer**	$\mathbf{R_t}$ (min)	**Conversion** (%)	$\boldsymbol{M_n}$ *Free polymer* (g/mol)	$\boldsymbol{M_w/M_n}$ *Free polymer* (g/mol)	$\boldsymbol{M_n}$ *degrafted polymer* (g/mol)	$\boldsymbol{M_w/M_n}$ *degrafted polymer* (g/mol)
1	$Si_{12}Br$	Sty	85	5.6	7,400	1.14	6,200	1.07
2	$Si_{12}Br$	Sty	232	19.2	20,000	1.22	16,000	1.21
3	$Si_{20}Br$	Sty	94	4.8	9,400	1.06	5,400	1.04
4	$Si_{20}Br$	Sty	242	18.6	18,000	1.21	17,200	1.17
5	$Si_{12}Br$	MMA	23	7.6	9,400	1.32	7,100	1.13
6	$Si_{12}Br$	MMA	70	18.2	21,300	1.34	17,000	1.31
7	$Si_{20}Br$	MMA	27	6.8	11,100	1.18	5,200	1.11
8	$Si_{20}Br$	MMA	77	20	17,200	1.22	15,300	1.25

Subscripts 12 and 20 in $Si_{12}Br$ and $Si_{20}Br$ correspond to the average diameter (nm) of the silica core respectively. The bromide concentration on both types of silica particles was adjusted to 0.4 mmol/g. For Sty polymerization, the molar ratios are [M]: [SiBr]: [CuBr]: [$CuBr_2$]: [PMDETA] = 500:1:1:0.06:1 at 90 ^{0}C and for MMA polymerization, the molar ratios is as follows [M]: [SiBr]: [2-EBriB]: [CuBr]: [PMDETA] = 500:1:0.06:0.8:0.8 at 70 ^{0}C.

The $[M]_0/[I]_0$ ratios have been varied from 200–1000 for the polymerization reactions. The results discussed here are those carried out at a monomer to initiator ratio of 500:1 for both styrene and methyl methacrylate polymerizations (standard deviations in the molar mass from different sets of experiments can be seen in the figures discussed below). Figures 4.2.1 (a) and (b) represent the kinetic plot and molar mass vs. conversion of styrene ATRP, respectively, from silica based initiators in the presence of deactivator $CuBr_2$.

Both kinetic and molar mass vs. conversion plots tend to be linear, as can be appreciated in Figure 4.2.1 (a) and (b). The molar mass distribution of the growing chains increases with time in the case of both particles. During the initial stages (lower conversions) of styrene polymerization, better control on the molar mass was achieved. The free polymer was recovered by centrifuging the polymerization mixtures and the supernatant solution was treated with THF and the process repeated two or three times until no precipitate formed when the supernatant was added to methanol. The surface-grafted polymer was isolated by etching

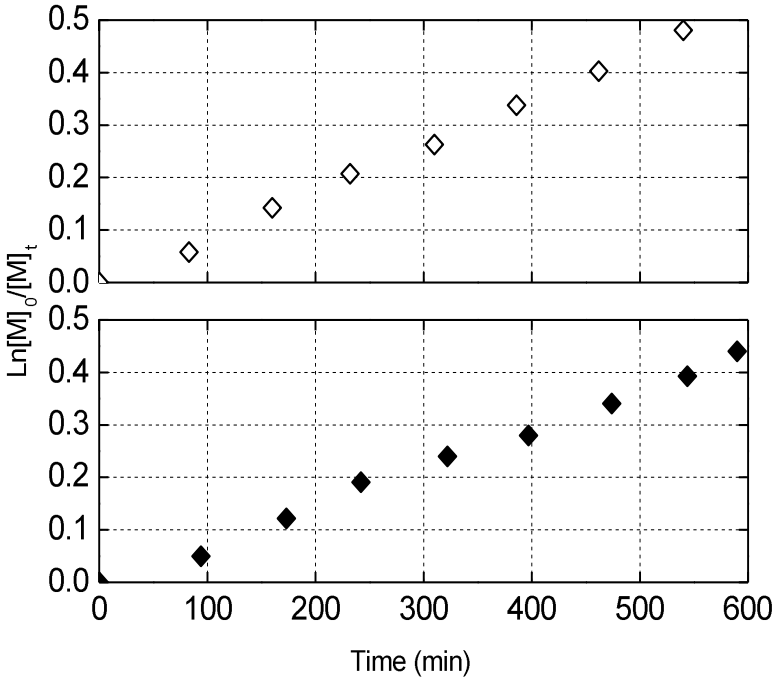
Ln[M]$_0$/[M]$_t$
0.5
0.4
0.3
0.2
0.1
0.0
0
100
200
300
400
500
600
Time (min)

(a)

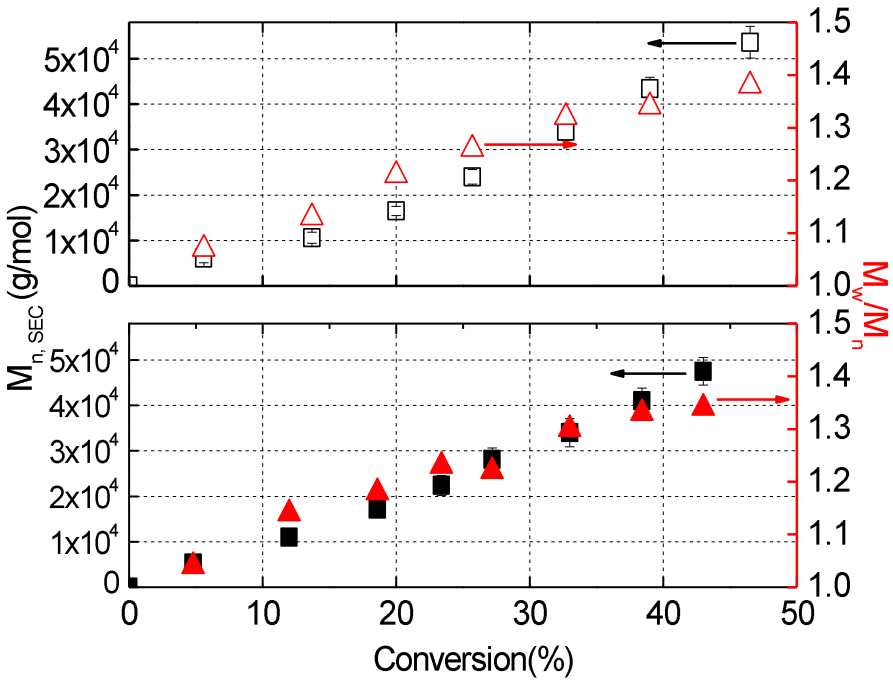
M$_{n,SEC}$ (g/mol)
5x10^4
4x10^4
3x10^4
2x10^4
1x10^4
0
M$_w$/M$_n$
1.5
1.4
1.3
1.2
1.1
1.0
0
10
20
30
40
50
Conversion(%)

(b)

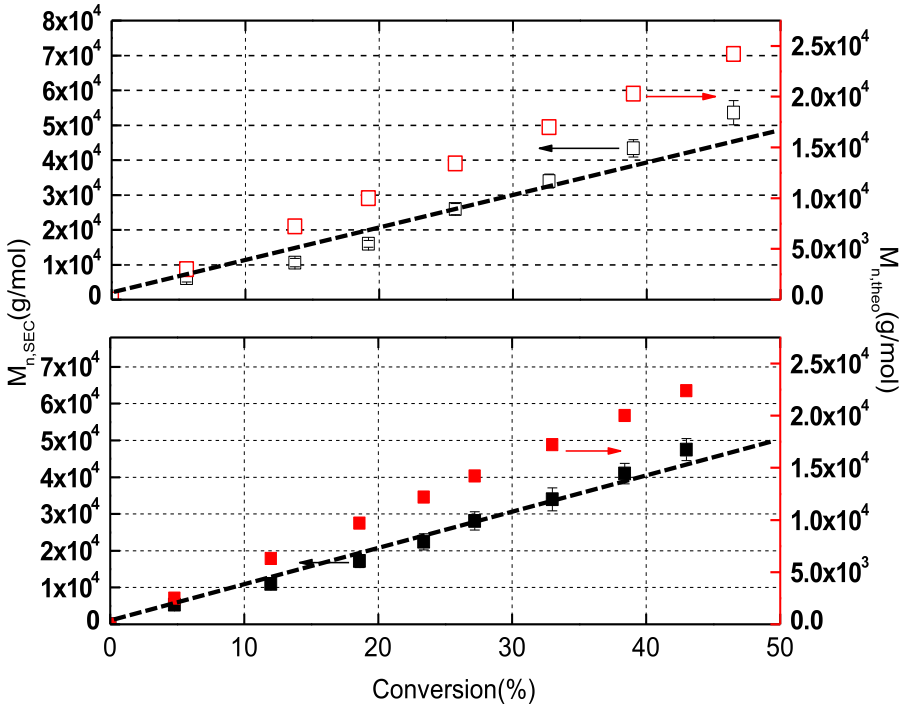

(c)

Figure 4.2.1. SI-ATRP of styrene at 90 ^{0}C from silica nanoparticles. (a) semi logarithmic plot of monomer conversion versus time from functionalized Si_{20} (♦) and Si_{12} (◊) particles respectively. (b) number average molar mass of degrafted PS vs. conversion from the surface functionalized Si_{20} (■, ▲) and Si_{12} (□, Δ) particles and (c) experimental and theoretical number average molar mass vs. conversion from Si_{20} (■, ■) and Si_{12} (□, □) in the presence of deactivator ($CuBr_2$). $M_{n(theo)}$= $[M]_0/[I]_0$ x % of conversion x $M_{\text{molar mass of monomer}}$. $[M]_0/[I]_0$ = initial monomer to initiator ratio.

One possible explanation for this difference is that, not all of the initiator sites on the nanoparticle surface initiated the growth of polymer chains, and this rationalization is consistent with the possibility that the growing chains sterically block access of the catalyst to the neighbouring initiation sites on the nanoparticle surface.[18] When the styrene polymerizations were carried out at low monomer to initiator ratio, a good control over molar mass was observed. Moreover, the discrepancy between the theoretical and experimental molar masses was found to

be less. When we compare the above polymerization reactions for the same monomer to initiator ratios, in the absence of Cu(II)Br_2 (not discussed in Table 4.2.2), the degrafted polystyrene chains from Si_{12} particles exhibit a number average molar mass of 28.2 kg/mol with a PDI value of 1.25 for 17.2 % conversion, whereas, a number average molar mass of 26.4 kg/mol with PDI value 1.3 from Si_{20} particles for 18 % conversion. The theoretical molar masses for the respective conversions from Si_{12} and Si_{20} particles are 8,950 g/mol and 9,400 g/mol respectively. Here, the discrepancy between experimental and theoretical molar mass is high for a targeting conversion of 20 %. This indicates that addition of the deactivator copper(II) species was found to be efficient up to 20 % conversion. Above 20 % conversion (especially above 25 %), the GPC curves (see Figure 4.2.2) of the degrafted polystyrene chains show slight peak broadening (34 kg/mol from Si_{12} particles) that may arise from the beginning of small amount of interparticle radical coupling reactions. Finally at higher molar mass (53 kg/mol for Si_{12} and 47 kg/mol for Si_{20}), a bimodal molar mass distribution arise from the cross linking between polymer chains. It is more prominent in the case of 12 nm sized particles. The corresponding changes in M_w/M_n values (see Figure 4.2.1 (b)) support above conclusions.

The light scattering experiments carried out on the hybrid nanoparticles showed the existence of discrete particles. The hydrodynamic diameter of the hybrid nanoparticles also increased with the molar mass of the pendant polymer (shown in Table 4.2.4). In the case of styrene polymerization, crosslinking/radical coupling between chains on two different particles was found at higher conversions, as indicated by a large increase in hydrodynamic diameter versus conversion.

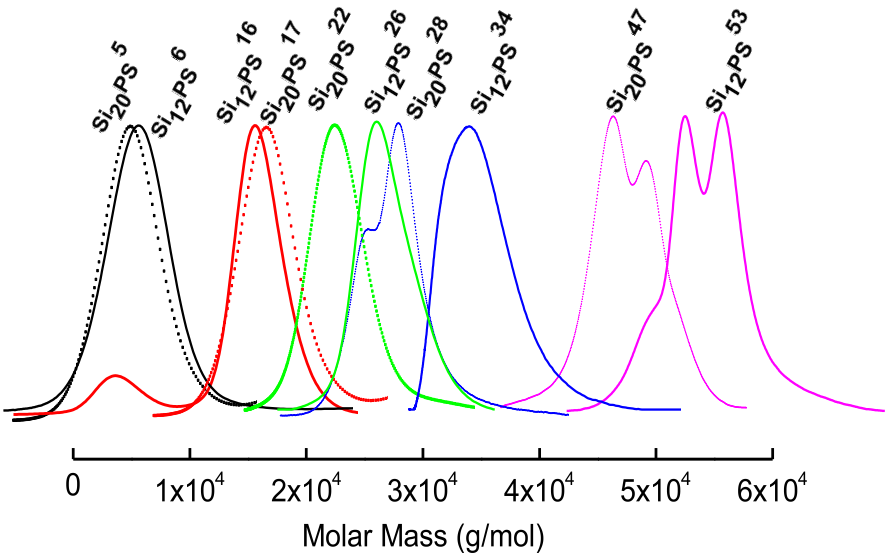

Figure 4.2.2. GPC (signal from UV detector) curves of PS degrafted from Si_{12} and Si_{20} silica particles at different conversions. Curves with solid lines are for polystyrene degrafted from Si_{12} and dotted lines are those from Si_{20} particles respectively. (The subscript, x and superscript a in Si_xPS^a denote the average core diameter of silica nanoparticle and molecular weight of degrafted PS in kg/mol, respectively)

4.2.2.2. SI-ATRP kinetics of MMA from initiator functionalized Si_{12} and Si_{20} particles

The procedure for surface initiated ATRP of MMA polymerization was described in chapter 3. The polymerization reactions of methyl methacrylate were carried out in the presence of low catalyst concentration ([$CuBr_2$]: [PMDETA] = 0.8:0.8, compared to styrene polymerization) for the same $[M]_0/[I]_0$ initiator ratio (500:1) and in the presence of free initiator, 2-ethylbromoisobutyrate (0.06 mol eq), at 70 °C. After PMMA grafting reactions, the C=O stretching band was found to be stronger near 1750 cm^{-1}, as observed by ATR-FT-IR analysis. Moreover, the antisymmetric C-O-C stretching mode in esters gives rise to a very strong and quite broad band near 1200 cm^{-1} (Chapter 4.1, Figure 4.1.1e). More precisely, ^{1}H-NMR spectrum

(Chapter 4.1, Figure 4.1.6, curve B)) of degrafted PMMA chains supports the conclusion of the successful degrafting reactions. Unlike styrene polymerization, sacrificial initiator was adopted instead of the $CuBr_2$ deactivator for MMA polymerizations. In the presence of deactivating species, the rate of reaction and percentage of conversion was found to be very slow especially at lower monomer to initiator ratios. The M_w/M_n values of the degrafted polymers are more or less comparable with those of the sacrificial initiator system (Table 4.2.2). In the presence of sacrificial initiator, good control over molar mass and faster reactions was achieved for MMA polymerization up to 20 % conversion. Increasing the monomer to initiator ratio also tends to the formation of more free polymer in the reaction media. One possible explanation can be as follows: since the system is diluted there might be a competition arising between sacrificial initiator and initiator grafted silica particles towards polymerization. Figure 4.2.3(a-c) shows the MMA polymerizations data from Si_{12} and Si_{20} based initiators.

The number average molar mass vs. conversion plot shows that the molar mass increases gradually with time. Here also, good control of molar mass was observed below 20 % conversion. In MMA polymerization reactions, a difference in molar mass of $\leq$ 7000 g/mol and $\leq$ 5000 g/mol were observed for PMMA chains grown from Si_{12} and Si_{20} particles, respectively, when compared with their respective theoretical molecular weights near to 20 % conversion.

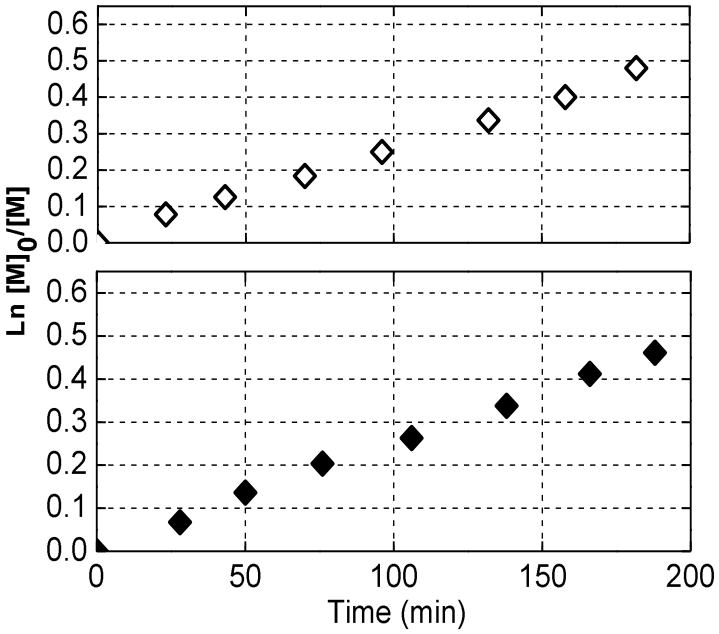
Ln [M]0/[M]
0.0
0.1
0.2
0.3
0.4
0.5
0.6
0
50
100
150
200
Time (min)

(a)

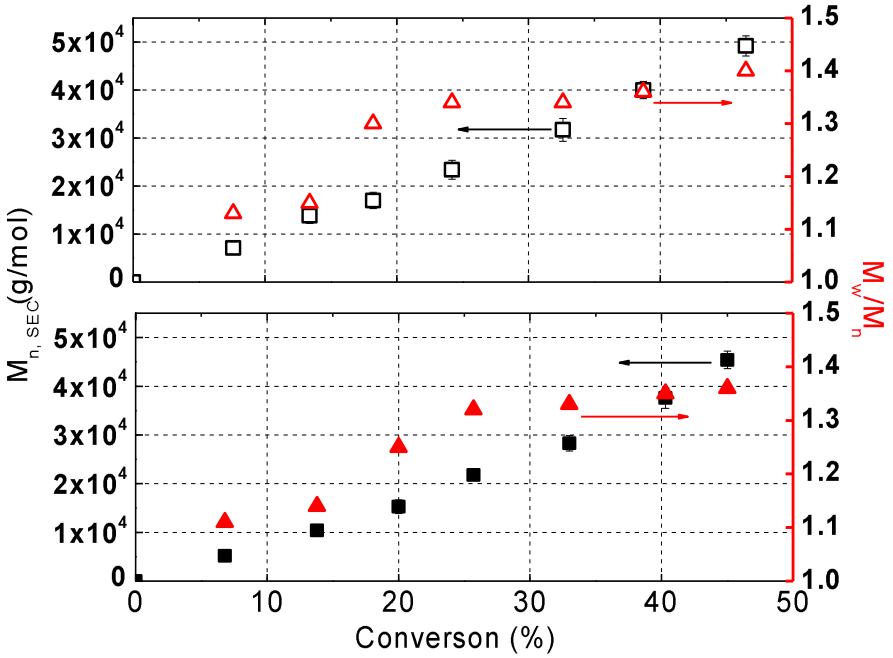
Mn, SEC(g/mol)
Mw/Mn
0
1x10^4
2x10^4
3x10^4
4x10^4
5x10^4
1.0
1.1
1.2
1.3
1.4
1.5
0
10
20
30
40
50
Converson (%)

(b)

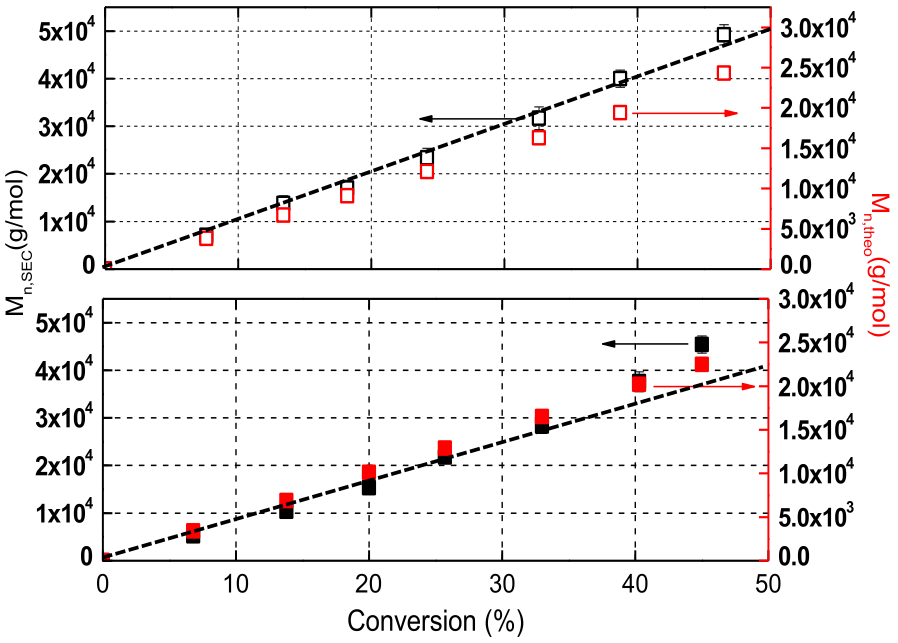

(c)

Figure 4.2.3. SI-ATRP of MMA at 70 ^{0}C from silica nanoparticles. (a) semi logarithmic plot of monomer conversion versus time from functionalized Si_{20} (♦) and Si_{12} (◊) particles respectively. (b) number average molar mass of degrafted PMMA vs. conversion from the surface functionalized Si_{20} (■, ▲) and Si_{12} (□, Δ) particles and (c) experimental and theoretical molar mass vs. conversion from Si_{20} (■, ■) and Si_{12} (□, □) in the presence of sacrificial initiator (2-EBriB). $M_{n(theo)}$= $[M]_0/[I]_0$ x % of conversion x $M_{\text{molar mass of monomer}}$. $[M]_0/[I]_0$ = initial monomer to initiator ratio.

When polymerization reactions were carried out in the absence of sacrificial initiator for the same monomer to initiator ratio, the molar mass of degrafted PMMA chains from Si_{12} particles was 30.5 kg/mol with a polydispersity 1.33 for 18.4 % conversion. Similarly, from Si_{20} particles, a molar mass of 26.6 kg/mol was obtained for a conversion 17.8 % with a polydispersity of 1.3. The respective theoretical molar masses from Si_{12} and Si_{20} particles are 9,200 g/mol and 8,900 g/mol. The difference between experimental and theoretical molar masses is high in the absence of sacrificial initiator. Moreover, molar mass distribution of surface-grafted chains is higher than of free polymer indicating a different growth of polymer chains from solution and surface

leading to lack of control on polymerization. This is more prominent with smaller particles like Si_{12} and may arise from the interparticle segregation during polymerization.

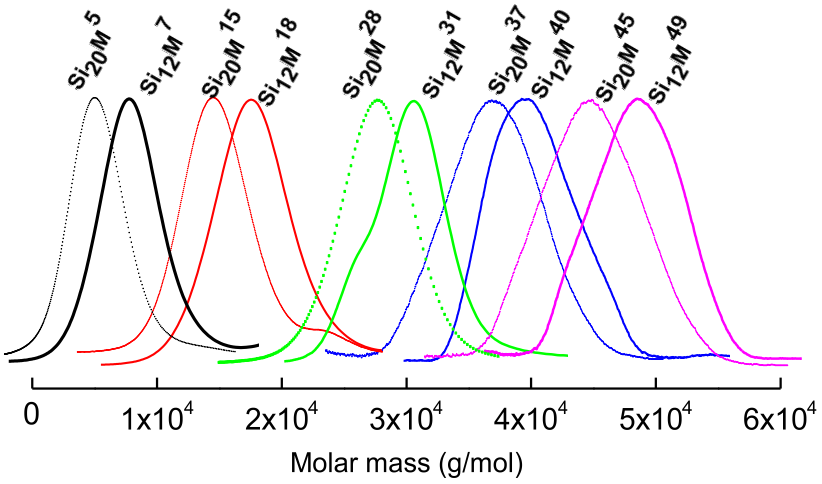

Figure 4.2.4. GPC (signal from IR detector) curves of PMMA degrafted from Si_{12} and Si_{20} silica particles at different conversions. Curves with solid lines are for PMMA degrafted from Si_{12} and dotted lines are those from Si_{20} particles respectively. (The subscript *x* and superscript *b* in Si_xM^b denotes the average core diameter of silica nanoparticle and molecular weight of degrafted PMMA in kg/mol, respectively)

So, one possible explanation can be that the concentration of added free initiator is adequate and efficient to control growth of polymer chains from surface and solution up to 20 %. The rate of polymerization from Si_{12} particles is comparatively higher than that from Si_{20}Up to 20 % conversion, for similar concentration of brominated silica particles, better control of polymerization was observed from Si_{20} particles. The increasing molar mass of growing chains might lead to aggregation and it might be more prominent in the case of polymerization from smaller Si_{12} particles than Si_{20} particles. The loss of initiator efficiency and control over polymerization is observed at higher conversions by the discrepancy in molar mass. The

concentration of the added sacrificial initiator might be efficient for polymerizations only up to 20 % conversion. Above this value, the GPC curves (see Figure 4.2.4.) of degrafted PMMA chains from both sets of particles exhibit peak broadening at high conversions pointing towards the occurrence of cross linking or branching. This interpretation is supported by the increase of polydispersities observed from the dependence of molar mass vs. conversion plots (Figure 4.2.3 (b)).

It is known that the polymerization occurred both in solution and from the surface of the silica particles. Therefore, the rate of growth of polymer chains from surface initiated styrene polymerization (in the presence of $CuBr_2$ deactivator) and MMA polymerizations (in the presence of free initiator, 2-ethylbromoisobutyrate) from both phases has been checked. Table 4.2.2 also describes the molar mass distribution of free polymer generated from styrene and MMA polymerizations of Si_{12} and Si_{20} particles. The molar mass and the PDI of the free polymer generated in solution from surface initiated styrene and MMA polymerization show only a small difference from the corresponding values of the degrafted polymer chains. This indicates that almost the same rate of polymerization occurred from surface and in solution for styrene (in the presence of deactivator, $CuBr_2$) and MMA (in the presence of free initiator) polymerizations up to 20 % conversion. Again in MMA polymerization, one could see that the polymerization reaction is controlled up to 20 % conversion as it is the case for styrene polymerization. Apart from the reported studies, the overall reaction kinetics of styrene and MMA polymerization from either modified silica nanoparticles indicate the efficiency of polymerization reaction even at higher bromide concentration (0.4 mmol/g). The reaction control and the behavior of either polymer modified Si_{12}/Si_{20} particles just beyond 20 % conversion was investigated by the following thermal characterization.

4.2.2.3. Thermal characterization of polymer modified silica nanoparticles

It is known that the glass transition temperature (T_g) is strongly influenced by the mobility of polymer chains. T_g values of polymer tethered silica particles depend on the graft molecular weight, weight fraction of silica content and the nature of silica particles. Differential scanning calorimetry (DSC) was used to analyse the behaviour or the dependence of T_g in PS/PMMA tethered Si_{12}/Si_{20} nanoparticles near 20 % conversion (good control on polymerization) and in those particles synthesized just beyond 20 % conversion in order to check the control over polymerization reaction is existing or not (Table 4.2.3). For styrene polymerization, the T_g value of $^{54}Si_{12}PS_{46}{}^{16}$ particles (superscript 54 for the weight fraction of Si_{12} particles in %; subscript 12 for average core diameter in nm; subscript 46 for weight fraction of grafted PS in % and superscript 16 for graft molecular weight in kg/mol) at 19 % conversion was observed at 98±1 ^oC and for corresponding $^{55}Si_{20}PS_{45}{}^{17}$ particles at 18 % conversion is 96±1 ^oC. The T_g value of PS modified Si_{12} particles is found to be slightly higher than respective Si_{20} particles. At 26 % conversion, $^{46}Si_{12}PS_{54}{}^{24}$ particles show a slight increase in T_g value to 100±1 ^oC and for the corresponding $^{46}Si_{20}PS_{54}{}^{22}$ particles at 24 % conversion is 97±1 ^oC.

Table 4.2.3 T_g values in PS/PMMA tethered Si_{12}/Si_{20} nanoparticles near 20 % conversion and beyond 20 % conversion

Grafted polymer	**Fraction of polymer** (Wt.-%)	M_n (kg/mol)	T_g (^0C)	**Diameter of SiO_2** (nm)
PS	46	16	98	12
	45	17	96	20
	54	24	100	12
	54	22	97	20
PMMA	48	17	115	12
	45	15	113	20
	56	23	118	12
	55	22	115	20

For MMA polymerization, $^{52}Si_{12}M_{48}^{17}$ and $^{55}Si_{20}M_{45}^{15}$ particles exhibited T_g values of 115±1 ^oC and 113±1 ^oC at 18.2 % and 20 % conversions respectively. Like styrene polymerization, similar behaviour was observed for MMA polymerization beyond 20 % conversion. At 24 % conversion, $^{44}Si_{12}M_{56}^{23}$ particles show a T_g value of 118±1 ^oC. Whereas, the $^{45}Si_{20}M_{55}^{22}$ particles have a T_g value of 115±1 ^oC at 26 % conversion.

The slight increase in the value of glass transition temperature from either polymer tethered silica (Si_{12} and Si_{20}) nanoparticles beyond 20 % conversion can be due to the evolution of T_g with molecular weight and the weight fraction of silica in the hybrid particles. Similar observation was made by Matyjaszewski et al.[11] from silica (20 nm) nanoparticles grafted with polystyrene chains. Moreover, the DSC curves do not show any broad T_g, no asymmetry and bimodality (not shown) that can be arise from interparticle crosslinking. So, this discards the possibility of interparticle crossslinking from either modified Si_{12}/S_{20} particles for respective conversions (beyond 20 %). The T_g value of either polymer tethered Si_{12} particles was observed to be always slightly higher than Si_{20} particles may arise from the effect of *curvature* of particles. This again point towards the efficiency of the present system with high initiator concentration (0.4 mmol/g) to control polymerization at conversions above 20%. The thermal characteristics of untethered chains just beyond 20 % conversion might give more insight into the relation between glass transition temperature and molecular weight than the grafted ones. But the occurrence of bimodal or broadened peaks in the GPC curves of degrafted polystyrene and poly(methyl methacrylate) chains at higher conversion are the most definite proof for the lack of reaction control.

4.2.2.4. Morphology of polymer grafted silica particles

The morphology of spherical polymer brushes (PB's) in the solid state was analyzed by using transmission electron microscopy (TEM). Dilute solutions of initiator modified silica particles and polystyrene/PMMA grafted Si_{12} and Si_{20} colloids in good solvent toluene were cast onto carbon coated TEM grids and analyzed after evaporation of the solvent. Figure 4.2.6 (a) represents the TEM image of well dispersed Si_{12} particles grafted by polystyrene (34 kg/mol) with 67 wt % polymer content. The calculated diameter of the resulting $Si_{12}PS_{62}$[34] was 84 ± 3 nm, the value is in accordance with the value obtained from DLS (see Table 4.2.4). Figures 4.2.5 (b) and (c) represent clusters of polystyrene (7 kg/mol, 28 wt %) and PMMA (17 kg/mol, 60 wt %) grafted Si_{12} silica particles. One observation from the above figures is that the shorter the grafted chains, the shorter will be the distance between particles.[11]

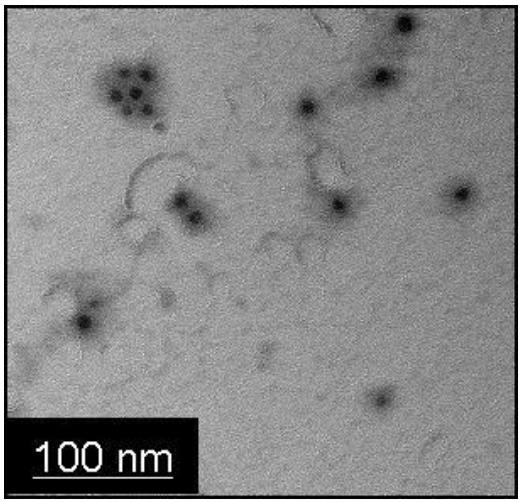

(a)

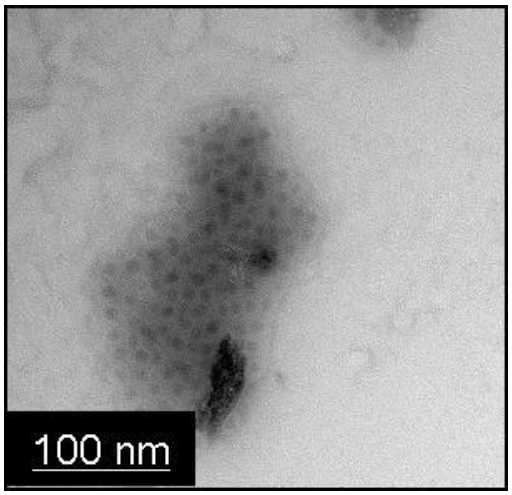

(b)

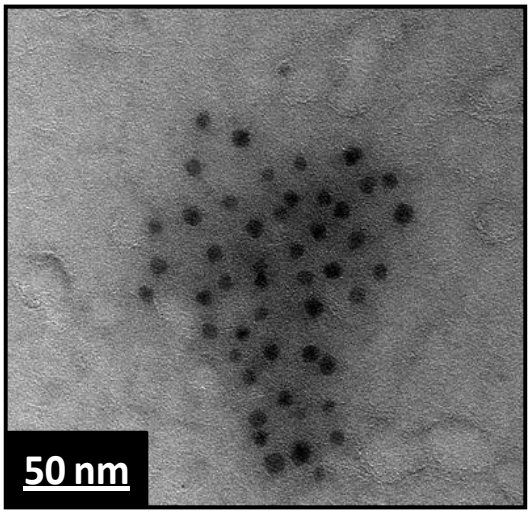

(c)

Figure 4.2.5. Selective TEM images of polymer grafted Si_{12} colloids casted onto a carbon-coated copper grid (a) ultrathin films of Si_{12} PS^{34} ($M_{n\ tethered\ PS}$ = 34 kg/mol) (b) $Si_{12}PS^{7}$ ($M_{n\ tethered\ PS}$ = 7 kg/mol) (c) $Si_{12}M^{17}$ ($M_{n\ tethered\ PMMA}$ = 17 kg/mol).

4.2.2.5. Size distribution of polymer brushes

Silica nanoparticles (12 and 20 nm) grafted with polystyrene and poly(methyl methacrylate) of various molar masses have been prepared. Table 4.2.4. summarizes the observed average diameters (approximate) of silica polymer brushes synthesized at higher conversions obtained from DLS measurements.

The variations in average diameters of polymer brushes at higher conversion are explained on the basis of the results from kinetics and GPC measurements. The basic dimensions of silica nanoparticles have been measured as follows. First a drop of diluted solution, as obtained from the supplier, was dried on a carbon-coated grid and imaged by TEM. The number-average particle diameters D_n = 12 ± 5 nm and D_n = 20 ± 5 nm were determined, respectively, by direct measurement of not less than hundred nanoparticles. Secondly, the above sample solutions were

subjected to DLS measurements, the resultant diameters obtained are higher than the TEM analysis, $2R_h = 14 \pm 2$ nm for Si_{12} and $2R_h = 22 \pm 4$ nm for Si_{20} particles. Both measurements indicate that the base particle dimensions are greater than those expected from the average particle dimensions (12 and 20 nm) advertised by the manufacturer. The difference between D_n and $2R_h$ is attributed to the polydispersity effects, since the DLS measurements are strongly weighted by larger particles.

Table 4.2.4. Details of the grafted molar mass and hydrodynamic diameter calculated from DLS measurements.

Sample Code [a]	G_p Wt.-% [b]	M_w/M_n	M_n (kg/mol) [c]	σ/a^2 (chains/nm^2) [d]	$2R_h$ (nm) [e]
Si_{12} PS_{62}^{34}	62	1.32	34	0.16	74±9
Si_{12} PS_{80}^{53}	80	1.38	53	0.2	100±10
$Si_{12}M_{58}^{31}$	58	1.34	31	0.15	77±9
$Si_{12}M_{83}^{48}$	85	1.4	50	0.27	130±10
Si_{20} PS_{58}^{28}	58	1.22	28	0.19	56±8
Si_{20} PS_{75}^{47}	75	1.34	47	0.3	115±9
$Si_{20}M_{53}^{28}$	53	1.33	28	0.16	75±5
$Si_{20}M_{68}^{46}$	68	1.36	46	0.32	130±10

a) $Si_xPS_y^a$ or $Si_xM_y^b$, subscripts x and y stands for average particle diameter in nms (here it is 12 and 20) and wt. fraction (%) of grafted polymer chains measured from TGA and superscripts a and b for molecular weight of grafted PS and PMMA in kg/mol. PS for polystyrene and M for poly (methyl methacrylate) b) wt. fraction (%) of grafted polymer obtained from TGA. C) molecular weight of degrafted polymer d) graft density determined from TGA measurements[27] e) calculated from DLS measurements.

The DLS measurements of polystyrene/poly(methyl methacrylate) coated Si_{12} and Si_{20} nanoparticles were carried out in solvent toluene at room temperature. The hydrodynamic radii of isolated, non interacting and coiled homopolymers like PS and PMMA of various molecular weights in good solvent toluene at temperature close to room temperature was reported in literature.[28-30] Some of these reported values were determined through DLS and other methods, on an inter-laboratory analysis basis. On the above basis, in the range of molecular weights (for

both PS and PMMA) given in present work, the hydrodynamic radii ranges between 4 to 8 nm if these macromolecules assumed an isolated, non interacting, coiled conformation. If either Si_{12} or Si_{20} silica particles are decorated with such kind of macromolecules, the size should be increased from 18 to 30 nm with increasing M_n of the polymer. Certainly, this is the lower limit.

Taking into account of above facts, in the present case, the unusual increase in the hydrodynamic diameters of silica grafted with polymer brushes at higher conversion are explained by combining the results from kinetics and GPC measurements. Both types of silica particles (Si_{12} and Si_{20}) grafted with polystyrene and poly(methyl methacrylate) show a common trend of increasing hydrodynamic radius with increasing molar mass. This indicates that the chains adopted a stretched conformation from the surface. Combining the results from GPC and DLS gives valuable information about the extent of chain transfer and chain termination occurring during polymerization from different particle surfaces. The hydrodynamic diameter of the polystyrene grafted Si_{12} and Si_{20} particles shows a gradual increase of size with the length of polymer brush. Patterson et al.[11] reported the size distribution of PS grafted from 20 nm silica nanoparticles synthesised by ATRP under conditions avoiding interparticle radical coupling. They measured a close to linear evolution of M_n with sizes that locates in between fully extended and fully coiled chains.

However, much larger hydrodynamic diameters are measured for polystyrene/silica nanohybrids characterized by the highest molar mass of degrafted polymer chains ($Si_{12}PS_{80}^{53}$, 53,000g/mol and $Si_{20}PS_{75}^{47}$, 47,000g/mol). Considering the fact that DLS measurements are highly weighted by the existence of larger particles, these results points towards the possibility of inter/intra-particle radical coupling reactions or particle segregation at very higher conversions as assessed on the basis of kinetic studies and the molar mass distributions obtained from GPC (Figure

4.2.2). Indeed, this could leads to the formation of aggregates of PS coated nanoparticles and increasing the amount of bigger particles in the sample.

When the hydrodynamic diameter of particles $Si_{12}PS_{62}^{34}$ (34,000 g/mol) and $Si_{20}PS_{58}^{28}$ (28,000 g/mol) are compared, the effective diameters are 74 ± 9 nm and 56 ± 8 nm for PS chains characterized by PDI values 1.32 and 1.22, respectively. The observed hydrodynamic diameter of $Si_{20}PS_{58}^{28}$ (56 ± 8 nm) is lower than the one reported by Patterson et al.[11] for PS grafted (about 30,000 g/mol, $2R_h$~90 nm) 20 nm sized silica particles measured in solvent toluene, while they claim the absence of interparticle coupling reactions. Among the above polystyrene grafted Si_{12} and Si_{20} particles, PS grafted Si_{12} have larger diameter than the corresponding Si_{20}. Further, kinetic studies shows that the reaction from Si_{20} particles is better controlled when compared to the same from Si_{12}. Since the size of the Si_{20} core is larger but the initiator molecular surface density is essentially the same as for Si_{12} particles (~ x molecules of initiator/ nm^2), the polymer chains are more stretched and more sterically crowded when compared to silica particles with smaller core diameter, due to the weaker curvature of the surface.[31] On increasing the molecular weight of tethered PS chains the hydrodynamic diameter was also found to be increased (already discussed in previous paragraph). With the above few points one cannot predict whether the evolution of size is linear. But the obtained values of hydrodynamic diameter from either modified silica particles are below the one reported by Patterson et al.[11] Since the initiator density on both Si_{12}/Si_{20} particles is much higher (0.4 mmol/g) than in the publication (0.135 mmol/g), one could expect more extended polymer brushes. All the above observations lead to the inference that, in the present case no significant interparticle radical coupling occurs and the large size measured are possible without this coupling. Also, the bimodal behaviour/peak broadening observed at higher conversions may result from intraparticle radical coupling.

Similarly, DLS experiments were carried out with dispersion of PMMA grafted silica particles. The Si_{12} particles modified with PMMA show a wider variation in the hydrodynamic diameter for $Si_{12}M_{58}^{31}$ (77 ± 9 nm, for 31,000 g/mol) and $Si_{12}M_{85}^{50}$ (130 ± 10 nm, for 50,000 g/mol) in comparison with the other samples. A similar behavior was observed for PMMA chains degrafted from Si_{20} particles. The lack of reaction control and the probability of radical coupling at higher conversions (as in PS grafted silica particle discussed above) on the basis of broadened peaks in GPC is an indication to the strong increase of hydrodynamic diameter in solvent. The grafting densities of the respective tethered chains are also presented in Table 4.2.4. Moreover, on the basis of the above results, control over the molar mass is achievable when the reaction is carried out with deactivator ($CuBr_2$) or sacrificial initiator (2-EBriB) in the case of styrene or MMA polymerization from particle surfaces, respectively. Also, the interparticle segregation was found to be higher with smaller particle size.

4.2.3. Conclusions

The efficiency of initiator grafted Si_{12} and Si_{20} particles (discussed in chapter 4.1) towards styrene and MMA polymerizations was studied. For this, the initiator concentration was kept the same on both particles. The reaction was found to be under good control up to 20 % conversion. Here we investigated the efficiency of carrying out styrene/MMA polymerization from silica colloidal initiators having higher concentration (0.4 mmol/g) than those previous reported studies at lower initiator concentration. The rate and control on MMA polymerization was found to be better up to 20 % from Si_{20} particles. The rate of MMA polymerization from Si_{12} particles was found to be faster than from Si_{20}. Slight increase in T_g value was observed for either polymer tethered Si_{12} nanoparticles than Si_{20} particles. Absence of asymmetry or bimodality in DSC curves from either Si_{12}/S_{20} particles discards the possibility of interparticle crosslinking reactions

for the respective conversions beyond 20 %. This again point towards the efficiency of the present system with high initiator concentration (0.4 mmol/g) to control polymerization at conversions above 20% to good extend. The rate and control on MMA polymerization was found to be better from Si_{20} particles. The rate of MMA polymerization from Si_{12} particles is faster than from Si_{20}. On the basis of above reactions from both type of particles, chances of aggregation through interparticle coupling seems to be more important when particle size decreases. Even though studies reported the linear behaviour of increasing hydrodynamic diameter of silica grafted PS with increasing molar mass, the observed values under similar conditions in the present work are below their values.

4.2.4. References

1. J. S. Wang, K. Matyjaszewski, *Macromolecules* 1995, 28, 7901.
2. J. S. Wang, K. Matyjaszewski, *J. Am. Chem. Soc*. 1995, 117, 5614.
3. K. Matyjaszewski, J. Xia, *Chem. Rev*. 2001, 101, 2921.
4. M. Kamigaito, T. Ando, M. Sawamoto, *Chem Rev*. 2001, 101, 3689.
5. W. A. Braunecker, K. Matyjaszewski, *Prog. Polym. Sci*. 2007, 32, 93.
6. N. V. Tsarevsky, K. Matyjaszewski, *Chem. Rev*. 2007, 107, 2270.
7. X. Y. Huang, M. Wirth, *J. Anal. Chem*. 1997, 69, 4577.
8. M. Ejaz, S. Yamamoto, K. Ohno, Y. Tsujii, T. Fukuda, *Macromolecules* 1998, 31, 5934.
9. M. Alexandre and P. Dubois in *"Macromolecular Engineering: Precise Synthesis,Materials Properties, Applications"*, Vol.4, Chapter 2, K. Matyjaszewski, Y. Gnanou and L. Leibler. Wiley-VCH; Weinheim, 2007, 2033-2070.
10. R. Barbey, L. Lavanant, D. Paripovic, N. Schüwer, C. Sugnaux, S. Tugulu, H. A. Klok, *Chem. Rev*. 2009, 109, 5439-5452.
11. D. A. Savin, J. Pyun, G. D. Patterson, T. Kowalewski, K. Matyjaszewski, *J.Polym. Sci. Part B: Polym. Phys.* 2002, *40*, 2667-2676.
12. J. P. A. Heuts, T. P. Davis, *Macromol. Rapid Commun*. 1998, 19, 371.
13. H. Fischer, *J. Polym. Sci., Part A: Polym Chem*. 1999, 37, 1885.
14. D. A. Shipp, K. Matyjaszewski, *Macromolecules* 2000, 33, 1553.

15. A. Goto, T. Fukuda, *Prog. Polym. Sci*. 2004, 29, 329.
16. M. Al-Harthi, L. S. Cheng, J. B. P. Soares, L. C. Simon, *J. Polym. Sci, Part A: Polym Chem*. 2007, 45, 2212.
17. W. Tang, K. Matyjaszewski, *Macromol. Theory Simul*. 2008, 17, 359-375.
18. K. Matyjaszewski, P. J. Miller, N. Shukla, B. Immarapom, A. Gelman, B. B. Luokala, T. M. Siclovan, G. Kickelbick, T. Vallant, H. Hoffmann, T. Pakula, *Macromolecules* 1999, 32, 8716.
19. T. von Werne, T. E. Patten, *J. Am. Chem. Soc*. 2001, 123, 7497-7505.
20. G. Carrot, S. Diamanti, M. Manuszak, B. Charleux, J. –P. Vairon, *J. Polym. Sci. Part B: Polym. Chem*. 2001, *39*, 4294-4301.
21. T. von Werne, T. E. Patten, *J. Am. Chem. Soc*., 1999, 121, 7409-7410.
22. J. Pyun, S. Jia, T. Kowalewski, G. D. Patterson, K. Matyjaszewski, *Macromolecules* 2003, *36*, 5094-5104.
23. A. E. Harrak, G. Carrot, J. Oberdisse, C. E. Baron, F. Boue, *Macromolecules* 2004, *37*, 6376-6384.
24. K. Ohno, T. Morinaga, K. Koh, Y. Tsujii, T. Fukuda, *Macromolecules*, 2005, 38, 2137.
25. M. Husseman, E. Mamstrom, M. McNamara, M. Mate, D. Mecerreyes, D. Benoit, J. Hedrick, P. Mansky, E. Huang, T. Russel, C. Hawker, *Macromolecules* 1999, 32, 1424.
26. J. Pyun, S. Jia, T. Kowalewski, G. D. Patterson, K. Matyjaszewski. *Macromolecules* 2003, 36, 5094-5104.
27. M. Save, G. Granvorka, J. Berard, B. Charleux, C. Boissière, D. Grosso, C. Sanchez, *Macromol Rapid Commun*, 2006, *27*, 394.
28. K. Huber, S. Bantle, P. Lutz, W. Burchard, *Macromolecules*, 1985, *18*, 1461-1467.
29. L.J. Fetters, N. Hadjichristidis, J. S. Lindner, J. W. Mays, *J. Phys. Chem. Ref. Data*, 1994**,** *23*, 619-640
30. T. Arai, N. Sawatari, T. Yoshizaki, Y. Einaga, H. Yamakawa, *Macromolecules*, 1996, *29*, 2309-2314.
31. M. K. Corbierre, N. S. Cameron, M. Sutton, K. Laaziri and R. B. Lennox, *Langmuir*, 2005, 21, 6063-6072.

4.3. Study of the Mechanical, Thermal and Morphological Characteristics of PMMA Composites Comprising Modified Si_{12} and Si_{20} Particles: Effect of Silica Core Size, Graft Density and Graft Molar Mass

4.3.1. Introduction

Nanoscale particles have generated great interest in the field of polymer composites owing to the potential benefits associated with a large surface area-to-volume ratio and dimensions equal to or smaller than the polymer coil radii of gyration.[1] In order to achieve maximal property improvement, optimal structure control and good dispersion of NP's (NP's) in a polymer matrix is necessary. This applies to mixtures with all sorts of polymers like homopolymers, block copolymers and also random copolymers. However, in the absence of particle-particle repulsive forces, van der Waals attraction between NP's favors clustering and gross aggregation.[2-3] This can be reduced to a good extend by surface modification.[4-5]

As we have seen in the introduction and in Chapter 4.2, nowadays grafting of long polymer chains onto the surface functionalized NP's (*grafting from* technique), more precisely *core-shell* particles, received much attention in order to facilitate their better dispersion in a polymer matrix. In most cases, the matrix and graft polymers contain identical repeat units but may have different molecular weights. A good compatibility between graft and matrix polymers can be achieved by using polymer combinations characterised by a negative Florry-Huggins interaction parameter. The extend of dispersion, rheological behavior[6] and thermo mechanical behaviour[7] of polymer matrix containing polymer grafted particles is determined by several parameters including the graft density (σ)[8-9] of anchored chains, length (L) of tethered and matrix polymer chains[10-13], the chemical composition and molecular weight of the graft (M_g) and matrix (M_m)

polymers,[14] polymer-particle interaction energy[15] and the size (*curvature*)[16-18] and nature of NP's. Computer modelling studies have shown that molecular weight of the grafted polymer chains and the density of surface attachment contribute to the degree of swelling of the grafted chains in the matrix polymer.[13,19]

Relative to the graft size, in low and high molecular weight matrices, uniform dispersion and extensive aggregation are obtained, respectively.[20-25] Most of these works were carried out in films and in dispersions. To our knowledge, no detailed work regarding the changes in the mechanical properties of polymer composites by considering all these parameters has been reported yet. A question arising in the present context is, how the nature of dispersion and final tensile and impact properties of a polymer nanocomposite with constant matrix molar mass is influenced by the grafted particles of varying particle size, graft density and chain length?.

Theoretical calculations and simulations showed that depending on the size relative to the length of the polymer chain and surface chemistry, NP's can either be located in the middle of the domain or at the interface separating two domains.[23] Bates et al. [14] described the mixing behaviour of silica NP's, grafted with polystyrene chains of various molecular weights in homopolymer and block copolymer. Increasing the molecular weight of polystyrene homopolymer matrix induces aggregation of grafted silica particles. All the above studies regarding the dispersion of grafted NP's in homopolymer or block copolymer matrices were done in solvent casted films.

In the present research work, for the first time the effect of varying molecular weights, graft density of tethered polymer chains and the core size of silica NP's on dispersion and the final tensile and impact properties of PMMA composite have a constant graft molar mass is investigated. In order to make sure a defined quantity of modified or unmodified particles in

polymer matrix, first they were trapped in the polymer matrix by solvent casting, dried and followed by the melt compounding of stripes from composite films. The morphological characterization of ultracut thin films of nanocomposite extrudates was carried out by means of transmission electron microscopy (TEM) analysis.

4.3.2. Discussion of Results

4.3.2.1. Mechanical properties of PMMA composites with Silica-*g*-(PMMA) particles

Grafting of poly(methyl methacrylate) (PMMA) on silica particles, Si_{12} and Si_{20} was carried out by the general procedure described in Chapter 3. A commercial PMMA matrix having a molar mass of 49,000 g/mol and PDI value 1.8 was chosen for composite preparation. Three different grafting densities in the ranges ≤ 0.2, ≤ 0.3, and ≤ 0.5 chains / nm^2 were chosen for tethering polymer chains from both Si_{12} and Si_{20} particles. The details of silica-polymer hybrid particles used for composite preparation are given in Table 4.3.1.

The composites were prepared according to the method described in Chapter 3. The detailed description of the mechanical properties of PMMA and its composites containing Si_{12} and Si_{20} (*core*) modified by PMMA (*shell*) of varying graft density is given in Table 4.3.1 and Table 4.3.2, respectively. The percentage of silica content in the PMMA composites was varied from 0 to 2 wt %. Pristine PMMA shows a tensile modulus of 3400 ± 45 MPa, tensile strength of 75 ± 1 MPa, elongation at break of 5 ± 2 %and impact strength of 15 ± 1 kJ/m^2. The difference in the sizes of silica core particles (Si_{12} (12 nms) and Si_{20} (20 nms)) chosen for the present study is relatively small.

Table 4.3.1. Details of various PMMA modified Si_{12} and Si_{20} particles synthesised by *grafting from* polymerization used for composite preparation

Sample code	M_n (kg/mol) [a)]	G_p Wt.- (%) [b)]	**Silica content** (%) [c)]	σ (chains/nm^2) [d)]	T_b (nm) [e)]	T_g (^oC) [f)]	T_g (^oC) [g)]
$Si_{12}M_{58}^{31}$	31	58	42	0.15	28	115.7	111.8
$Si_{12}M_{83}^{48}$	48	83	15	0.27	50	118.7	
$Si_{12}M_{92}^{72}$	72	92	8	0.43	72	120	117.6
$Si_{20}M_{53}^{28}$	28	53	42	0.16	21	115.3	111.7
$Si_{20}M_{68}^{46}$	46	68	32	0.32	54	118	
$Si_{20}M_{88}^{67}$	67	88	12	0.46	68	118.2	117.3

$Si_xM_y^a$: the subscripts x and y corresponds to average particle diameter in nm and weight fraction of grafted polymer measured from thermogravimetry (TGA) respectively; superscript a for molecular weight of grafted polymer. a) molecular weight of degrafted PMMA chains. b) weight fraction (%) of grafted polymer determined by thermogravimetric measurement c) weight fraction of silica (%) measured from TGA d) graft density e) approximate brush thickness calculated theoretically from DLS measurements using the equation, $T_b = (D_{Si\text{-}P.B}\text{-}D_{Si})/2$, where $D_{Si\text{-}PB}$ is the approx. diameter of polymer brush grafted silica in nm measured from DLS and D_{Si} is the diameter of pristine core silica particle in nm f) glass transition temperature obtained from DSC measurements. g) glass transition temperature of degrafted PMMA chains using HF.

By the addition of both sets of unmodified, Si_{12} and Si_{20}, particles some improvement in tensile and impact properties is obtained. The nanocomposite containing 1.5 wt % of Si_{12} particles shows better tensile and impact properties when compared to the one with Si_{20} particles (Table 4.3.2 and Table 4.3.3). This point toward the fact that the size of pristine NP's may have some influence on the properties, even though the improvement is not much.

It is an already observed fact that NP's can improve mechanical properties of composites at small loadings. An improvement in tensile and impact properties was observed by Hong et al.[26] in PMMA composites. Similarly, Bikiaris et al.[27] observed a small improvement in tensile and impact strength as well as elongation at break of isotactic polypropylene (iPP) composites containing 2.5 wt% silica NP's prepared by melt compounding. However, the mechanical

properties of the unmodified silica nanoparticle-reinforced poly(ethylene 2,6-naphthalate) (PEN) composites tended to be worse than those of pristine PEN.[28]

Further, mechanical properties of films of polyisoprene -silica hybrids prepared by sol-gel process show a maximum improvement in tensile strength and elongation at break for a net silica content of 10 wt%.[29] Polyamide-6 showed a decrease in tensile modulus, elongation at break and impact strength with increasing silica content.[30] Thus controlling the interactions and hence the spatial dispersion of NP's is critical to the ultimate goal of producing polymer nanocomposites with desired macroscale properties. Experimental studies have already shown that unmodified NP's aggregate into clusters and hinder further spatial dispersion due to the lack of proper interfacial adhesion between the matrix and NP's.[21,31] This indicates the necessity of surface modification. As already described before (Chapter 4.1), (3-glycidoxypropyl) trimethoxysilane (GPS) is used as the silane coupling agent for anchoring ATRP initiator (2-BriB) followed by grafting of PMMA chains. In the present case, we checked the compatibility of epoxy silane modified Si_{12} and Si_{20} particles in PMMA matrix towards mechanical properties. In both cases, a slight improvement in tensile modulus, impact and tensile strength was observed in comparison to the pristine silica containing composites (Table 4.3.2 and Table 4.3.3). Even though the improvement is not so large, an improvement in tensile modulus was observed for $PMMA^{49}\_Si_{12}G^{12}$ composites.

Epoxy silanes are widely used for particle-based coating applications because of their capability to improve interfacial strength between inorganic and organic phases in composite bulk materials leading to increased abrasion resistance, hardness etc.[32-34] Moreover, Hong et al.[26] reported an improvement in mechanical properties like tensile strength, flexurial and impact strength of PMMA composites containing silane modified silica particles. They adopted KH570 silane ((γ–

methacryloxypropyl) trimethoxysilane) as the coupling agent for grafting poly (methyl methacrylate) chains in the presence of AIBN (Azo-bisisobutyronotrile) initiator.

Table 4.3.2. Mechanical properties of pure PMMA (Plexiglas 6N glassklar) and PMMA composites containing pristine silica, silane modified silica and PMMA grafted Si_{12} particles extruded at 210 ^{o}C.

Sample code	**Tensile strength** σ_m (MPa)	**Tensile modulus** E (MPa)	**Elongation at break** ε_B (%)	**Impact strength** (*unnotched*) a_{cU} (kJ/m^2)	T_g (±1 ^{o}C) DSC	T_d (±1 ^{o}C) TGA
$PMMA^{49}$	75±1	3400±45	5±1	15±1	96.0	381.3
$PMMA^{49}\_^{1}Si_{12}$	75±2	3460±28	4±1	16±1		
$PMMA^{49}\_^{1.5}Si_{12}$	77±1	3530±30	3±2	16±1	98.6	390
$PMMA^{49}\_^{2}Si_{12}$	72±2	3390±46	2±1	14±2		
$PMMA^{49}\_^{1.5}Si_{12}G^{12}$	76±1	3573±36	3±2	17±1	98.7	391.4
$PMMA^{49}\_^{1}Si_{12}M_{58}^{31}$	77±2	3530±52	3±2	18±1		
$PMMA^{49}\_^{1.5}Si_{12}M_{58}^{31}$	80±2	3750±44	3±1	21±1	101.8	397.3
$PMMA^{49}\_^{2}Si_{12}M_{58}^{31}$	76±3	3620±38	2±1	17±2		
$PMMA^{49}\_^{1}Si_{12}M_{83}^{48}$	76±2	3532±40	3±1	15±2		
$PMMA^{49}\_^{1..5}Si_{12}M_{83}^{48}$	74±1	3630±39	3±1	14±1	100.2	398.2
$PMMA^{49}\_^{2}Si_{12}M_{83}^{48}$	71±2	3447±42	2±1	13±2		
$PMMA^{49}\_^{1}Si_{12}M^{72}$	67±2	3360±30	3±2	13±2		
$PMMA^{49}\_^{1.5}Si_{12}M_{92}^{72}$	66±3	3382±43	2±1	12±2	99.6	398.0
$PMMA^{49}\_^{2}Si_{12}M_{92}^{72}$	65±2	3265±43	2±1	11±1		

The tensile properties and impact results shown here are an average of those obtained from six samples of Dog bones (tensile measurements) and Composite blocks (impact measurements) respectively. $PMMA^{49}$: superscript 49 stands for the molecular weight (kg/mol) of PMMA matrix used for composite preparation. $PMMA^{49}\_^{x}Si_{12}$: superscript, x denotes the wt.- % of silica in the composite and subscript 12 denotes the average diameter of silica core in nm. $PMMA^{49}\_^{1.5}Si_{12}G^{12}$: superscript 1.5 denotes wt.- % of silica in the composite, G stands for (3-glycidoxypropyl) trimethoxysilane (GPS) and superscript 12 denotes the weight fraction (%) of coupled silane obtained from TGA. $PMMA^{49}\_^{x}Si_{12}M_y^{a}$: superscripts x and a denotes the wt-. % of silica in the composite and molecular weight (kg/mol) of grafted PMMA respectively; subscript y stands for weight fraction of grafted polymer (%) measured from TGA. Standard deviation is shown for values obtained from tensile and impact measurements. The results shown in table is obtained from PMMA composite incorporated with silica-polymer hybrid particles obtained after ATRP from colloidal silica initiators coupled through 12 wt % of GPS. T_g and T_d for glass transition temperature and temperature of decomposition of composites.

Other studies also reported an increase in the mechanical properties of polyisoprene (PI) and polyamide-6 (PA-6) composites by using silica modified by suitable coupling agents.[29-30] The utility of end-grafted polymer chains on NP's and several factors that control the dispersion have been already reviewed in the introductory part. For a comparative study, the silica content was varied from 0 to 2 wt % for polymer grafted Si_{12} and Si_{20} particles having different graft densities. In the entire PMMA-hybrid silica composites an optimum improvement in properties is observed for systems with silica content of 1.5 wt%. When we compare the properties of PMMA (M_n=49,000 g/mol) composites containing either $Si_{12}M_{58}^{31}$ (M_n=31,000 g/mol, graft density σ = 0.15, T_b=31 nm) or $Si_{20}M_{58}^{28}$ (M_n=28,000 g/mol, σ= 0.19, T_b=28 nm) particles, PMMA grafted Si_{12} shows improved properties.

One would expect a better property for those composites having similar molecular weight for matrix and grafted polymer. But in the case of PMMA composites containing either $Si_{12}M_{83}^{48}$ (M_n=48,000 g/mol σ = 0.27, T_b=50 nm) or $Si_{20}M_{68}^{46}$ (M_n=46,000 g/mol σ = 0.32, T_b=54 nm) particles, tensile and impact properties are found to reduced further with increasing silica content. But a slight improvement in tensile modulus was observed at 1.5 wt% loading of modified particles in both cases.

Here also PMMA modified Si_{12} particles lead to slightly better properties than the modified Si_{20} particles. In the present case, as we increase the molar mass of tethered chains beyond that of the molar mass of the matrix, the properties of the resultant composites exhibit no further improvement by the addition of either $Si_{12}M_{92}^{72}$ (M_n=72,000 g/mol σ = 0.43, T_b=72 nm) or $Si_{20}M_{88}^{67}$ (M_n=67,000 g/mol σ = 0.46, T_b=68 nm) particles.

Table 4.3.3. Mechanical and thermal properties of pure PMMA (Plexiglas 6N glassklar) and PMMA composites containing pristine silica, silane modified silica and PMMA grafted Si_{20} particles extruded at 210 ^{o}C.

Sample code	**Tensile strength** σ_m (MPa)	**Tensile modulus** E (MPa)	**Elongation at break** ε_B (%)	**Impact strength** (*unnotched*) a_{cU} (kJ/m^2)	T_g (±1 ^{o}C) DSC	T_d (±1 ^{o}C) TGA
$PMMA^{49}$	75±1	3400±45	5±2	15±1	96.0	381.0
$PMMA^{49}\_^{1}Si_{20}$	76±1	3430±36	4±2	16±2		
$PMMA^{49}\_^{1.5}Si_{20}$	76±2	3492±28	3±2	16±2	98.3	387.3
$PMMA^{49}\_^{2}Si_{20}$	72±3	3437±48	2±2	14±1		
$PMMA^{49}\_^{1.5}Si_{20}G^{7}$	77±1	3505±28	3±1	17±1	98.6	389.5
$PMMA^{49}\_^{1}Si_{20}M_{58}^{28}$	77±1	3575±27	4±2	16±1		
$PMMA^{49}\_^{1.5}Si_{20}M_{58}^{28}$	76±2	3660±48	3±2	18±1	101.2	397.0
$PMMA^{49}\_^{2}Si_{20}M_{58}^{28}$	72±1	3520±45	2±1	15±2		
$PMMA^{49}\_^{1}Si_{20}M_{68}^{46}$	73±1	3544±61	3±2	14±1		
$PMMA^{49}\_^{1.5}Si_{20}M_{68}^{46}$	72±2	3632±34	3±2	13±2	100.4	398.3
$PMMA^{49}\_^{2}Si_{20}M_{68}^{46}$	70±2	3466±33	2±1	12±1		
$PMMA^{49}\_^{1}Si_{20}M_{88}^{67}$	70±1	3420±61	3±1	13±2		
$PMMA^{49}\_^{1..5}Si_{20}M_{88}^{67}$	67±2	3347±46	2±1	11±2	99.0	398.2
$PMMA^{49}\_^{2}Si_{20}M_{88}^{67}$	65±3	3280±53	2±1	9±2		

The tensile properties and impact results shown here are an average of those obtained from six samples of Dog bones (tensile measurements) and Composite blocks (impact measurements) respectively. $PMMA^{49}$: superscript 49 stands for the molecular weight (kg/mol) of matrix PMMA used for composite preparation. $PMMA^{49}\_^{x}Si_{20}$: superscript, x denotes the wt.- % of silica in the composite and subscript 20 denotes the average diameter of silica core in nm. $PMMA^{49}\_^{1.5}Si_{20}G^{7}$: superscript 1.5 denotes wt % of silica in the composite, G stands for (3-glycidoxypropyl) trimethoxysilane (GPS) and superscript 7 stands for the weight fraction (%) of coupled silane obtained from TGA. $PMMA^{49}\_^{x}Si_{20}M_{y}^{a}$: superscripts x and a denotes the wt-. % of silica in the composite and molecular weight (kg/mol) of grafted PMMA respectively; subscript y stands for weight fraction of grafted polymer (%) measured from TGA. Standard deviation is shown for values obtained from tensile and impact measurements. The results shown in table is obtained from PMMA composite incorporated with silica-polymer hybrid particles obtained after ATRP from colloidal silica initiators coupled through 12 wt % of GPS. T_g and T_d for glass transition temperature and temperature of decomposition of composites.

For a better understanding, the optimum tensile and impact properties obtained for PMMA and its composites for 1.5 wt % of various surface modified Si_{12} and Si_{20} particles are given in Figure 4.3.1 (a and b). Further, the variation in the tensile and impact properties of polymer modified

Si_{12} and Si_{20} particles in PMMA composites for a net silica content of 1.5 wt % are shown in Figure 4.3.2 (a and b). As mentioned before, Hong et al. [26] also reported some improvement in impact strength and tensile modulus of PMMA composites by the addition of PMMA modified silica particles. They prepared PMMA modified silica particles through solution polymerization. Similar studies were reported by Rong et al. [35] for various polymer modified silica particles incorporated into polypropylene. They observed an optimum improvement in mechanical properties for a composite with 3.3 vol% of silica content.

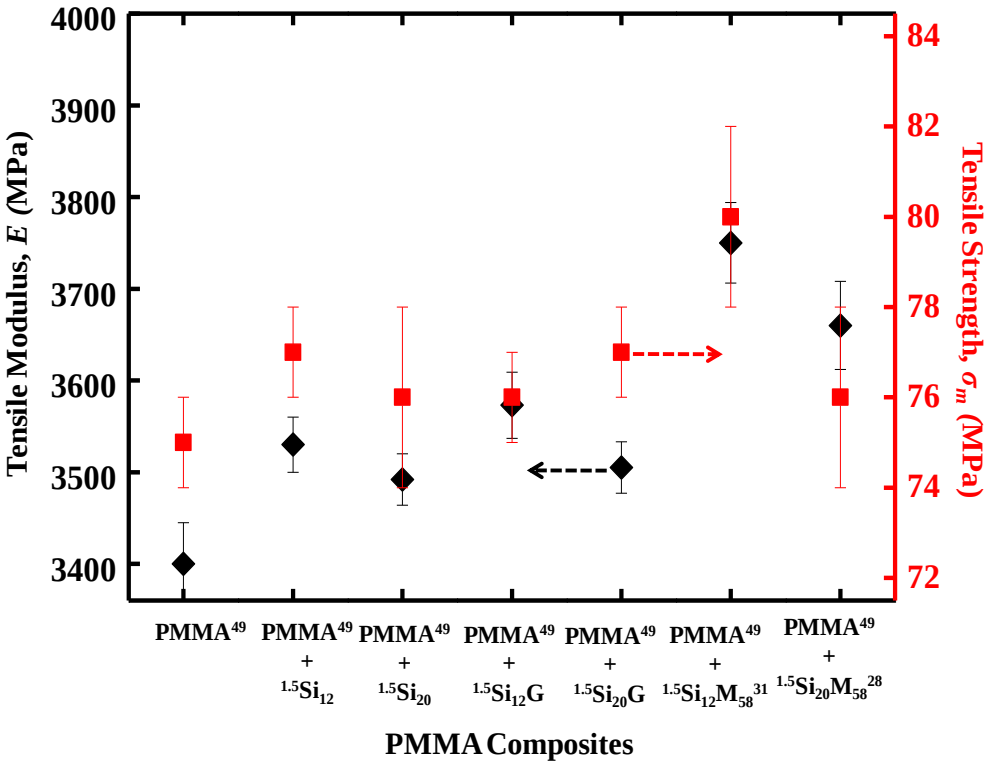

(a)

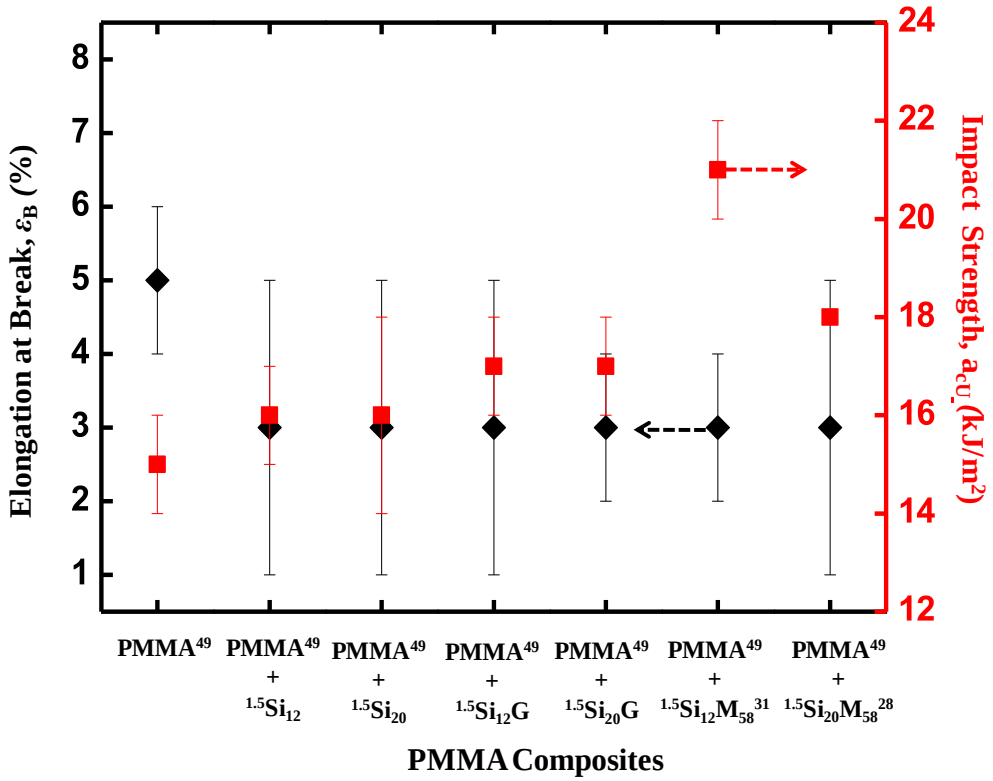

(b)

Figure 4.3.1. (a) Variation of Tensile modulus and Tensile strength and (b) Elongation at break and Impact strength of pure PMMA^{49} matrix, PMMA^{49} composites containing 1.5 wt % of pristine silica NP's (Si_{12} and Si_{20}), silica particles modified GPS ($Si_{12}G$ and $Si_{20}G$, G stands for GPS), silica particles modified by PMMA ($Si_{12}M_{58}^{31}$, $Si_{20}M_{58}^{28}$, M stands for tethered PMMA polymer, 31 and 28 denotes the molar mass of tethered PMMA chains from 12 and 20 nm sized silica NP's respectively.

On the basis of the current results obtained from the systematic study of mechanical properties of hybrid silica containing PMMA composites, "*wetting*" or "*dewetting*" phenomenon between the polymer brush and the matrix polymer might be the possible factor that regulates the dispersion or interfacial adhesion of modified particles in the matrix. This phenomenon depends on several factors, as graft density of tethered chains, molar mass of grafted and matrix polymer, length of the grafted and matrix polymer chains and curvature of the silica core particles.

In the present scenario, among all the composites, better properties are shown by modified Si_{12} particle systems. The best values are obtained with Si_{12} particles modified by PMMA having a molar mass of 31,000 g/mol, graft density of 0.15 chains/nm^2, and an approximate brush thickness of 31 nm.

This point towards the fact that the size of the core particle, graft density, and molar mass of grafted chains influence the "wetting" of polymer brush in polymer matrix and thus the final properties of the composite.

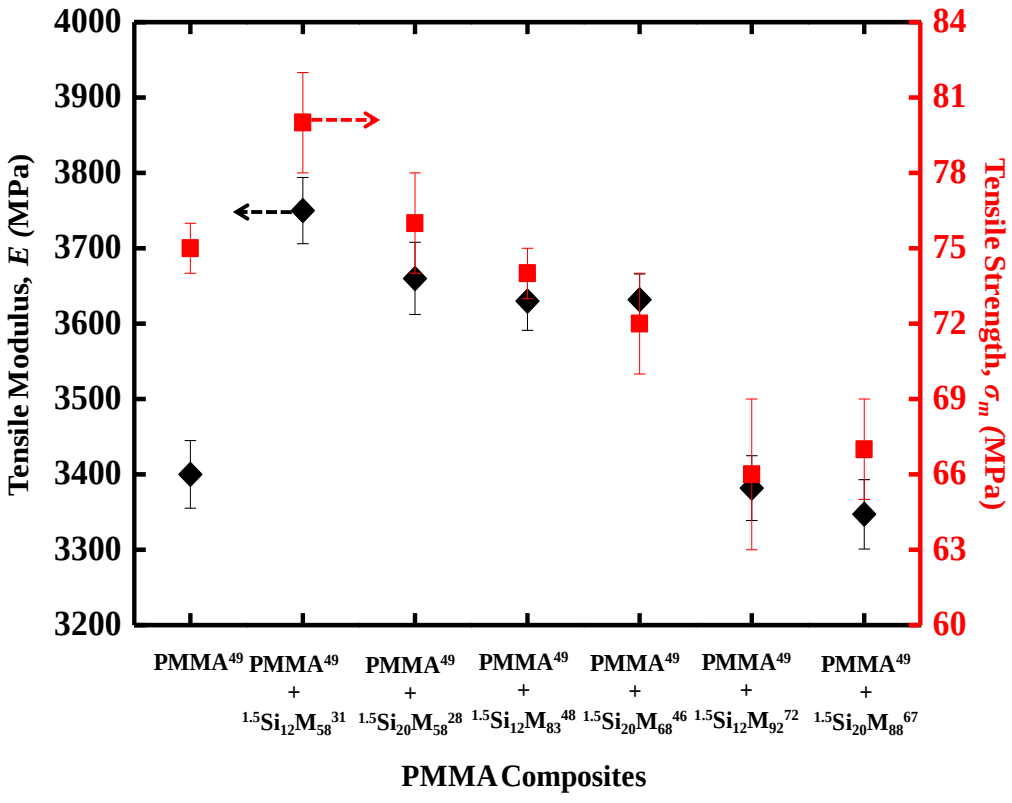

(a)

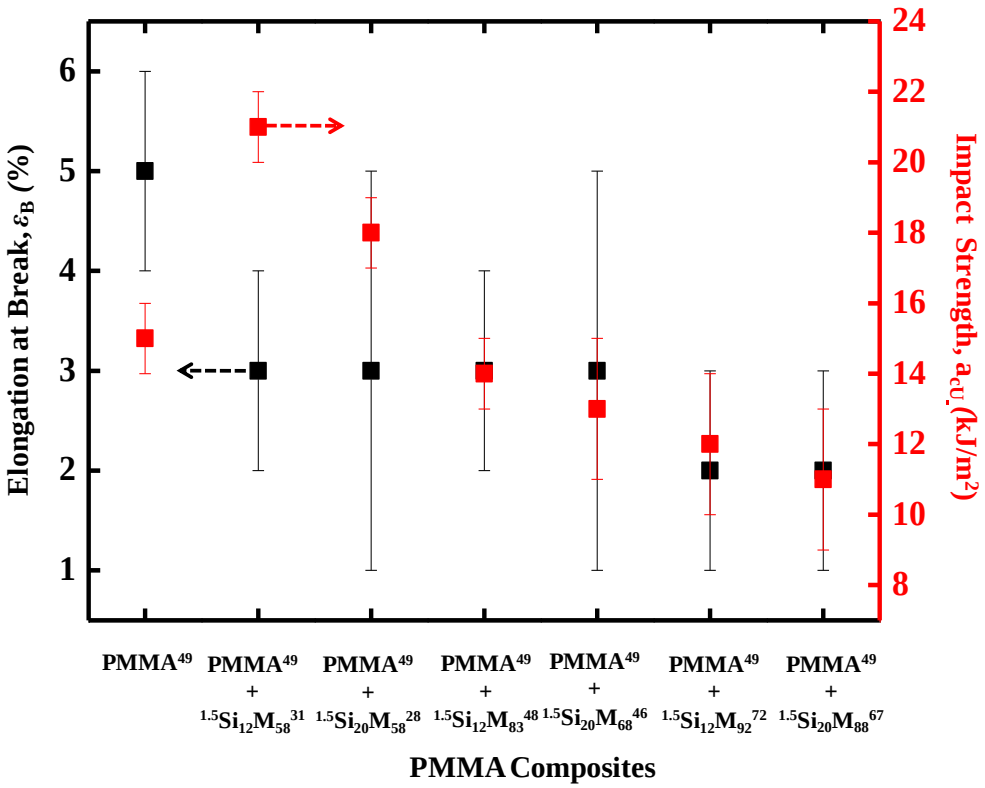

(b)

Figure 4.3.2. (a) Variation of Tensile modulus and Tensile strength and (b) Elongation at break and Impact strength of pure PMMA^{49}, PMMA^{49} composites contain 1.5 wt% of Si_{12} and Si_{20} silica NP's modified by PMMA polymer chains of varying molecular weights. $^{1.5}Si_aM_b^c$, the superscripts 1.5 and c denotes the weight fraction of silica (%) and molecular weight of grafted chains in kg/mol respectively, subscripts a and b correspond to the average core diameter of silica particle (in nm) and weight fraction of grafted polymer chains (%) measured from TGA analysis, M stands for grafted PMMA polymer.

The present work is not going into the details of the "dry brush" or "wet brush" limits. Most of the reported works were about the nature of dispersion of PS grafted particles in respective polymer films or in solutions.[6-7,14] To our knowledge, a less number of systematic studies has

been reported yet regarding the nature of dispersion of grafted particles in polymeric melt and their behaviour towards mechanical properties. [7,13,31,36]

It is known that a layer of (matrix) polymer will dewet from a chemically identical planar brush layer, as long as $L_g << L_m$ (L_g for grafted chain length and L_m for matrix chain length) and if the graft density, σ, follows $\sigma^2 L_m >> 1$ (L is the chain length).[7,37-42] Borukhov and Leibler [19] have shown that "in order to stabilize colloidal suspensions in polymer melts it is typically necessary to utilize polymer grafts whose degree of polymerization (N_g) is equal to or greater than that of the polymer matrix (N_m) as a result of the inability of the matrix to wet short brushes."

When we compare the overall mechanical properties of PMMA composites with polymer grafted silica particles, depletion in properties was observed for those composites containing grafted particles having increasing high graft density (~ 0.47 chains/nm^2), brush thickness and molar masses ($Si_{12}M_{92}^{72}$ and $Si_{20}M_{88}^{67}$) higher than the matrix polymer (see Table 4.3.1). Both Si_{12} and Si_{20} particles shows same behaviour. Composites containing grafted silica particles having medium graft densities (0.27-0.32 chains/nm^2) and similar molar mass ($PMMA^{49}\_S_{12}M_{83}^{48}$ and $PMMA^{49}\_Si_{20}M_{68}^{46}$) to that of matrix polymer (49,000 g/mol) are expected to show better properties due to a proper dispersion by "*wetting*" phenomenon and thus better interfacial adhesion between matrix and grafted particles. Here also we observed a decreasing behaviour of properties, which is still better than the former. We saw in Chapter 4.2 (see Table 4.2.2), the possibility of interparticle crosslinking and resulting abnormal particle size distribution at higher conversions on the basis of combined results from GPC and DLS. This might lead to self aggregation of particles and hinders the proper dispersion in the matrix. As mentioned before, $Si_{12}M_{58}^{31}$ particles having a graft density 0.15 chains/nm^2 and average brush thickness 31nm (calculated from DLS) exhibit good properties among all composites. When we compare the same with $Si_{20}M_{58}^{28}$ particles, having a graft density 0.19 chains/nm^2 and brush thickness 17nm,

the properties tend to decrease. Even though $Si_{12}M_{58}$[31] particles possess higher brush thickness (compared to $Si_{20}M_{58}$[28]), the lower graft density and small size of the silica core might be the deciding factors for property improvement in this PMMA matrix system. Recently, Xu et al. [43] made self-consistent mean-field theoretical studies in order to gain a better understanding of the interaction of polymer grafted spherical NP's (NP) in polymer melts and Harton et al. [13] studied the phase behaviour of dispersions of polymer-grafted NP's in polymer matrices. The studies of Xu et al.[43] study revealed that, "for the specific case of N_m=N_g (N stands for degree of polymerization) that the effective NP-NP interaction depends strongly on the graft density and NP radius. For sufficiently small radius and sufficiently low grafting densities, it was predicted that effective interactions between polymer-grafted NPs will be repulsive whereas increasing graft density and or NP radius leads to regions of net NP-NP attractions." So, this might be a possible reason why PMMA modified Si_{12} particles, $Si_{12}M_{58}$[31], exhibit better properties in the current PMMA matrix for a given molar mass than the corresponding Si_{20} particles. This can be better appreciated from the morphological characterisation of composite. Overall observations indicate that changing the molar mass of matrix polymer, grafting densities and graft molar mass core size and the synthetic pathway of preparing grafted particles, it is also possible further to tailor the mechanical properties of modified Si_{12} or even Si_{20} particles as well.

4.3.2.2. Thermal properties of PMMA modified silica nanoparticles and their composites with PMMA matrix

Before switching into the discussion of thermal properties of PMMA-modified silica nanocomposites, let us go through the variation in the glass transition temperature of various PMMA modified silica (Si_{12} and Si_{20}) particles used for the composite preparation (Table 4.3.1).

T_g strongly depends on the mobility of polymer chain segments. It is known that addition of filler materials to polymer liquid increases T_g if there are strong attractive forces between the polymer and filler surface. Moreover, differences between the T_g's of composite and matrix materials have been reported to decrease with lower filler contents in the blend.[44-45] When we compare the T_g's of PMMA modified either Si_{12} or Si_{20} NP's, the grafted polymer chains with low molar mass have lower T_g when compared to those with higher molar mass. The weight fraction of silica (42 %) present in those particles grafted with low molar mass, $Si_{12}M_{58}^{31}$ and $Si_{20}M_{58}^{28}$ is higher than those grafted with higher molar mass, $Si_{12}M_{83}^{48}$ (17 %), $Si_{20}M_{68}^{46}$ (32 %) and $Si_{12}M_{92}^{72}$ (8 %), $Si_{20}M_{88}^{67}$ (12 %). This is concluded from the decrease in T_g value obtained for cleaved PMMA chain when compared to that of bound PMMA chains (Table 4.3.1). The behaviour is unique for both sets of particles. When we closely compare the T_g values of surface modified silica particles, the values of modified Si_{12} particles are slightly higher than the respective Si_{20} particles. This difference may arise from the surface chemistry of the two kinds of particles. Figure 4.3.3 represents the variation of T_g for a given graft density and brush thickness from both sets of modified particles. The nature of interaction in polymer modified silica systems is different from conventional filled materials.

Usually, fillers serve to increase T_g by the adsorption of polymer chains, thereby decreasing the mobility of the chains closest to the surface. In the case of spherical polymer brushes, the mobility of the chains is further reduced by the covalent bonding of polymer chains with silica particles instead of adsorption, and raises the average T_g. A similar observation was made by Savin et al.[46] in their polystyrene (PS) modified silica particles. Now let us go into the details of thermal behaviour of PMMA composites containing pristine and surface modified silica NP's.

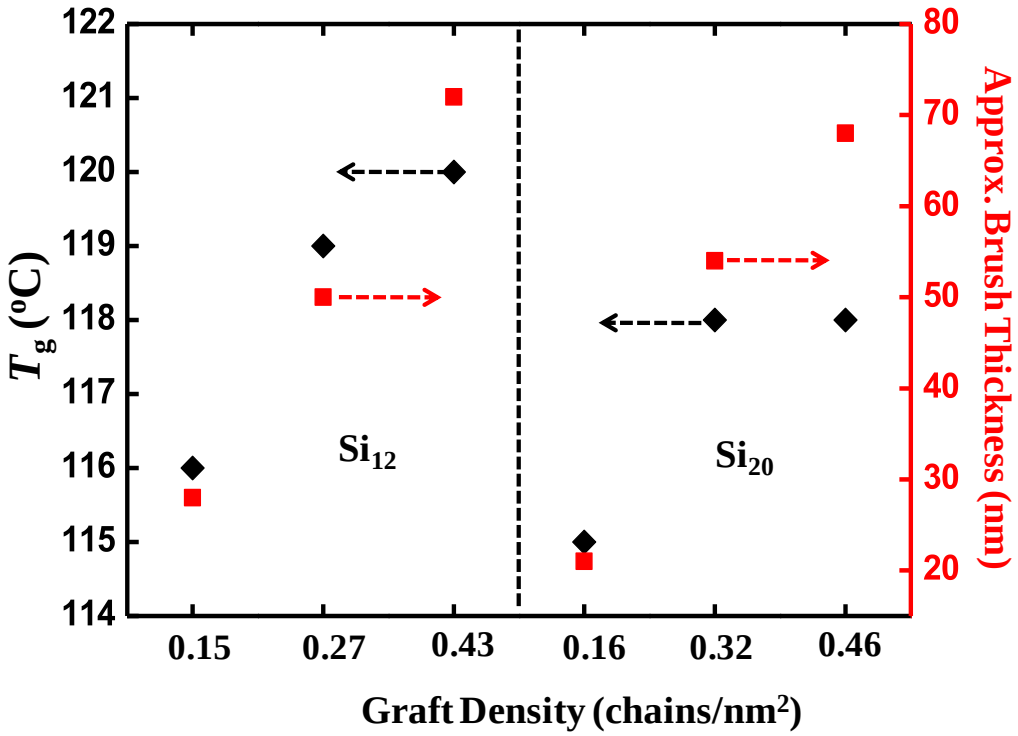

Figure 4.3.3. Variation of T_g for a given brush thickness and graft density for PMMA modified Si_{12} (left side of the partition) and Si_{20} (right side of the partition) NP's.

By the addition of pristine Si_{12} and Si_{20} NP's into the PMMA matrix, the decomposition temperature raised to 390 °C and 387.3 °C, respectively. Small increase in decomposition temperature (T_d) was observed for Si_{12} filled PMMA composites. It should arise from the size of NP's. By the addition of surface modified silica NP's (see Table 4.3.2 and Table 4.3.3), the T_d values are further increased or delayed the thermal decomposition arising from the improved compatibility of surface modified constituents with the matrix polymer. Both surface modified Si_{12} and Si_{20} particles show more or less parallel behaviour towards the thermal decomposition PMMA composites. The increase in decomposition temperature by the addition of pristine and modified NP's in a PMMA matrix has already been observed before.[47]

The above paragraph discussed the effect of polymer grafting on silica particles on T_g values. Thermomechanical properties of polymer composites, especially the T_g value can be profoundly affected by addition of nanofillers.[48-52] It has been reported that T_g of a polymer can change due to the addition of nanofiller.[53] Elastic modulus, hardness, conductivity and various other physical properties can change by several orders of magnitude in the vicinity of T_g. Hence, facile tuning of nanocomposite T_g could allow us to control the usable temperature range of these materials.

Polymer modified NP's in a matrix material can change the thermal and mechanical properties by several factors, such as the type of interactions between the NP's and the polymer chains, graft density of polymer chain and the distribution and diameter of the NP's. As we already saw in the previous paragraphs, the T_g of the polymer chains is affected by their grafting on silica particles. But the variation is not as high as in the reported literature.[53] As we observed better mechanical properties for those composites having a net silica content of 1.5 wt%, T_g values of those systems are chosen for discussion. A dramatic increase in T_g values was not observed in PMMA composites when incorporated with either of the PMMA modified silica NP's (see, Table 4.3.1 and Table 4.3.2). Composites containing modified particles having a graft density of 0.15 and 0.19 chains/nm^2 (PMMA^{49}_$^{1.5}$Si$_{12}$M$_{58}$^{31} and PMMA^{49}_$^{1.5}$Si$_{20}$M$_{58}$^{28} respectively) show a slight decrease in T_g when compared to others. Glass transition temperature of polymer nanocomposites are influenced by the relative strength of the chain-particle interactions, particle dispersion and the interparticle spacing in the matrix polymer. Recently, Green et al.[48] showed that, one can tailor T_g values by controlling the concentration of gold NP's, nanoparticle size, graft density of PS chains and graft chain degree of polymerization. Moreover, Bansal et al.[7] showed that "the T_g of polymer nanocomposite material decreased under conditions where the PS grafted silica NP's/host chains were non-wetting." The graft density of modified NP's is found to be very sensitive in designing nanocomposites within a particular range of T_g.

In the present context, a small improvement in T_g and the mechanical properties was observed for those grafted silica particles having lower graft density ($Si_{12}M_{58}^{31}$, 0.15 chains/nm^2 and $Si_{20}M_{58}^{28}$, 0.19 chains/nm^2) having molar mass lower than the matrix PMMA (M_n=49,000 g/mol). The weight fraction of silica (42 wt%) in these particles is higher when compared to other modified particles. Among them, $Si_{12}M_{58}^{31}$ particles having a graft density of 1.5 chains/nm^2 show better thermal and mechanical properties for 1.5 wt % silica content in the composite. Increase in graft density and size of Si_{20} core in $Si_{20}M_{58}^{28}$ than the previous one might be the factor responsible for depletion in properties. We have not investigated in detail the critical limit of graft density for proper wetting of silica polymer brushes in the current PMMA matrix. The small improvement in T_g and mechanical properties of current composites indicates the influence of particle size, graft density and weight fraction of silica in the grafted particles Irrespective of size of particles, those grafted with higher molar masses and graft density, including the possibility of formation of cross linked chains (discussed in Chapter 4.2) might increase the particle aggregation and hinder proper wetting or particle dispersion in the matrix polymer.

4.3.2.3. Morphology of PMMA composites with PMMA modified Si_{12} nanoparticles

Controlling the extent of aggregation for getting better dispersion of NP's in a polymer matrix is one of the biggest challenge in order to achieve the desired properties of nanocomposites. Grafting of polymer chains onto NP's can control the particle aggregation to a good extend and eases the particle dispersion in a polymer matrix.

Bansal et al.[7] studied the wetting and dewetting behaviour of silica (core diameter 14 nm) grafted polystyrene (PS) in a polystyrene matrix by varying the molar mass of the matrix polymer. They

found that "dewetting occurs when $M_m < M_g$ for a particular chain length". This agrees to the findings of Bates et al. [14] In which they observed a better dispersion of PS grafted silica NP's (average diameter of 17 ± 4 nm), when the molecular weight of the matrix PS was roughly equal to or smaller than the graft molecular weight. Most recently, Chevigny et al.[6] and Akcora and his co workers[31] also reported how to fine tune the dispersion of polystyrene grafted silica NP's (average diameter of silica core was 14 nm) in PS composite films of varying graft density by varying molar mass of matrix and graft polymer. They correlated the experimental results with simulations in order to explain the orientation of NP's in films prepared under different annealing conditions and the rheological response from various dispersed systems.[7,13,36] Very recently, Akcora and his co-workers[54] reported the segmental dynamics in PMMA-grafted nanoparticle composites. They studied the dispersion behaviour and rheology of PMMA modified particles in PMMA matrix of varying graft molar mass and matrix molar mass for a given graft density. They observed that, "modified particle is miscible or well dispersed, when the matrix molar mass is lower than the graft molar mass for a given graft density". The rheological studies indicate that segmental mobility of grafted chains slightly decreases with the aggregation of particles. In combination, these results suggest that the mechanical reinforcement in these situations is driven by the formation of a particle network with the grafted polymers providing the bridges.

The results indicate that the variation in thermal and mechanical properties is a consequence of changing graft density, molar mass of graft polymer chain and size of core particles. Besides the experimental errors and limitations, good mechanical and thermal properties were observed for composites comprised of ${}^{1.5}Si_{12}M_{58}{}^{31}$ particles having a graft density 0.15 chains/nm^2 for a molar mass of 31,000 g/mol in a PMMA matrix of 49,000g/mol.

One possible explanation for the poor dispersion and poor mechanical properties with particles with increasing graft molar mass and graft density may arise due to some cross linking or interparticle coupling occuring during synthesis (discussed in Chapter 4.2). The level of dispersion of these particles in the matrix is analysed by transmission electron microscopy (TEM). The results from composites having polymer modified Si_{12} particles of different graft density is subjected to discussion in the present Chapter. TEM images of ultrathin cuts of PMMA composite samples containing 1.5 wt % of modified $^{1.5}Si_{12}M_{58}^{31}$ and $^{1.5}Si_{12}\ M_{83}^{48}$ is shown in Figure 4.3.4 (a and b). The TEM image shows a good dispersion of $^{1.5}Si_{12}M_{58}^{31}$ particles having a graft density, 0.15 chains/nm^2 for a molar mass of 31,000 g/mol in $PMMA^{49}\_^{1.5}Si_{12}M_{58}^{31}$ composite. The $^{1.5}Si_{12}M_{83}^{48}$ particles, having higher a graft density of 0.27 chains/nm^2 and a molar mass of 48,000 g/mol similar to that of matrix polymer exhibit more aggregation. Further increase of graft density and graft molar mass to 0.43 chains/nm^2 and 72,000 g/mol, respectively ($^{1.5}Si_{12}M_{92}^{72}$), lead to a worse dispersion than the previous ones. A close observation of the TEM image (a) shows very small well separated aggregates but no big clusters as in Figure 4.3.4 (b).

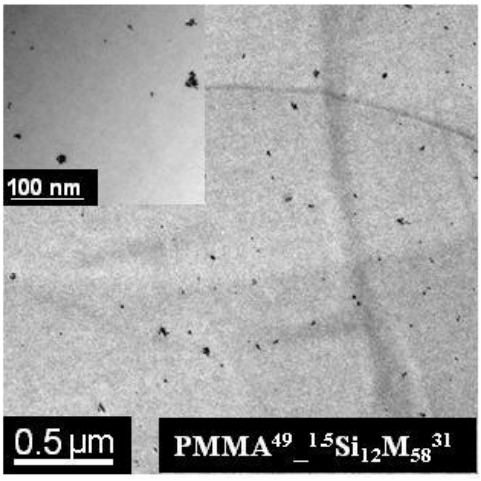

(a)

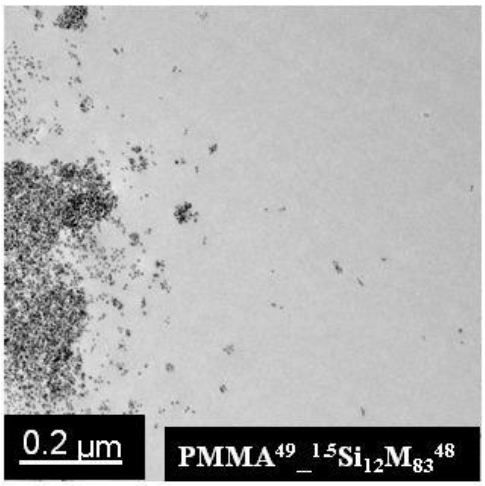

(b)

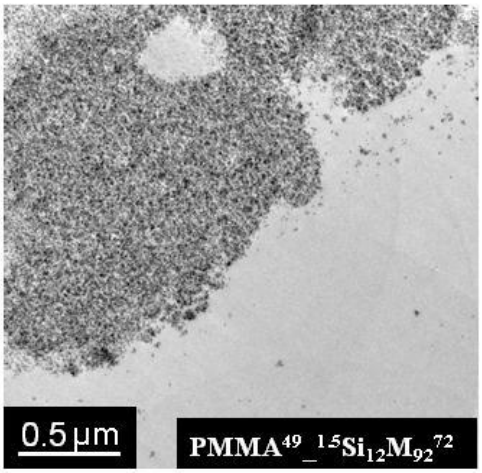

(c)

Figure 4.3.4. Selective TEM images of ultra thin cuts of (a) $PMMA^{49}\_^{1.5}Si_{12}M_{58}^{31}$, graft density 0.15 chains/nm^2 and (b) $PMMA^{49}\_^{1.5}Si_{12}M_{83}^{48}$, graft density 0.27 chains/nm^2 (c) $PMMA^{49}\_^{1.5}Si_{12}M_{92}^{72}$, graft density 0.43 chains/nm^2 extrudates containing a net silica content of 1.5 wt%.

A good dispersion and an improved *wetting* behaviour of $^{1.5}Si_{12}M_{58}^{31}$ particles in the composite might be obtained as a result of respective graft density, graft molar mass and particle size in a given matrix molar mass. This inference is further confirmed by the improved mechanical and thermal properties of $PMMA^{49}\_^{1.5}Si_{12}M_{58}^{31}$ composite obtained when compared to others.

4.3.3. Conclusions

In this Chapter, the influence of graft density, molar mass of graft chains and size of silica core on the mechanical, thermal and morphological properties of PMMA composites for a constant matrix molar mass (49,000 g/mol) were investigated. Silica particles having average core diameters 12 nm (Si_{12}) and 20 nm (Si_{20}) were chosen for surface modification. Grafting densities in the range, ≤ 0.2, ≤ 0.3, and ≤ 0.5 chains/nm^2 were chosen for grafting molar masses which are

lower, nearly equal and higher than the matrix polymer from Si_{12} and Si_{20} particles, respectively. Overall evaluation indicates that modified Si_{12} having a graft density 0.15 chains/nm^2 and graft molar mass 31,000 g/mol gives some improvement in mechanical and thermal properties. This is further confirmed by TEM characterisation, in which a good dispersion of respective particles in the matrix polymer was observed. . Overall observations indicate that changing the molar mass of matrix polymer, graft densities and graft molar mass core size and the synthetic pathway of preparing grafted particles, it is also possible further to tailor the mechanical properties of modified Si_{12} or even Si_{20} particles as well.

4.3.4. References

1. D. Zhou, J. E. Mark, *J. Macromol. Sci. Pure. Appl. Chem*., 2004, A41, 1221.
2. S.T. Selvan, J. P. Spatz, H. A. Klok, M. Moller, *Adv. Mater*., 1998, 10, 132.
3. R. Sengupta, A. Bandyopadhyay, S. Sabharwaj, T. K. Chaki, A. K. Bhowmick, *Polymer*, 2005, 46, 3343.
4. Q. W. Yuan, J.E. Mark, *Macromol. Chem. Phys*., 1999, 200, 206.
5. J. Lee, V. C. Sundar, J. R. Heine, M. G. Bawendi, K. F. Jensen, *Adv. Mater*., 2000, 12, 1102.
6. C. Chevigny, F. Dalmas, E. D. Cola, D. Gigmes, D. Bertin, F. Boué, J. Jestin, *Macromolecules*, 2011, 44, 122-133.
7. A. Bansal, H. Yang, C. Li, B. C. Benicewicz, S. K. Kumar, L. S. Schadler, *J. Polym. Sci, Part B: Polym. Phys*., 2006, 44, 2944-2950.
8. C. Xu, K. Ohno, V. Ladmiral, R. J. Composto, *Polymer*, 2008, 49, 3568-3577.
9. G. D. Smith, D. Bedrov, *Langmuir*, 2009, 25, 11239-11243.
10. H. Hasegawa. Y. Aoki, M. Doi, *Macromolecules*, 1996, 29, 6656-6662.
11. P. G. Ferreira, A. Ajdari, L. Leibler, *Macromolecules*, 1998, 31, 3994-4003
12. M. Aubouy, G. H. Fredrickson, P. Pricus, E. Raphael, *Macromolecules*, 1995, 28, 2979-2981.
13. S. E. Harton, S. K. Kumar, *J. Polym. Sci, Part B: Polym. Phys*., 2008, 46, 351-358.
14. Q. Lan, L. F. Francis, F. S. Bates, *J. Poly. Sci: Part B: Poly. Phys*., 2007, 45, 2284-2299.
15. K. T. Marla, J. C. Meredith, *J. Chem. Theory. Comput*., 2006, 2, 1624-1631.
16. R. C. Ball, J. F. Marko, S. T. Milner, T.A. Witten, *Macromolecules*, 1991, 24, 693-703.

17. K. R. Shull, K. I. Winey, E. L. Thomas, E. J. Kramer, *Macromolecules*, 1991, 24, 2748.
18. J. Kalb, D. Dukes, S. K. Kumar, R. S. Hoy, G. S. Grest, *Soft Matter Conference*, Royal Society of Chemistry, 2010.
19. I. Borukhov, L. Leibler, *Macromolecules*, 2002, 35, 5171.
20. G. Lindenblatt, W. Schartl, T. Pakula, M. Schmidt, *Macromolecules*, 2001, 34, 1730.
21. M. K. Corbierre, N. S. Cameron, M. Sutton, K. Laaziri, R. B. Lennox, *Langmuir*, 2005, 21, 6063.
22. F. S. Bates, G. H. Fredrickson, *Ann. Rev. Phys. Chem*., 1990, 41, 525.
23. M. R. Bockstaller, E. L. Thomas, *Phys. Rev. Lett*., 2004, 93, 1661.
24. R. B. Thompson, V. V. Ginzburg, M. W. Matsen, A. C. Balazs, *Science*, 2001, 292, 2469.
25. A. C. Balazs, T. Emrick, T. P. Russel, *Science*, 2006, 314, 1107.
26. R. Y. Hong, H. P. Fu, Y. J. Zhang, L. Liu, J. Wang, H. Z. Li, Y. Zheng, *J. Appl. Polym. Sci*., 2007, 105, 2176-2184.
27. D. N. Bikiaris, G. Z. Papageorgiou, E. Pavlidou, N. Vouroutzis, P. Palatzoglou, G. P. Karayannidis, *J. Appl. Polym. Sci*., 2006, 100, 2684.
28. S. H. Kim, S. H. Ahn, T. Hirai, *Polymer*, 2003, 44, 5625.
29. X. Y. Shang, Z. K. Zhu, J. Yin, X. D. Ma, *Chem. Mater*., 2002, 14, 71.
30. F. Yang, Y. C. Ou, Z. Z. Yu, *J. Appl. Polym. Sci*., 1998, 69, 355.
31. P. Akcora, H. Liu, S. Kumar, J. Moll, Y. Li, B. Benicewicz, L. S. Schadler, D. Acehin, A. Z. Panagiotopoulos, V. Pryamitsyn, J. Ilavsky, P. Thiyagarajan, R. H. Colby, J. Douglas, *Nat. Mater*., 2009, 8, 354-359.
32. E. P. Plueddemann, "*Silane Coupling Agents*", Plenum, New York, 1982.
33. E. R. Pohl, F. D. Osterholtz *in* "*Molecular Characterisation of Composite Interfaces*" (H. Ishida and G. Kumar, Eds.) Plenum, New York, 1985, 157.
34. M. W. Daniels, L. F. Francis, *J. Colloid Interface Sci*., 1998, 205, 191-200.
35. M. Z. Rong, M. Q. Zhang, Y. X. Zheng, H. M. Zeng, R. Walter, K. Friedrich, *Polymer*, 2001, 42, 167.
36. D. L. Green, J. Mewis, *Langmuir*, 2006, 22, 9546-9553.
37. R. A. L. Jones, E. J. Kramer, M. H. Rafailovich, J. Sokolov, S. A. Schwarz, *Phys. Rev. Lett*., 1989, 62, 280.
38. A. C. Costa, M. Georghegan, P. Vlcek, R. J. Composto, *Macromolecules*, 2003, 36, 9897.
39. Y. Liu, M. H. Rafailovich, J. Sokolov, S. A. Schwarz, X. Zhong, A. Eisenberg, E. J. Kramer, B. B. Sauer, S. Satija, *Phys. Rev. Lett*., 1994, 73, 440.
40. R. Oslanec, A. C. Costa, R. J. Composto, P. Vlcek, *Macromolecules*, 2000, 33, 5505.
41. A. C. Costa, R. J. Composto, P. Vlcek, *Macromolecules*, 2003, 36, 3254.
42. K. R. Shull, *Macromolecules*, 1996, 29, 8487.

43. J. Xu, F. Qui, H. Zhang, Y. Yang, *J. Polym. Sci. PartB: Polym. Phys*., 2006, 44, 2811-2820.
44. S. N. Tong, M. L. Chen, P. Wu, in "*Analysis of Transition Temperatures in Polymer-Filler Systems*" J. Mitchel, Jr, Ed,; Oxford University Press, New York, 1992, Vol 2, 329-345.
45. S. M. Aharoni, *Polym. Adv. Technol*., 1998, 9,169-201.
46. D. A. Savin, J. Pyun, G. D. Patterson, T. Kowalewski, K. Matyjaszewski, *J. Polym. Sci. PartB: Polym. Phys*., 2002, 40, 2667-2676.
47. S. Etienne, C. Becker, D. Ruch, B. Grignard, G. Cartigny, C. Detrembleur, C. Calberg, R. Jerome, *J. Therm. Anal. Cal*., 2007, 87, 101-104.
48. H. Oh, P. F. Green, *Nat. Mater*., 2009, 8, 139-143.
49. V. Pyramitsyn, V. Ganesan, *Macromolecules*, 2006, 39, 844-856.
50. A. Bansal, H. Yang, C. Li, B. B. Benicewicz, S. K. Kumar, L. S. Schadler, *Nat. Mater*., 2005, 4, 693.
51. G. D. Smith, D. Bedrov, L. Li, O. A. Byutner, *J. Chem. Phys*., 2002, 117, 9478-9489.
52. G. Tsagaropoulos, A. Eisenburg, *Macromolecules*, 1995
53. P. Xiao, M. Xiao, K. Gong, *Polymer*, 2001, 42, 4813.
54. P. Akcora, H. Liu, S. Kumar, V. G. Sakai, Y. Li, B. Benicewicz, L. S. Schadler, *Macromolecules*, 2010, 43, 8275-8281.

4.4. Dispersion Characteristics and Impact Properties of (PS-*b*-PMMA) Composites with Si_{12}-*g*-(PMMA) Particles Prepared by Melt Processing

4.4.1. Introduction

As we discussed in the previous chapters, applications of polymer modified nanoparticles (NP's) have been widely extended to block copolymers (BCP's) as well. Block copolymers consist of two or more chemically different polymer chains joined covalently at their ends. The dissimilar blocks of narrow disperse block copolymers tend to undergo microphase separation into well-ordered domains due to the positive enthalpy and small entropy of mixing. The property of microphase separation in block copolymers give rise to diverse morphologies and can provide an effective means to control the particle location and dispersion while preparing composites. Such spatially regular composites will have high impact in nanotechnology, exploiting their unique mechanical,[1] electrical,[2] optical,[3-4] and magnetic[5] properties.

One can tailor the properties of nanocomposites by controlling the nature of dispersion as well as ordering of nanoparticles in the (co) polymer matrix and opening new possibilities on the front of developing new materials.[6] On the basis of self consistent field theory (SCFT) calculations, Reister and Fredrickson[7] investigated the phase behaviour of diblock copolymer with polymer-tethered NP's and showed the pronounced effect of the overall size of the particles including the shell on the region of microphase separation. They also studied the ways to increase the loading of NP's in an ordered phase without macrophase separation by tuning the length and number of tethered polymer chains in the shell. Size-selective organization of inorganic NP's has been validated by Bockstaller et al.[8] On the basis of number of theoretical calculations, they showed that "larger particles will organize at the center of a preferred domain to reduce the overall free energy, while the smaller particles concentrate at the block copolymer interface to gain

maximum translational entropy".[9-10] Kramer and his co-workers[11-12] also investigated the nanoparticle induced phase transitions in bulk diblock/inorganic particle composites and later the effects of areal density of homopolymers on the localization behaviour of NP's in diblock copolymer composites. Yeh et al.[13] studied the morphological change of a given block copolymer system by the selective dispersion of quantum dots.

Most of the above mentioned studies have focussed on relatively small NP's of metals or metallic oxides. Usually, the diameter of nanoparticles (d) are relative to the block copolymer domain dimensions ($d/L < 0.3$, where L is the respective domain spacing).[14-15] Very few studies reported the dispersion behaviour of polymer modified silica nanoparticles in block copolymer matrices. There are not many systematic studies dealing with the variation of matrix molecular weight and particle dimension on nanoparticle dispersion in ordered block copolymers. Bates et al.[16] reported the above effects for the first time in ordered block copolymers. In their studies, they described the mixing behaviour of silica NP's grafted with polystyrene in poly(styrene-*b*-butadiene) (PS-*b*-PB) having lamellar morphology. They discovered that, NP's grafted with low molecular weight tend to aggregate and those with higher molecular weight showed a better dispersion in PS-*b*-PMMA block copolymer for a comparatively higher matrix molar mass. All the above studies regarding the dispersion of grafted NP's in block copolymer matrices were done in solvent casted films. Due to the complex morphological changes that can occur during processing, almost no study has been reported yet regarding the dispersion behaviour of polymer modified NP's in glassy block copolymer composites prepared by melt mixing.

In the present studies, glassy block copolymer, PS-*b*-PMMA (SM) having ordered lamellar (SM_L) and cylindrical (SM_C) morphologies were chosen as the matrix for composite preparation. The localization behaviour of PMMA modified Si_{12} particles in block copolymer matrix and the resultant morphology of composite prepared by melt mixing was investigated through

transmission electron microscopy (TEM) and small angle X-ray scattering (SAXS). This chapter also describes a comparative study of the impact properties and the morphology of the respective composites.

4.4.2. Discussion of results

4.4.2.1. Morphology of (PS-*b*-PMMA) composites with PMMA modified silica nanoparticles

The procedure for the preparation of PS-*b*-PMMA (SM) composites containing PMMA grafted silica particles were described in Chapter 3. Further details of surface functionalization followed by polymer grafting reactions were discussed detail in Chapters 4.1 and 4.2, respectively.

Because of the disparity in the values of periodicities (*d*) calculated from TEM analysis, we rely on the values calculated from small angle x-ray scattering (SAXS) for ordered periodicities. The block copolymers with lamellar and cylindrical morphology were have a periodicity of 56 nm and 57 nm respectively.

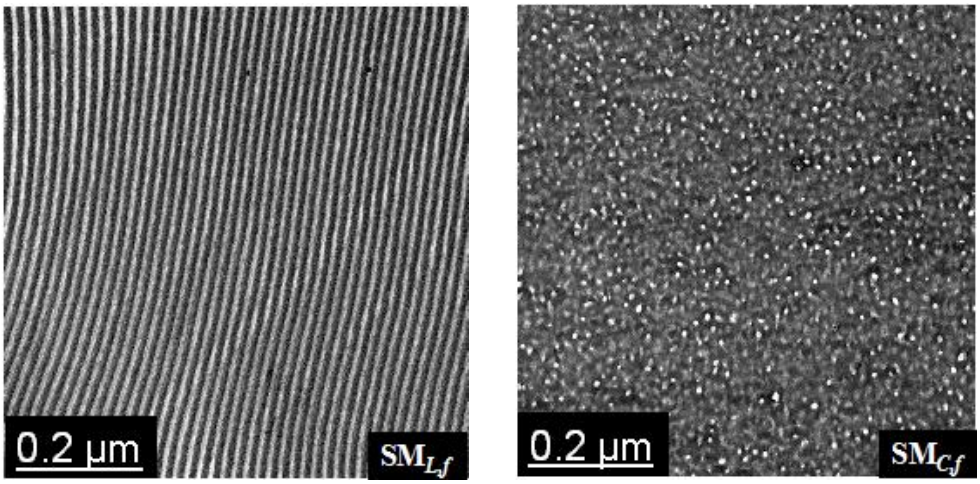

(a) (b)

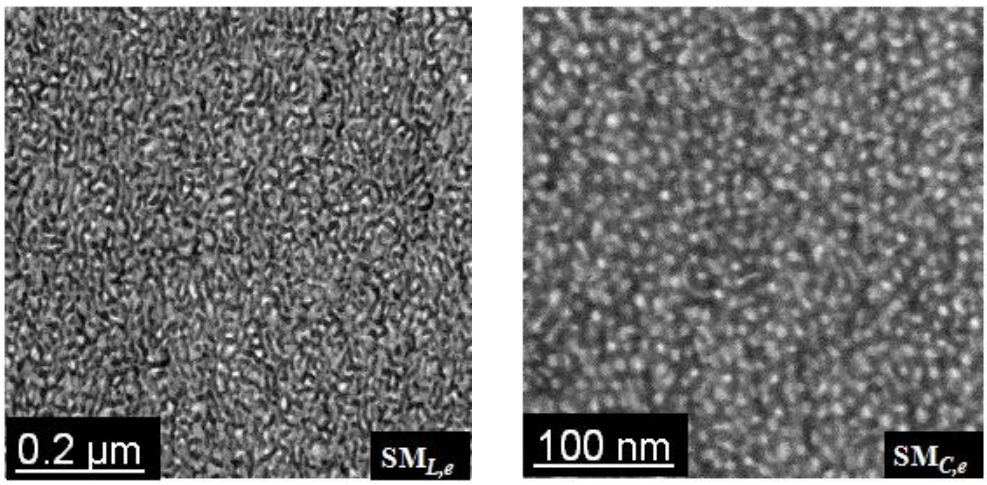

(c) (d)

Figure 4.4.1. TEM images of pristine block copolymer films (a) $SM_{L,f}$ (b) $SM_{C,f}$ obtained after annealing at 210 ^{o}C and ultra thin cuts of extrudates (c) $SM_{L,e}$ (d) $SM_{C,e}$ after processing at 210 ^{o}C. In order to obtain a good contrast the block copolymer films were stained with RuO_4. White contrast in the picture corresponds to PMMA domain and gray to PS domain. The subscripts *f* stand for film and *e* for extrudate.

The size of the core particle, molecular weight of the tethered chains and overall size of polymer grafted particles are important in particle dispersion and localization. PMMA modified Si_{12} particles are utilized in the present studies. Si_{12} particles having a graft molar mass, 18,000 g/mol ($Si_{12}M_{50}^{18}$) were chosen for studying the mode of dispersion. The size of $Si_{12}M_{50}^{18}$ particle (calculated from DLS measurements) is less than the periodicity of both types of bock copolymers and approximate brush thickness is also less than the average diameter of one block. Figure 4.4.1 (a - d) represents the TEM images of bulk films ((a) $SM_{L,f}$ and (b) $SM_{C,f}$) and ultra thin cuts of extrudates ((c) $SM_{L,e}$ and (d) $SM_{L,e}$) obtained from pristine SM_L and SM_C block copolymers. The purpose of these figures is to show the difference in the orientation of blocks in

BCP's during annealing and processing. Both annealing of films and extrusion of BCP's were carried out at 210 ^{o}C.

The disparity and the frustration in the morphology of extrudates may be due to the complex morphological behaviour occur during the processing conditions. The dispersion characteristics was studied by varying the content of silica in modified silica particles from 0.5-1.5 wt% in the block copolymer composite (see Figure 4.4.2 (a-d)). By analysing the TEM images (see Figure 4.4.2 (a and c)) of composites containing 0.5 wt% of silica, the modified silica nanoparticles tend to occupy or organise in the PMMA domain of the block copolymer. When the silica content increased to 1.5wt %, particles tend to form small aggregates in the case of lamellar type of $SM_{L,e}\_^{1.5}Si_{12}M_{50}^{18}$ composite (see Figure 4.4.2 (b)). But these small aggregates are dispersed well apart from each other. Still one could observe some particles located in the PMMA domain. But more pronounced is the tendency of particles to locate in either domains at higher loadings of silica. A similar conclusion was made by Bates et al.[16] for the distribution of their PS modified silica particles in lamellar PS-*b*-PB composite film. Whereas in $SM_{C,e}\_^{1.5}Si_{12}M_{50}^{18}$ composite (see Figure 4.4.2 (d)) prepared from cylindrical type of

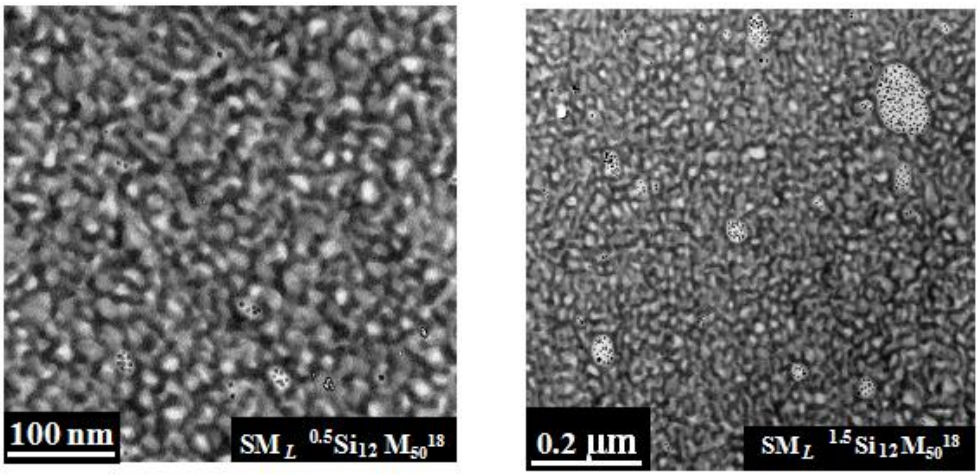

(a) (b)

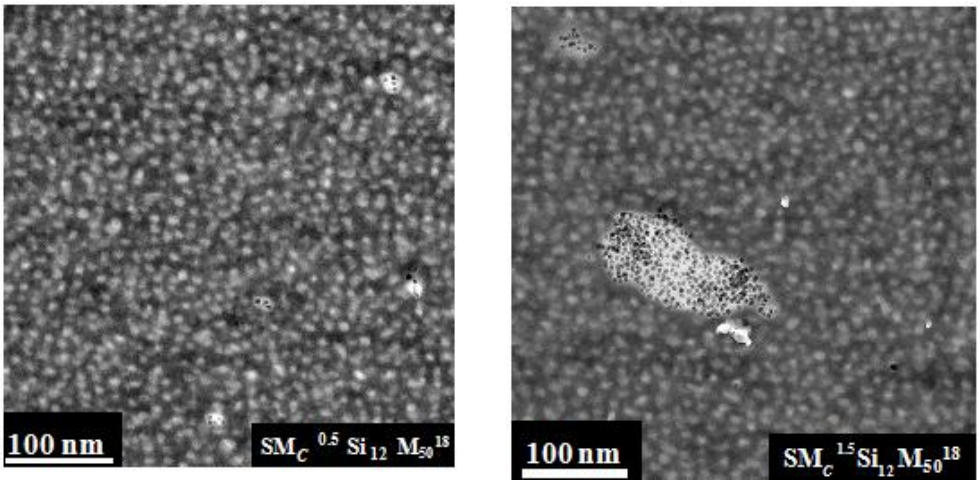

(c) (d)

Figure 4.4.2. TEM images of ultra thin cuts of block copolymer filled with modified silica composites after impact measurements. (a) $SM_{L,e\_}{}^{0.5}Si_{12}M_{50}{}^{18}$ (b) $SM_{L,e\_}{}^{1.5}Si_{12}M_{50}{}^{18}$ (c) $SM_{C,e\_}{}^{0.5}Si_{12}M_{50}{}^{18}$ (d) $SM_{C,e\_}{}^{1.5}Si_{12}M_{50}{}^{18}$ obtained by extrusion at 210 ^{o}C at a rotation speed of 10 rpm for a processing period of 25 min. In order to obtain a good contrast the block copolymer films were stained with RuO_4. White contrast in the picture corresponds to PMMA domain and gray to PS domain. The superscripts 0.5 and 1.5 stand for silica content of modified particles in wt%.

block copolymer, irrespective of the size distribution of modified particles, instead of particle localisation or dispersion, agglomerate formation was observed.

Further, SAXS analysis (Figure 4.4.3) of the respective composites gives more information about how the distribution of the modified particles affects the periodicity of block copolymer matrices. As mentioned before, the lamellar type of block copolymer has a periodicity 56 nm (shown in Figure 4.4.3 (i) and (ii)). After the addition of 0.5 wt % of $Si_{12}M_{50}{}^{18}$ particles, the periodicity of $SM_{L,e\_}{}^{0.5}Si_{12}M_{50}{}^{18}$ (see curve (a) in Figure 4.4.3 (i)) increases to 57.6 nm, this obviously due to the presence of modified silica particles. The additional peak appears at 2.3 (q^3) other than the typical lamellar morphology arises from the form factor of silica particles. Form factor gives information about the size distribution of silica particles in block copolymer matrix

through fitting analysis of theoretical curves with that of experimental curves obtained from scattering measurements. The form factor of spherical particles with radius R is calculated by the following equation,[17-18]

$$P(q, R) = 9\left(\frac{\text{Sin}(qR) - qR\,\text{Cos}(qR)}{(qR)^3}\right)^2 \quad \text{.....} \quad \text{(Equation 4.4.1)}$$

Where, q is the scattering vector obtained from SAXS measurements and R was chosen as the variable parameter for the fitting analysis. The form factor was calculated for each scattering curves obtained from block copolymer-modified silica composites and are shown by curves b in Figure (i-iv).

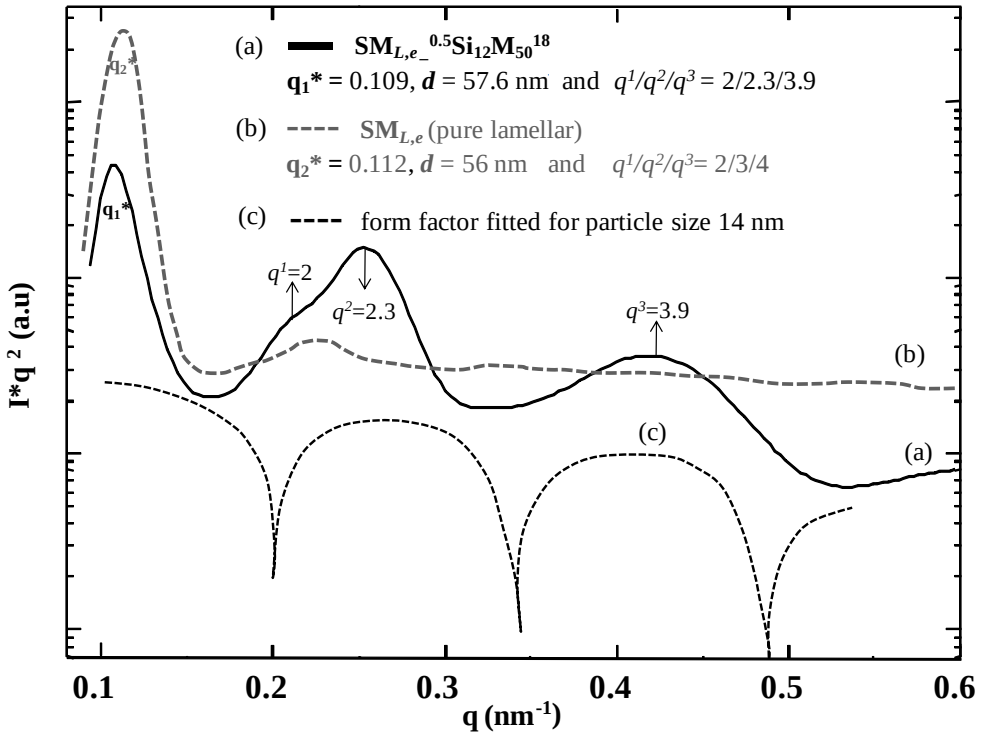

(i)

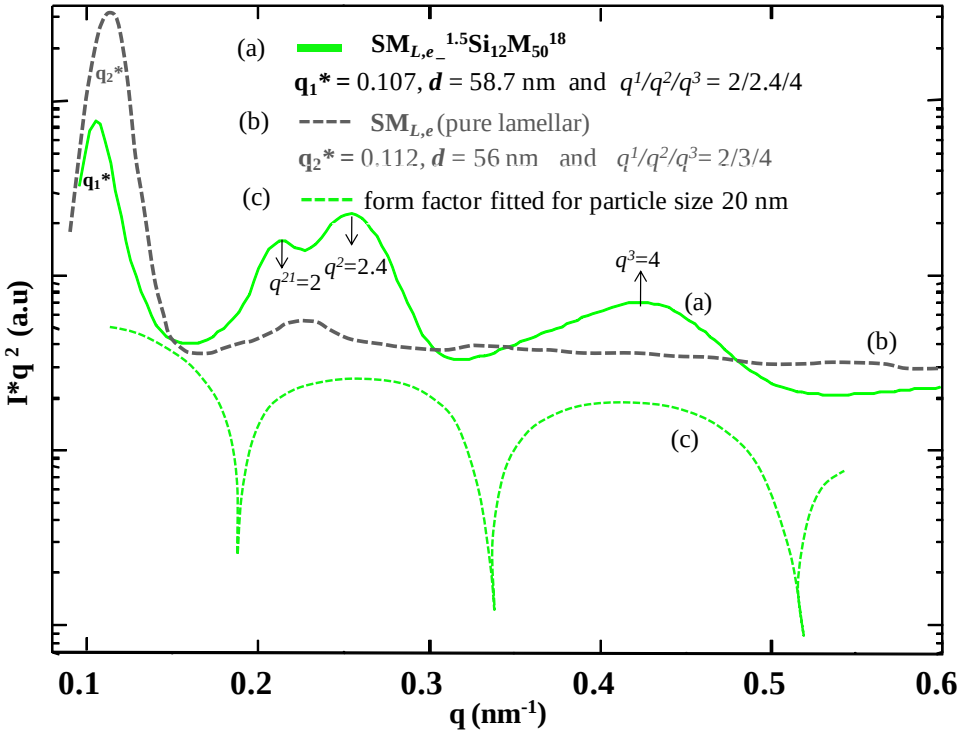

(ii)

Figure 4.4.3. SAXS curves of ultra thin cuts of BCP-modified silica composites. The changes in periodicity, *d* (2π/q*) and respective q^x (q*/q) values, of lamellar (SM_L) BCP and their composites (i) [(a) $SM_{L,e}$_$^{0.5}Si_{12}M_{50}^{18}$ (b) pure $SM_{L,e}$ (c) Form factor] (ii) [(a) $SM_{L,e}$_$^{1.5}Si_{12}M_{50}^{18}$ (b) pure $SM_{L,e}$ (c) Form factor] are shown in the inset of figure. Superscripts 0.5 and 1.5 correspond to the wt% of silica in the composite. The respective peak positions of SAXS curves are shown adjacent to the colour code in the inset of figure.

The form factor calculation shows the presence of silica core nanoparticles with 14 nm diameter. This size of commercially available silica nanoparticles (12 nm sized) used in the present study were found to have a size distribution in the range of 14 nm when analysed by DLS experiments (discussed in Chapter 4.2). Similarly, for 1.5 wt% silica content, the periodicity of $SM_{L,e}$_$^{1.5}Si_{12}M_{50}^{18}$ (curve (b) in Figure 4.4.3 (ii)) further arises to 58.7 nm. This is due to the increase in silica content (peak at q^3=2.4, due to form factor) and secondly from the small

aggregates in the composite. Further, the form factor calculation shows approximate fitting for size distribution of 20 nm. This should obviously arise from the formation of small aggregates (as seen in Figure 4.4.2 (b)).

A similar behaviour was observed for composites having cylindrical type of block copolymer matrix. The periodicity of the block copolymer matrix in $SM_{C,e}\_^{0.5}Si_{12}M_{50}{}^{18}$ composite with 0.5 wt% of silica content shifted from 57nm of the pristine block copolymer to 58.7 nm, shown by curve (a) in Figure 4.4.4 (i). The shift in the peak positions as observed in curve (a) of Figure 4.4.4 (i) when compared to that of pure block copolymer (curve (b) in Figure 4.4.4 (i)) can be explained due to the presence of modified silica nanoparticles.

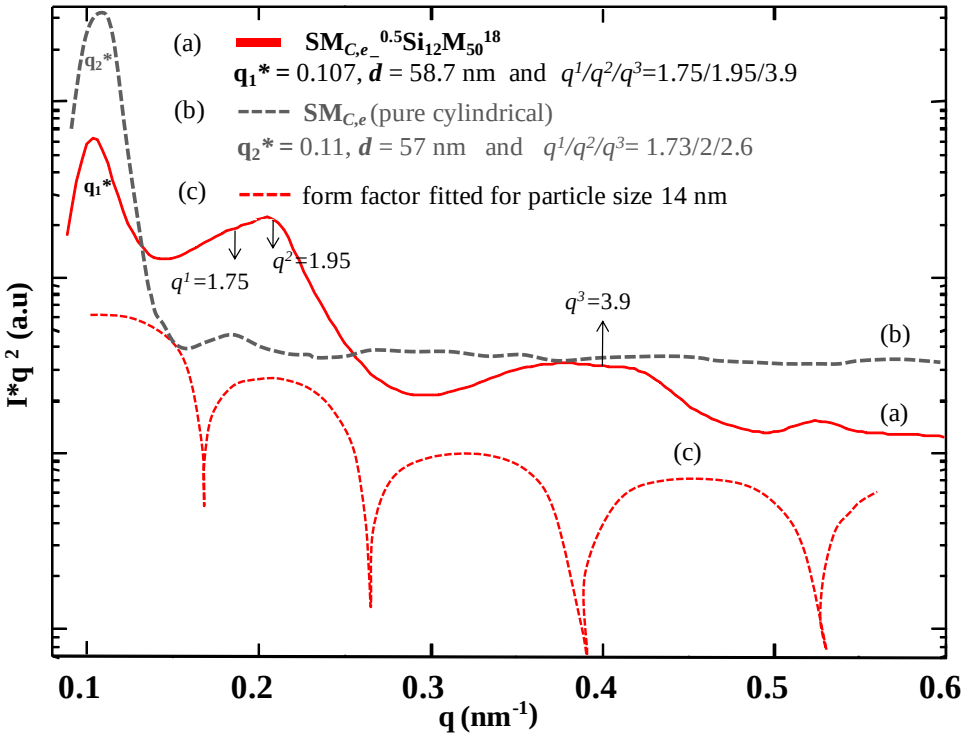

(i)

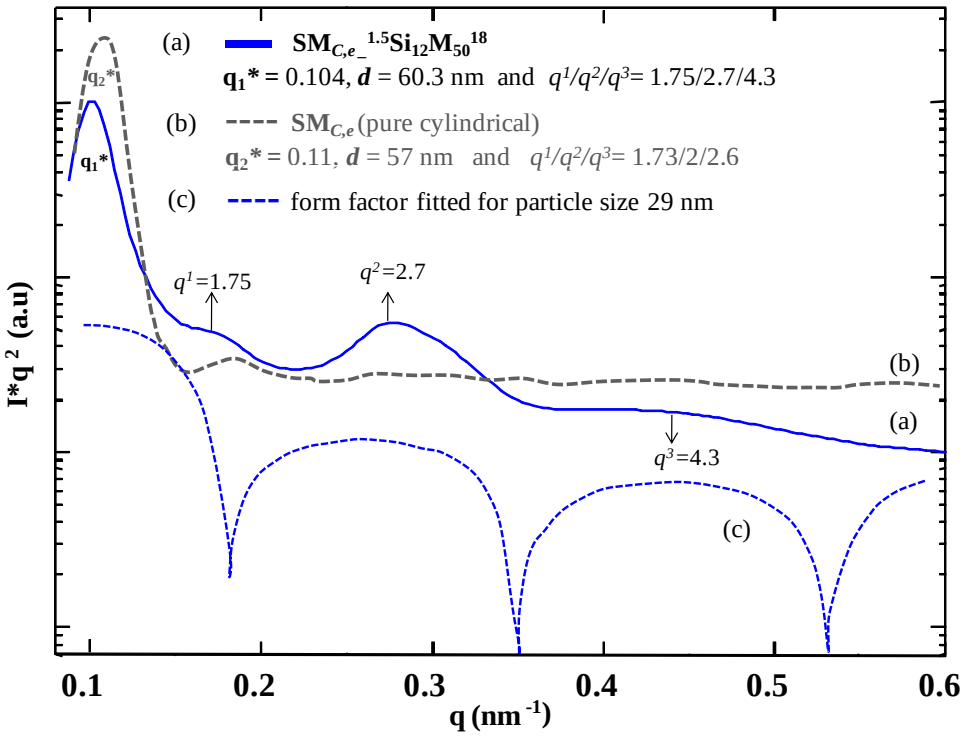

(ii)

Figure 4.4.4. SAXS curves of ultra thin cuts of BCP-modified silica composites. The changes in periodicity, *d* (2π/q*) and respective q^x (q*/q) values, of cylindrical (SM_L) BCP and their composites (i) [(a) $SM_{C,e}$_$^{0.5}Si_{12}M_{50}^{18}$ (b) pure $SM_{C,e}$ (c) Form factor] (ii) [(a) $SM_{C,e}$_$^{1.5}Si_{12}M_{50}^{18}$ (b) pure $SM_{C,e}$ (c) Form factor] are shown in the inset of figure. Superscripts 0.5 and 1.5 correspond to the wt% of silica in the composite. The peak positions of SAXS curves are shown adjacent to the colour code in the inset of figure.

The size of silica nanoparticles was found to be the same as 14 nm from the form factor calculation. When the silica content increased to 1.5 wt%, the periodicity of composite, $SM_{C,e}$_$^{1.5}Si_{12}M_{50}^{18}$, rises to 60.3 nm (curve (a) in Figure 4.4.4 (ii)). Form factor calculation shows a large size distribution of silica nanoparticles (in the range of 29 nm) should arise from the aggregate formation. The abnormal increase in periodicity is an indication of agglomerate formation in $SM_{C,e}$_$^{1.5}Si_{12}M_{50}^{18}$ composite and this is confirmed by the TEM image shown in Figure 4.4.2 (d).

4.4.2.2. Impact properties of (PS-*b*-PMMA) composites with PMMA modified silica nanoparticles

The influence of localisation of particles in either domains or more precisely the dispersion of modified silica particles in a block copolymer matrix is further analysed by the impact properties of the above composites. Impact measurements were carried out with unnotched specimen. Pristine SM_L and SM_C showed an impact resistance of 10±0.8 kJ/m^2 and 13±1.5 kJ/m^2, respectively. After the addition of 0.5 wt% silica, the impact resistance of $SM_{L,e\_}{}^{0.5}Si_{12}M_{50}{}^{18}$ and $SM_{C,e\_}{}^{0.5}Si_{12}M_{50}{}^{18}$ composites were improved to 12±1.8 kJ/m^2 and 15 ± 0.7 kJ/m^2, respectively. These improvements in impact properties may be an indication of the improved dispersion of silica particles in the BCP matrices as we observed in Figure 4.4.2 (a and c). For 1.5 wt% of silica, the impact resistance of $SM_{C,e\_}{}^{1.5}Si_{12}M_{50}{}^{18}$ composite decreases sharply to 8±1.8 kJ/m^2 from the pristine value 13±1.5 kJ/m^2. This indicates the possibility of formation of aggregates instead of proper dispersion. This is further confirmed by the respective TEM image (Figure 4.4.2 (d)). Whereas for the same silica content, the impact resistance of $SM_{L,e\_}{}^{1.5}Si_{12}M_{50}{}^{18}$ composite was decreased to 8±1.3 kJ/m^2. This decrease in value is not high as compared to $SM_{C,e\_}{}^{1.5}Si_{12}M_{50}{}^{18}$ composite. This infers that, there can be obviously small aggregates in $SM_{L,e\_}{}^{1.5}Si_{12}M_{50}{}^{18}$ but smaller than those present in the $SM_{C,e\_}{}^{1.5}Si_{12}M_{50}{}^{18}$ composite.

4.4.4. Conclusions

The morphology of PS-*b*-PMMA block copolymer composites with PMMA modified particles shows that the particles tend to occupy in the PMMA domain at low loadings (0.5 wt%) but upon increasing the content of modified silica particles (1.5 wt%) aggregation occurs and occupation of either domains was observed. Further, the impact properties of either block copolymer composites show slight improvement for 0.5 wt% of silica content. The extent of aggregation

seems to be higher in a block copolymer matrix having cylindrical morphology than a lamellar morphology. This can be visualized from TEM images and from the impact properties.

4.4.4. References

1. G. A. Buxton, A. C. Balazs, *Phys. Rev. E* 2003, 67, 031802.
2. S. Torquato, S. Hyun, A. Donev, *Phys. Rev. Lett*. 2002, 89, 266601.
3. M. Maldovan, A. M. Urbas, N. Yufa, W. C. Carter, E. L. Thomas, *Phys. Rev. B* 2002, 65, 165123.
4. M. R. Bockstaller, E. L. Thomas, *Phys. Rev. Lett*. 2004, 93, 166106.
5. B. H. Sohn, R. E. Cohen, *Chem. Mater*. 1997, 9, 264-269.
6. J. Huh, V. V. Ginzburg, A. C. Balazs, *Macromolecules* 2000, 33, 8085-8096.
7. E. Reister, G. H. Fredrickson, *J. Chem. Phys*. 2005, 123, 214903.
8. M. R. Bockstaller, Y. Lapetnikov, S. Margel, E. L. Thomas, *J. Am. Chem. Soc*. 2003, 125, 5276-5277.
9. R. B. Thompson, V. V. Ginzburg, M. W. Matsen, A. C. Balazs, *Science* 2001, 292, 2469-2472.
10. J. Y. Lee, R. B. Thompson, D. Jasnow, A. C. Balazs, *Faraday. Discuss*. 2003, 123, 121-131.
11. B. J. Kim, J. J. Chiu, G. R. Yi, D. J. Pine, E. J. Kramer, *Adv Mater*. 2005, 17, 2618-2622.
12. B. J. Kim, J. Bang, C. J. Hawker, E. J. Kramer, *Macromolecules* 2006, 39, 4108-4114.
13. S. W. Yeh, T. L. Wu, K. H. Wei, Y. S. Sun, U. S. Jeng, K. S. Liang, *J. Polym Sci., Polym. Phys. Ed.* 2005, 43, 1220-1229.
14. R. M. Ho, T. Lin, M. R. Jhong, T. M. Chung, B. T. Ko, Y. C. Chen, *Macromolecules* 2005, 38, 8607-8610.
15. M. R. Bockstaller, R. A. Mickiewicz, E. L. Thomas, *Adv. Mater*. 2005, 17, 1331-1349.
16. Q. Lan, L. F. Francis, F. S. Bates, *J. Poly. Sci: Part B: Poly. Phys*. 2007, 45, 2284-2299.
17. G. Kostorz, Small-angle scattering and its applications to material science, in *Treatise on Materials Science and Technology*, Vol. 15, G. Kostorz (ed.), Academic Press, New York, 1982, p.227.
18. P. K. Pranzas, Basics of Small-Angle Scattering Methods in , *Neutrons and Synchrotron Radiation in Engineering Materials Science*, From Fundamentals to Material and Component Characterization, W. Reimers, A. R. Pyzalla, A. Schreyer, H. Clemens (eds.), WILEY-VCH Verlag GmbH& Co. KGaA, Weinheim, 2008, p.235.

4.5. Mechanical Properties of PMMA Composites Prepared from Silica-*g*-(PBMA-*b*-PMMA) (*double shell*) Particles: Synthesis, Characterization and Mechanical Properties of Composites

4.5.1. Introduction

The outstanding optical properties, weather resistance and good mechanical strength made poly(methyl methacrylate) (PMMA) as a widely used commodity plastic since a long time. Its brittleness manifests itself as a limiting factor for being used in other fields of applications. The classical method for improving the toughness of a polymer matrix is achieved by either incorporating discrete amount of rubbery like modifier particles[1-2] or through the addition of modified/unmodified inorganic nanofillers.[3-4]

Emulsion polymerization and mechanical blending are the two common methods adopted for the preparation of rubber-toughened polymer composites.[5-7] Sufficient stress transfer between the modifier phases and the matrix is necessary for an efficient toughening mechanism. For this, the rubbery phase needs to adhere to the matrix. Generally, this is achieved through a core-shell particle structure.[8,9] It can be either (i) elastomeric core-external shell (*single shell*) or (ii) glassy core-elastomeric shell-external shell (*double shell*), which promotes good adhesion and reduces agglomeration.[8] The glassy core can be any glassy polymer depending on the nature of matrix used for the studies.

Secondly, the unique effects of inorganic nanoparticles in the polymer matrix can be effective only when the particles are well dispersed. However, the typical filler contents needed for such an enhancement of performance are as high as 20% by volume. The high filler loading leads to agglomeration of particles in the polymer matrix and thereby depreciates the processability of polymer. This may increase the final weight of the composites and adversely effect their

application in industry, especially in the field of electrical and electronic products. Sometimes, the resulting polymer matrix with nanoparticles exhibits properties even worse than conventional particle/polymer systems. Published works[10-13] reported that considerable improvement in mechanical properties can be achieved at very low volume contents of nanosized fillers in the range (1-5 vol %). Here arises the necessity of surface modification of particles (as discussed in introductory chapters and in Chapters 4.1-4.3). As mentioned before, an improvement in mechanical properties of PMMA composites was observed for a net silica content of 1.5 wt %.

As known, silica particles have been used as fillers to improve the mechanical properties, especially impact properties of glassy homopolymers. Chapter 4.3. discussed the results obtained on the dispersion and final mechanical properties of PMMA/modified silica nanocomposites in terms of size distribution and polymer graft density. The results showed no significant improvement in the mechanical properties of PMMA composites. But, PMMA composites with silica core modified by a block copolymer outer shell having an elastomeric block (inner shell) for the property enhancement have not been reported yet. Here we adopted the "*grafting from*" approach for the synthesis of poly(butyl methacrylate) (PBMA)-*b*-poly(methyl methacrylate) (PMMA) block copolymer (double shell) from silica particles using the well known atom transfer radical polymerization (ATRP).[14-16] The purpose of the outer PMMA shell is to enhance the dispersion of double shell particles in a PMMA matrix.

On the basis of the results obtained in Chapter 4.3, composites comprised of PMMA coated Si_{12} particles show better mechanical properties than composites comprised of PMMA coated Si_{20} particles. This indicates the influence of the surface chemistry of silica core on properties. Hence, in the present context, the Si_{12} particles were chosen for surface modification with double shell of block copolymers. Synthesis of PBMA grafted silica particles (Si_{12}-*g*-(PBMA)Br, macroinitiator) and further synthesis of PMMA second block was on the basis of reported ATRP

methods.[17-19] Epoxy silane was used to anchor ATRP initiator.[18] For the first time, here we tried to synthesize and investigate the effect of core–double shell particle containing elastomeric inner shell on the mechanical properties of PMMA composites for low wt% of silica content. The lower glass temperature (T_g) value of poly(butyl methacrylate) made us to explore its ability and influence in (co) polymer hybrid particles on mechanical properties and nature of dispersion in composites.

4.5.2. Discussion of Results

4.5.2.1. Synthesis and characterization of silica-*g*-(PBMA-*b*-PMMA) (*core-double shell*) particles

The bromination reaction was performed in two steps as described in Chapter 3. The first step involved the silanization of silica nanoparticles with epoxy silane. The second step consisted of an esterification of the terminal hydroxyl group of the vicinal diol obtained after epoxy hydrolysis with the 2-bromoisobutyryl bromide.

Bromide concentration on silica particles was maintained at 0.36 mmol/g (quantitatively measured from TGA). The above bromide concentration on silica particles used for grafting *double shell* particles is slighltly lower than that used in PMMA *single shell* particles (0.4 mmol/g, discussed in Chapter 4.2). The detailed synthesis of silica nanoparticles grafted with PBMA macroinitiator, Si_{12}-*g*-(PBMA)Br, followed by the synthesis of PMMA outer block was described in Chapter 3. The PBMA grafted silica particles were synthesized from silica colloidal initiators under the condition, [n-BMA]:[Si_{12}Br]:[Cu(I)Br]:[PMDETA] = 250:1:1:1 at 50 ^oC. The reaction was carried out in the solvent acetone. After reaction, a grafted molar mass of 26,000 g/mol of PBMA with a polydispersity (PDI) of 1.33 were obtained. TGA analysis showed a weight fraction of 70 wt % of PBMA on the Si_{12} particles (represented by Si_{12}-*g*-($PBMA_{70}^{26}$)-

Br). The second block (outer shell) of poly(methyl methacrylate) was synthesized from PBMA macroinitiator having a bromide concentration 0.04 mmol/g (measured quantitatively from TGA).The molar ratios are [MMA]:[Si_{12}-*g*-($PBMA_{70}^{26}$)-Br]:[CuBr]:[PMDETA] =1100:1:1:1. The reaction was carried out at 85 ^{o}C. The resultant molecular weight of the degrafted block copolymer was 37,000 g/mol (represented by $Si_{12}BCP^{37}$ in Table 4.5.1) with a polydispersity of 1.34. The mol fraction of PBMA block calculated from ^{1}H-NMR was found to be PBMA = 0.56. The TGA analysis of block copolymer hybrid silica particles shows a weight fraction of 85 % ($Si_{12}BCP_{85}^{37}$). The GPC curves of degrafted PBMA and PBMA-*b*-PMMA chains respectively are shown in Figure 4.5.1.

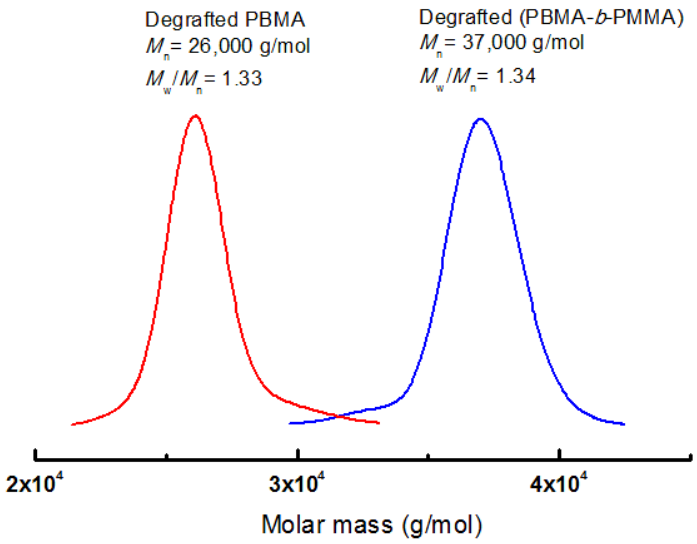

Figure 4.5.1. GPC curves of degrafted PBMA and PBMA-*b*-PMMA (co) polymer chains from silica particles, Si_{12}-*g*-$(PBMA)_{70}^{26}$-Br and Si_{12}-*g*-$(PBMA\text{-}b\text{-}PMMA)^{37}$ respectively

The yield of the final product was low because of the low efficiency of Si_{12}-*g*-(PBMA)Br macroinitiator to initiate PMMA polymerization. ^{1}H-NMR spectra (Figure 4.5.2) was used to complete the characterization of the grafted block copolymer. Figure 4.5.2. presents the ^{1}H-NMR

spectra of (a) pure PMMA (b) Si_{12}-*g*-($PBMA_{70}^{26}$)-Br macroinitiator, (c) block copolymer grafted silica particles, Si_{12}-*g*-(PBMA-*b*-$PMMA)_{85}^{37}$.

The NMR spectra allows the determination of the molar composition from the relative intensity of the resonance signals at 4 ppm (-OCH_2 protons of the butyloxy) for *n*-butyl methacrylate (*n*-BMA) and at 3.6 ppm (-OCH_3 protons of the methyloxy) for methyl methacrylate. Combined ATR-FTIR spectra of silica particles after each step of functionalization are shown in Figure 4.5.3.

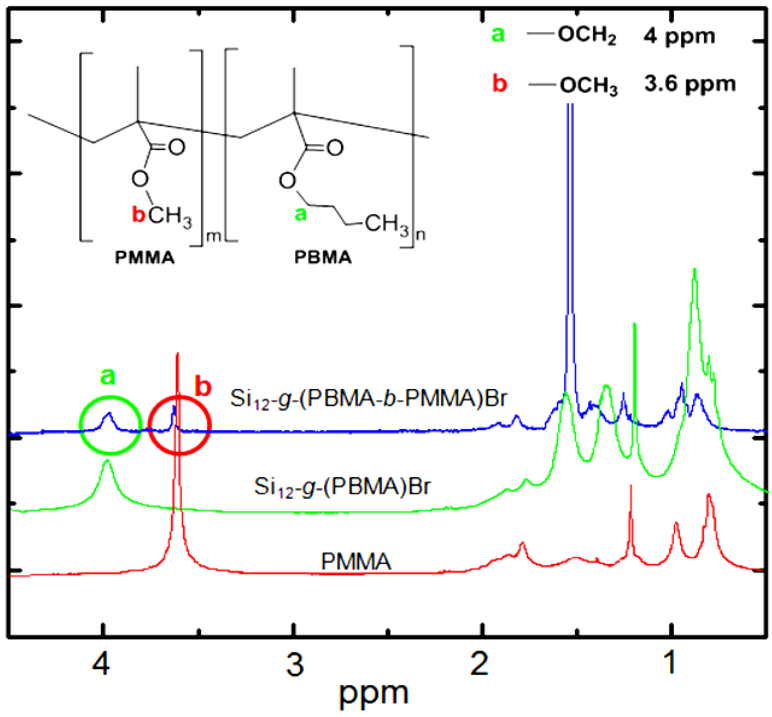

Figure 4.5.2. ^{1}H-NMR spectra of (a) pure PMMA (b) Si_{12}-*g*-$(PBMA)_{70}^{26}$-Br macroinitiator, (c) block copolymer grafted silica particles, Si_{12}-*g*-(PBMA-*b*-$PMMA)_{85}^{37}$.

The intensity of carbonyl (-C=O) stretching band near 1750 cm^{-1} for initiator anchored silica particles ($Si_{12}Br$) increases sharply after each step of grafting Si_{12}-*g*-($PBMA_{70}^{26}$)-Br and Si_{12}-*g*-(PBMA-*b*-$PMMA)_{85}^{37}$, coming from the ester moiety of the (co)polymer. Moreover, the antisymmetric C-O-C stretching mode in esters gives rise to a very strong and broad band around

the region, 1430-1460 cm^{-1}.

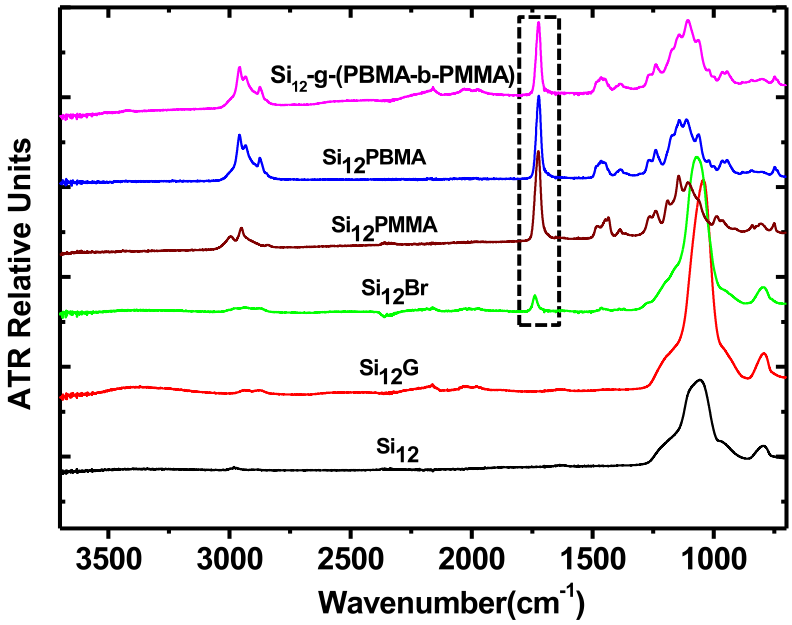

Figure 4.5.3. Combined ATR-FTIR spectra of (a) pristine silica particles, Si_{12} (b) silica particles after coupling with epoxy silane, $Si_{12}G$ (c) initiator grafted silica, $Si_{12}Br$ (d) PMMA modified silica particles, $Si_{12}PMMA$ (e) PBMA modified silica particles, Si_{12}-*g*-$(PBMA)_{70}^{26}Br$ (f) block copolymer grafted silica particles, Si_{12}-*g*-$(PBMA$-*b*-$PMMA)_{85}^{37}$.

4.5.2.2. Thermal characterization of silica-*g*-(PBMA-*b*-PMMA) (*core double shell*) particles

The phase study of diblock copolymer grafted silica nanoparticles was carried out by measuring the glass transition temperatures (T_g's) through differential scanning calorimetry (DSC). After grafting the PBMA shell on silica nanoparticles ($Si_{12}PBMA_{70}^{26}$), the T_g value raises to 47 ^oC. An equivalent free PBMA homopolymer (M_n=27,450 g/mol and M_w/M_n=1.32) was synthesized (as a reference) via ATRP using the initiator, ethyl-2-bromoisobutyrate, under similar reaction conditions showed a T_g value of 23 ^oC. The increase in T_g value of PBMA grafted silica particles

arises due to the decrease in the mobility of polymer chains through the covalent bond (strong interaction) between silica nanoparticles and the grafted polymer. A similar behaviour of increasing T_g was also observed after grafting PMMA shell on silica nanoparticles as discussed in Chapter 4.3. After grafting the outer PMMA shell, (Si_{12}-*g*-(PBMA-*b*-PMMA)$_{85}$[37], the T_g value of PMMA block was observed near 96 ^oC. This proves the successful grafting reaction of block copolymer on silica nanoparticles.

4.5.2.3. Mechanical properties and morphology of PMMA composites with silica-*g*-(PBMA-*b*-PMMA) (*core-double shell*) particles

The composites for mechanical and morphological characterization were prepared by the procedure described in Chapter 3. Even though studies reported that an improvement in mechanical properties of PMMA composites is achievable by the addition of pristine, silane modified or polymer modified silica nanoparticles at small loadings,[20-21] the improvement in properties is not significant when we compare them with the latest reported values obtained from a rubber toughened PMMA matrix.[9] Further, Chapter 4.3 discussed in detail the nature of dispersion and the mechanical properties of PMMA composites with silica core-single shell particles on the basis of some possible factors such as graft density, graft and matrix molar mass and core size. The present chapter investigates how silica core-double shell particles of given molar mass, elastomeric content and core size can affect the mechanical and morphological properties of PMMA composites.

PMMA composites of core-double shell particles were prepared for silica content varying in between 0-2.5 wt%. Optimum tensile and impact properties were observed at 1.5 wt %. Table 4.5.1 gives a description about the variation in mechanical properties of PMMA composites prepared from Si_{12} core-double shell particles.

The value of impact strength was found to improve (106 %) significantly. Similarly, elongation at break, modulus of elasticity and tensile strength were also found to increase 40%, 26 % and 12 % respectively. Figures 4.5.4 (a) and (b) describe the variation in tensile and impact properties of PMMA composites by varying amounts of core-double shell particles

Table 4.5.1. Tensile and impact properties of PMMA composites prepared from *silica core-double shell* particles.

Sample code	**Tensile modulus** *E* (MPa)	**Tensile strength** σ_m (MPa)	**Elongation at break** ε_B (%)	**Impact strength** (*unnotched*) a_{cU} (kJ/m^2)	T_g (^oC)
$PMMA^{49}$	3400±45	75±1	5±1	15±1	96±2
$PMMA^{49}\_^{1}Si_{12}BCP_{85}^{37}$	3760±60	80±1.8	7±1.2	20±2	99±1
$PMMA^{49}\_^{1.5}Si_{12}BCP_{85}^{37}$	4280±39	84±2.4	7±0.6	31±3	100±1
$PMMA^{49}\_^{2}Si_{12}BCP_{85}^{37}$	4120±64	82±1.9	5±1.3	26±1	101± 1
$PMMA^{49}\_^{2.5}Si_{12}BCP_{85}^{37}$	3810±47	78±1.6	4±0.7	22±2.5	102

$PMMA^{49}$: PMMA for the matrix polymer and the superscript 49 for the molar mass in g/mol. $PMMA^{49}\_^{x}Si_{12}BCP_{85}^{37}$: superscript x for wt% of silica content in matrix, BCP for grafted block copolymer on Si_{12} particles (Si_{12}-*g*-(PBMA-*b*-PMMA)$_{85}^{37}$), subscript 12 for average diameter of silica core particles and superscripts 37 and 85 for molar mass of grafted BCP in g/mol and weight fraction of grafted BCP (wt%) measured from TGA analysis respectively.

In the present studies, the optimum mechanical properties of PMMA composites are achieved at a loading of 1.5 wt% of silica core-double shell particles. The enhancement in mechanical properties, especially impact strength, shows the efficiency of core-double shell particles.

Recent studies of Suu[22] reported that unnotched specimen of PMMA composite achieved nearly 43 % improvement in impact strength for 7.5 wt % PMMA-modified natural rubber (MNR).

Beyond 1.5 wt % of silica content, the values of impact strength decreases but still the properties are better rather than either pure PMMA or those composites containing pristine and silane modified silica (Chapter 4.3). As already discussed in the introductory chapters and previous paragraphs, in contrary to the classical three

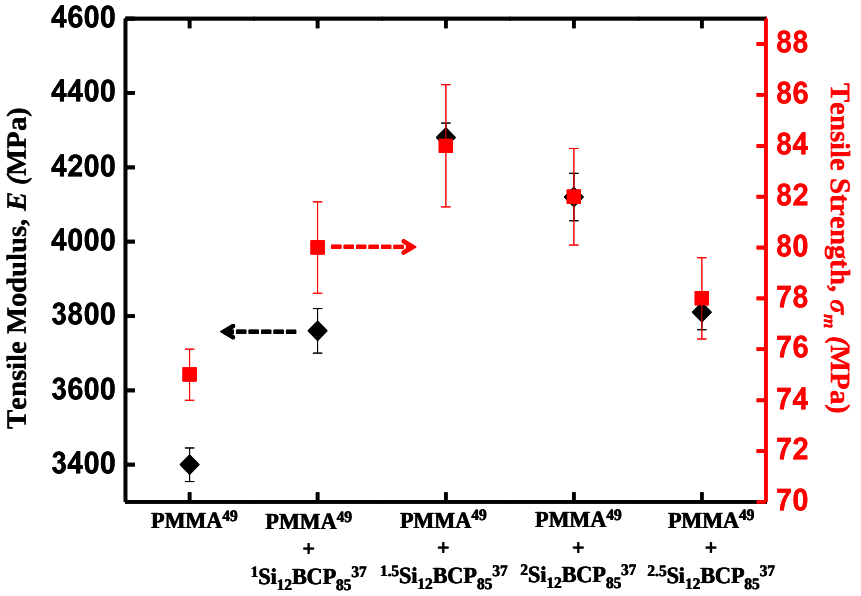

(a)

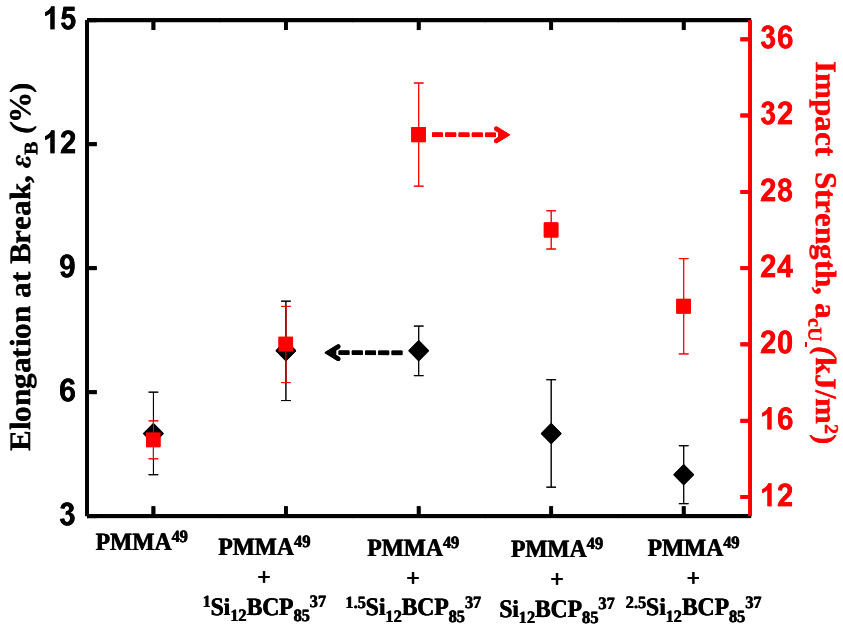

(b)

Figure 4.5.4. Variation of (a) tensile modulus and tensile strength and (b) elongation at break and impact strength of PMMA and its composites with 0-2.5 wt% loadings of silica core-double shell particles.

layered core shell (having hard glassy polymer core) and two layered (having soft core) structures, silica nanoparticles used as the inner core and PBMA as the inner shell with a PMMA outer shell in the present studies.

Mechanical properties of PMMA composites (Table 4.5.1) containing silica-*g*-(PBMA-*b*-PMMA) exhibit good results than those composites containing ungrafted (PBMA-*b*-PMMA) particles. These initial results reveal that PBMA linker in the core-double shell particle can act as an efficient stress transfer agent between modifier phases and the PMMA matrix. The mechanical properties of PMMA composites containing simply silica grafted PBMA (Si_{12}-*g*-($PBMA_{70}^{26}$)-Br) particles were also analysed. An optimum improvement in properties was observed at 2 wt % of silica content. The observed impact strength, tensile modulus, tensile strength and elongation at break were 23±1.8 kJ/m^2, 3880±48 MPa, 80±2.6 MPa and 7±2 %, respectively. Obviously these values are lower than those obtained by the addition of silica-double shell particles at 1.5 wt%. These observations show that the outer PMMA shell of silica core-double shell particles is necessary and indeed improves the dispersion of *double-shell* particles in PMMA matrix and altogether improves the mechanical properties of the composites. The TEM image (Figure 4.5.5) of ultra thin cut of PMMA composite sample after impact measurement is shown below.

One can observe small aggregates together with some isolated modified particles. These small aggregates might positively improve the mechanical properties of composites. DSC measurements (Table 4.5.1) of composites with double shell particles show not much improvement in the T_g values. These results demonstrate the possibility to use nanoparticles (silica in the present case) grafted with shells of polymer (depend upon the desire) to improve the properties (presently mechanical properties) in homopolymer matrices.

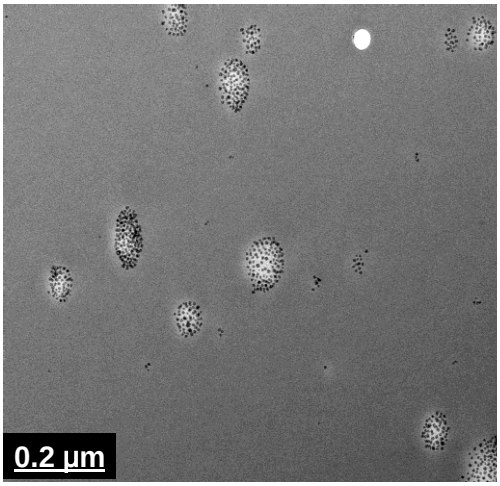

Figure 4.5.5. TEM image of ultra thin cut of $PMMA^{49}\_^{1.5}Si_{12}$-*g*-$(PBMA\text{-}b\text{-}PMMA)_{85}^{37}$ composite sample used for impact measurement having a net silica content of 1.5 wt%.

Apart from the present results, one could anticipate varying mechanical properties and dispersion of modified particles by varying the core size, weight fraction or graft density of PBMA inner block and outer PMMA shell and final size distribution of modified particles in polymer matrix. Following figures 4.5.6 (a-b) gives an overall impression of optimum mechanical properties of PMMA composites obtained with various surface modified Si_{12} particles adopted in the present work.

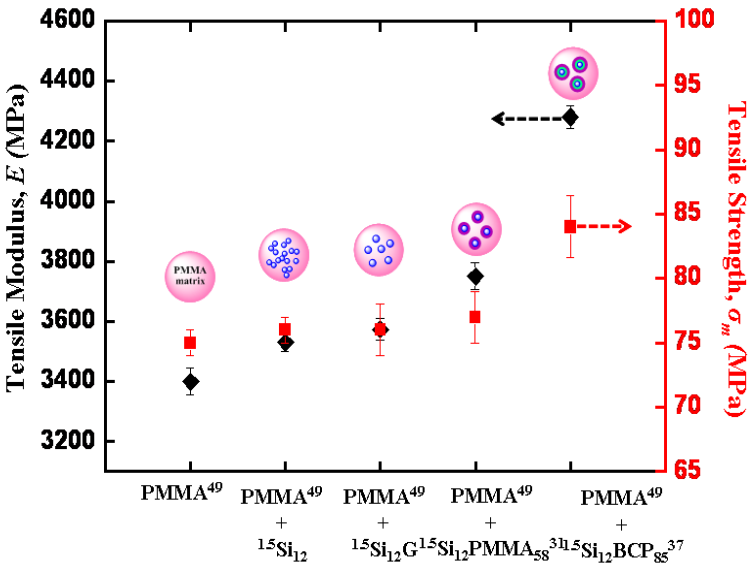

(a)

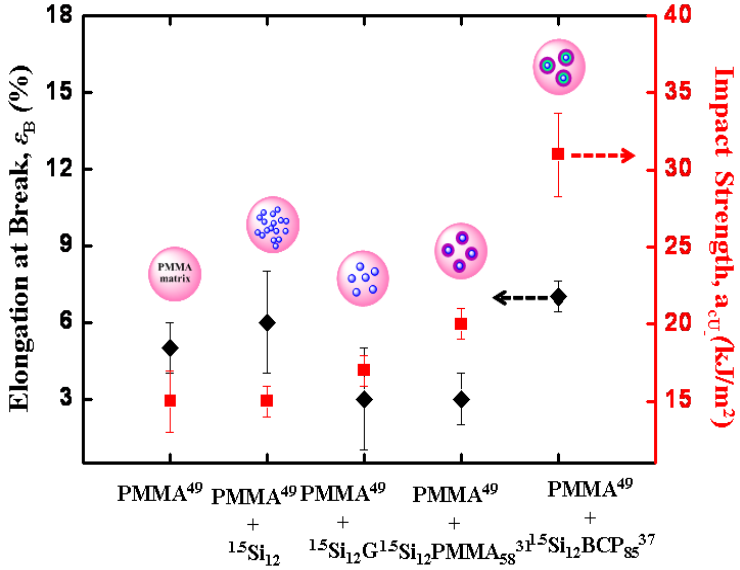

(b)

Figure 4.5.6. Optimum (a) tensile modulus and tensile strength and (b) elongation at break and impact strength of pure $PMMA^{49}$ and its composites obtained with 1.5 wt% loadings of Si_{12} ($PMMA^{49}$ + $^{1.5}Si_{12}$), GPS grafted Si_{12} ($PMMA^{49}$ + $^{1.5}Si_{12}G$), PMMA grafted Si_{12} ($PMMA^{49}$ + $^{1.5}Si_{12}PMMA_{58}^{31}$) and BCP grafted Si_{12} ($PMMA^{49}$ + $^{1.5}Si_{12}BCP_{85}^{37}$)

4.5.3. Conclusions

PMMA composites exhibit a significant improvement in mechanical properties, especially the impact properties for lower loadings (1.5 wt %) of silica particles (Si_{12}) grafted with PBMA-*b*-PMMA (double shell) block copolymer for a given graft molecular weight and size distribution. The observed improvement in mechanical properties with double shell particles is much better than other surface modified particles (Chapter 4.3). Also, the final transparency of the composite is also maintained to a good extent. These results open the door to use silica nanoparticles (of a given core size) grafted with polymeric shells (double shell in the present case) of desired characteristics to improve the mechanical properties of polymer composites, especially for light weight applications.

4.5.4. References

1. H. Keskkula, *Rubber-Toughened plastic*, American Chemical Society: New York, 1989, 289.
2. C. B. Bucknal, *Toughened Plastics*, Applied Science Publishers: London, 1977.
3. A. Savadori, M. Scapin, R. Walter, *Macromol. Symp*., 1996, 108, 1-289.
4. B. Pukanszky, *Particulate filled polypropylene composites*. In: J. Karger-Kocsis, editor. Polypropylene: an A-Z reference, Dordrecht: Kluwer Academic Publishers, 1999, 574-80.
5. J. Hooley, D. R. Moore, M. Whale, M. J. Williams, *Plastic and Rubber Processing and Application*, 1981, 1, 345.
6. H. Keskkula, *Rubber-Toughened plastic*, American Chemical Society: New York, 1989, 289.
7. O. Mauzac, R. Schirrer, *J. Appl. Polym. Sci*., 1989, 38, 2289.
8. C. Wrottecki, P. Heim, P. Gaillard, *Polym Eng Sci*., 1991, 31, 213.
9. R. Y. Hong, H. P. Fu, Y. J. Zhang, L. Liu, J. Wang, H. Z. Li, Y. Zheng, *J. Appl. Polym. Sci*., 2007, 105, 2176-2184.
10. M. Z. Rong, M. Q. Zhang, Y. X. Zheng, H. M. Zeng, R. Walter, K. Friedrich, *J. Mater. Sci. Lett*., 2000, 19, 1159.
11. M. Q. Zhang, M. Z. Rong, S. L. Yu, B. Wetzel, K. Friedrich, *Macromol. Mater. Eng*., 2002, 2, 111.
12. T. Naganuma, Y. Kagawa, *Comp. Sci. Technol*., 2002, 62, 1187.
13. Y. P. Zheng, Y. Zheng, R. C. Ning, *Mater. Lett*., 2003, 57, 2940.
14. (a) O. Prucker, J. Ruhe, *Macromolecules* 1998, 31, 602-613. (b) T. E. Pattern; K. Matyjaszewski,

Adv. Mater., 1998, 10, 901.

15. M. Alexandre and P. Dubois in Macromolecular Engineering: Precise Synthesis, Materials Properties, Applications″, Vol.4, Chapter 2, K. Matyjaszewski, Y. Gnanou and L. Leibler. Wiley-VCH; Weinheim, 2007, 2033-2070.
16. R. Barbey, L. Lavanant, D. Paripovic, N. Schüwer, C. Sugnaux, S. Tugulu, Vol.4, Chapter 2, K. Matyjaszewski, Y. Gnanou and L. Leibler. Wiley-VCH; Weinheim, 2007, 2033-2070.
17. R. Barbey, L. Lavanant, D. Paripovic, N. Schüwer, C. Sugnaux, S. Tugulu, H. A. Klok, *Chem. Rev*., 2009, 109, 5439-5452.
18. K. A. Davis, K. Matyjaszewski, Chin. *J. Polym. Sci*., 2004, 22, 195-204.
19. M. Fernández-García, J. Luis De La Fuente, M. Fernández-Sanz, E. L. Madruga, *J. Appl. Polym. Sci*., 2002, 84, 2683-2691.
20. S. Etienne, C. Becker, D. Ruch, B. Grignard, G. Cartigny, C. Detrembleur, C. Calberg and R. Jerome, *J.Therm. Ana. and Calori*., 2007, 87, 101-104.
21. H. Zou, S. Wu, J. Shen., *Chem. Rev*., 2008, 108, 3893-3957.
22. Y. G. Suu, "Studies on Mechanical Properties of Poly(methyl methacrylate) and Poly(methyl methacrylate)-Modified Natural Rubber Blend", Master Thesis, 2008.

Chapter 5. Summary and Conclusions

The outstanding optical properties, good mechanical strength and weather resistance made PMMA a widely used commodity plastic since a long time. But its brittleness manifests itself as a limiting factor for being used in other fields of applications. So, the present Ph.D work is mainly focussed to study and improve the dispersion and impact properties of composites based on commercially available PMMA matrix polymer (Plexiglass 6N Klar) filled with silica grafted homopolymer (*single shell*) or block copolymer (*double shell*) nanoparticles while retaining the transparency of matrix polymer to a good extent. Also, the localisation behavior of PMMA modified silica particles in glassy PS-*b*-PMMA diblock copolymer matrices for a given morphology on the impact properties was studied.

Controlling the extent of particle aggregation is one of the important issues that can improve the final mechanical properties of (co) polymer composites leads to the known concept of surface functionalisation of particles and is taken into account as a part of the present studies. Number of studies are still exploring in this area of research. So the efficient way is to decorate the particle surface with (co) polymer chains (hybrid nanoparticles). Hybrid nanoparticles in which polymer chains extended away from the colloidal silica core helps to minimise the steric crowding and enable good dispersion in polymer matrix (depending on the molar mass of matrix and grafted polymer). Here we adopted the "*grafting from*" approach for grafting (co) polymer chains by the well known atom transfer radical polymerisation (ATRP). This is usually achieved by initially functionalising the particles with a suitable silane linker followed by an esterification reaction with ATRP initiator. In order to avoid particle aggregation to a good extent, the particles were kept in solution until the initiator grafting step.

Small sized silica nanoparticles (SiNP's), 12 nm and 20 nm (Si_{12} and Si_{20} respectively) were chosen for current studies. Apart from the reported studies, efficiency of commercially available epoxy silane (GPS) linker for grafting ATRP initiator (2-BriB) was studied systematically in detail. Because, controlling the concentration of ATRP initiator is very important in regulating the graft density, molecular weight of tethered polymer chains and the final size distribution of polymer coated SiNP's. Esterificaton reaction was controllable in order to maintain a desired bromide concentration of ATRP initiator. Almost complete esterification or bromination of the terminal OH group of vicinal diol of silane modified silica was achievable. This was approved by the elemental and TGA analysis. Efficiency of these initiator grafted particles towards the kinetics of surface-initiated ATRP (SI-ATRP) was studied by means of simple styrenic and acrylic monomers like styrene and methyl methacrylate (MMA).

In the present scenario, it is necessary to study the SI-ATRP kinetics in order to develop well defined polymer grafted silica particles or silica–polymer brushes (SiPB's) of desired graft density, molecular weight and size distribution for their later application in the preparation and mechanical property analysis of final composites. Most of the SI-ATRP kinetics studies kept lower bromide concentration of ATRP initiator on silica particles (having either small or large size distribution) for efficient grafting polymerisation. But in the present work, the efficiency and consequences of grafting polymerisation from SiNP's having higher initiator concentration (0.4 mmol/g) for a given reaction condition at different conversions was investigated. On the basis of reviewed literatures and best of our knowledge, for the first time a comparative kinetic studies of styrene and MMA polymerisations were carried out from both small sized Si_{12} and Si_{20} particles keeping a constant bromide concentration. The results showed that the reaction is well controllable under these concentration from both sized particles for conversions up to 20 % and above to good extent for the given reaction condition. The control on MMA polymerization was found to be better from Si_{20} particles. The rate of MMA polymerization from Si_{12} particles was

found to be faster than from Si_{20}. On the basis of above reactions from both type of particles, chances of aggregation through interparticle coupling seems to be more important when particle size decreases. The consequences of cross linking/interparticle coupling were analysed by means of GPC and DLS experiments.

Recently, studies reported the dispersion behaviour and rheology of PMMA modified particles in PMMA matrix of varying graft and matrix molar mass for a given particle core size and polymer graft density. Most of these works were carried out in films and in dispersions. No detailed work regarding the changes in the impact and tensile properties of polymer composites by considering all the above parameters and particle core size has been reported yet. As already mentioned in the beginning, the purpose of the research work is to investigate the dispersion characteristics of PMMA modified (*single shell*) silica particles in PMMA matrix on the final impact and tensile properties of composite. Of the above synthesized polymer modified silica nanoparticles, PMMA modified Si_{12} and Si_{20} particles having three different graft densities, 0.15-0.19, 0.27-0.32, and 0.43-0.46 chains/nm^2 respectively, and graft molecular weights which are lower, nearly equal and higher than the matrix molecular weight were chosen for composite preparation. The silica content in the composite was varied from 0-2 wt%. Overall studies showed that PMMA composites comprised of modified silica particles with a core diameter of 12 nm (Si_{12}) have some improvement in impact and tensile properties than the corresponding 20 nm (Si_{20}) sized particles. This point towards the dependence of particle "*curvature*" on the final properties of composites. Among the various composites, Si_{12} particles having a graft density, 0.15 chains/nm^2 and graft molar mass 31,000 g/mol ($^{1.5}Si_{12}M_{58}{}^{31}$) exhibits slight improvement in impact and tensile properties of PMMA composites for a net silica content of 1.5 wt%. It was reported that considerable improvement in mechanical properties can be achieved at very low volume contents of nanosized fillers in the range (1-5 vol %)Increasing the amount of silica content beyond 1.5 wt% and graft molecular weight of either modified SiNP's was found to decrease the mechanical

properties and their dispersion in PMMA matrix. The TEM characterization of ultra thin cuts of $PMMA^{49}\_^{1.5}Si_{12}M_{58}^{31}$ composites showed a good dispersion of respective particles in the matrix polymer. It was concluded that the observed improvement in dispersion and mechanical properties of composite can be due to the "*wetting*" behavior of $^{1.5}Si_{12}M_{58}^{31}$ particles of given graft density and graft molecular weight with the matrix PMMA polymer. The optical transparency of the resultant composite was also retained to good extent. This indicates that one could anticipate improvement in dispersion or mechanical properties by varying the above parameters with the matrix polymer.

The above studies can be also extended to block copolymer matrices. Most of the morphological studies of block copolymer-nanoparticle composites have focussed on relatively small NP's (quantum dots) other than silica, relative to the block copolymer domain dimensions. All the above studies regarding the dispersion of grafted NP's in block copolymer matrices were done in solvent casted films. Due to the complex morphological changes that can occur during processing, almost no study has been reported yet regarding the dispersion behaviour of polymer modified NP's in glassy block copolymer composites prepared by melt mixing. The glassy block copolymer, PS-*b*-PMMA, having lamellar and cylindrical morphologies and PMMA modified (*single shell*) Si_{12} particles having a defined size distribution with respect to the block copolymer domain dimension with were chosen for studies. The silica content in the composite was varied up to 1.5 wt%. The localisation behaviour of PMMA modified Si_{12} particles in PS-*b*-PMMA composite prepared by melt mixing was analysed by TEM and SAXS measurements of ultra thin cuts of the specimen.

The morphological characterisation of either block copolymer-PMMA modified silica composite showed that the silica particles tend to occupy in the PMMA domain at low loadings (0.5 wt%) but upon increasing the silica content, up to 1.5 wt%, aggregation occurs and occupation in

either domains was observed. The above observation can be correlated with the impact measurements. The impact properties of either block copolymer composites show slight improvement for 0.5 wt% of silica content. Initial observation indicates that the extent of particle aggregation seems to be higher in block copolymer having cylindrical morphology than in a lamellar morphology.

So far, the dispersion characteristics and mechanical properties of PMMA composites with PMMA modified (*single shell*) silica particles was discussed. The observed improvement in impact and tensile properties are not significant. At this context, the idea behind classical way of toughening polymer matrix, through either (i) single shell (elastomeric core-external polymer shell) or (ii) double shell (glassy polymeric core-elastomeric inner shell-external polymer shell) particles, arose. Emulsion polymerization and mechanical blending were the two common methods adopted for the preparation of those rubber-toughened polymer composites. But, composites with silica core modified by a diblock copolymer (*double shell*) having an elastomeric block (inner shell) for the enhancement of impact property have not been reported yet.

In the present investigation the same "*grafting from*" approach is adopted for the synthesis of *double shell* silica particles (Si_{12}-*g*-(PBMA-*b*-PMMA) using ATRP. PBMA was chosen as the elastomeric inner shell. The purpose of PMMA outer shell was to enhance the dispersion of double shell particles in a PMMA matrix. The above synthesised particles were characterized by means of ^{1}H-NMR, ATR-FTIR, GPC and DSC analysis. The up scaling of these modified particles was found to be a limitation due to the low initiation efficiency of Si_{12}-*g*-(PBMA)Br macroinitiator. PMMA composites exhibited a significant improvement in mechanical properties, especially the impact properties (106 %) for lower loadings (1.5 wt %) of silica particles (Si_{12}) grafted with PBMA-*b*-PMMA (*double shell*) for a given graft molecular weight and size distribution. The observed improvement in impact properties is higher than those

reported works with PMMA composites of rubber modified particles. The transparency of the above composite was retained to a good extent. The observed improvement in mechanical properties of composites with double shell particles was found to be much better than the PMMA modified silica particles (*single shell*). Apart from the present results, one could anticipate varying mechanical properties and dispersion of modified particles by varying the core size, weight fraction or graft density of PBMA inner block and outer PMMA shell and final size distribution of modified particles in polymer matrix. These results open the door and the possibility of using silica nanoparticles (of a given core size) grafted with polymeric shells (double shell in the present case) of desired characteristics to improve the mechanical properties, especially the impact properties of polymer composites for light weight applications in future.

Chapter 6. Acknowledgement

I express my deep gratitude to Prof. Dr. Volker Abetz for giving me an opportunity to come to Germany in order to carry out my PhD research work in the Institute of Polymer Research, Helmholtz-Zentrum Geesthacht, through out these years. I really appreciate Your scientific support, ideas and assistance, especially during the discussions of my final thesis. Also, I am so great full to the DAAD-HGF fellowship for my doctoral studies. It is my pleasure to acknowledge that I have been a part in this new area of research that we begun in our institute in order to contribute my effort and skills and I hope it will be a success in future. It is a great privilege to have a mentor like Dr. Michaël Alexandre and have no words to thank him. I always have to remember his scientific support, patience, nice ideas and kindness from the initial stages of my research towards the end. I express my thanks to our former supervisor, Dr. Adriana Boschetti-de-Fierro for her supervision and good discussions during the short meetings and also thankful to present department leader Dr. Ulrich A. Handge for the nice discussions and comments during my presentations. I am also grateful to Dr. Julio Albuerne for those nice discussions and tips that I learnt from him.

I would also like to thank the beam line scientists of HASYLAB, Dr. Sérgio Funari, and Dr. Ulla Vainio for their support during the X-ray measurements and those funny moments with our fellow colleagues in the mean while.

I have to express my special thanks to Dr. Peter Simon, Mrs. Brigitte Lademann and Dr. Volkan Filiz of our Polymer Synthesis Department for providing me the matrix block copolymers for composite preparation. I really enjoyed the time, discussions and the coffee break that I

sometimes spent with my *PMM* team mates. My special thanks to Clarissa, Heinrich, Ilona, Ivonne, Sabrina, Thomas, Maren, Silvio, Carsten, Berthold, Holger, Petra, Peter, Allen, Daniel, Mukesh, Andreas, Mariela, Kristian, Marcio, Bing, Wiebke and Nahide. Also, my special regards to Mr. Kummerow, Carole, Anna, Maria, Jörg, Anja, Sergey and Meenakshi.

Finally, heartfelt thanks to my Appa and Amma, sister and brothers for their constant support, strength and prayers all these times. Above all, I thank God Almighty for whatever I achieved in my life until now.

Publications

1. Golda Louis Chakkalakal, Michaël Alexandre, Clarissa Abetz, Adriana Boschetti-de-Fierro and Volker Abetz, *Macromol. Chem. Phys.* 2012, 213, 513-528. (The contents of the paper are from Chapter 4.1 and Chapter 4.2 of Results and Discussions)

2. Golda Louis Chakkalakal, Michaël Alexandre, Adriana Boschetti-de-Fierro and Volker Abetz, *Macromol. Mater. Eng*. Published online 9 FEB 2012, DOI: 10.1002/mame.201100365. (The contents of the paper are from Chapter 4.5 of Results and Discussions)